ATOMIC LAYER EPITAXY

Contract No. N00014-85-K-0331

FINAL TECHNICAL REPORT

For the Period: 1 July 1984 through 31 October 1988

Submitted to:

Office of Naval Research
Head Electronics Division
800 North Quincy Street
Arlington, Virginia 22217-5000

Submitted by:

P. Daniel Dapkus, Professor
Department of EE/Electrophysics
University of Southern California
University Park
Los Angeles, California 90089-0483

For our final technical report

ATOMIC LAYER EPITAXY

Contract No. N00014-85-K-0331

For the Period: 1 July 1984 through 31 October 1988

We present

"Atomic Layer Epitaxy of III-V Compound Semiconductors by Thermal and Laser-Assisted Metalorganic Chemical Vapor Deposition"

A Final Dissertation by Steven P. DenBaars

Submitted to:

Office of Naval Research
Head Electronics Division
800 North Quincy Street
Arlington, Virginia 22217-5000

Submitted by:

P. Daniel Dapkus, Professor
Department of EE/Electrophysics
University of Southern California
University Park
Los Angeles, California 90089-0483

SECURITY CLASSIFICATION OF THIS PAGE

REPORT DOCUMENTATION PAGE

1a. REPORT SECURITY CLASSIFICATION **NOT CLASSIFIED**	1b. RESTRICTIVE MARKINGS
2a. SECURITY CLASSIFICATION AUTHORITY **N/A**	3. DISTRIBUTION / AVAILABILITY OF REPORT **APPROVED FOR PUBLIC RELEASE, DISTRIBUTION UNLIMITED**
2b. DECLASSIFICATION / DOWNGRADING SCHEDULE	
4. PERFORMING ORGANIZATION REPORT NUMBER(S) **53 4502 5066**	5. MONITORING ORGANIZATION REPORT NUMBER(S)
6a. NAME OF PERFORMING ORGANIZATION **UNIVERSITY OF SOUTHERN CALIFORNIA** 6b. OFFICE SYMBOL (*If applicable*)	7a. NAME OF MONITORING ORGANIZATION **OFFICE OF NAVAL RESEARCH**
6c. ADDRESS (*City, State, and ZIP Code*) **DEPT OF EE/EP, SSC 502** **LOS ANGELES, CA 90089-0483**	7b. ADDRESS (*City, State, and ZIP Code*) **800 NORTH QUINCY STREET** **ARLINGTON, VA 22217-5000**
8a. NAME OF FUNDING / SPONSORING ORGANIZATION **OFFICE OF NAVAL RESEARCH** 8b. OFFICE SYMBOL (*If applicable*)	9. PROCUREMENT INSTRUMENT IDENTIFICATION NUMBER **N00014-85-K-0331**
8c. ADDRESS (*City, State, and ZIP Code*) **800 NO QUINCY STREET** **ARLINGTON, VA 22217-5000**	10. SOURCE OF FUNDING NUMBERS PROGRAM ELEMENT NO / PROJECT NO / TASK NO / WORK UNIT ACCESSION NO

11. TITLE (*Include Security Classification*)
ATOMIC LARYER EPITAXY OF III-V COMPOUNDS

12. PERSONAL AUTHOR(S)
P.D. DAPKUS

13a. TYPE OF REPORT	13b. TIME COVERED	14. DATE OF REPORT (*Year, Month, Day*)	15. PAGE COUNT
FINAL TECHNICAL	FROM **7/1/84** TO **10/31/88**	**1/31/89**	**226**

16. SUPPLEMENTARY NOTATION

17. COSATI CODES			18. SUBJECT TERMS (*Continue on reverse if necessary and identify by block number*)
FIELD	GROUP	SUB-GROUP	

19. ABSTRACT (*Continue on reverse if necessary and identify by block number*)

20. DISTRIBUTION / AVAILABILITY OF ABSTRACT ☒ UNCLASSIFIED/UNLIMITED ☐ SAME AS RPT ☐ DTIC USERS	21. ABSTRACT SECURITY CLASSIFICATION
22a. NAME OF RESPONSIBLE INDIVIDUAL **HARRIET VIGOREN CONTRACT ADMINISTRATOR**	22b. TELEPHONE (*Include Area Code*) **213 743 7762** 22c. OFFICE SYMBOL

DD FORM 1473, 84 MAR — 83 APR edition may be used until exhausted. All other editions are obsolete.

SECURITY CLASSIFICATION OF THIS PAGE

ATOMIC LAYER EPITAXY OF III-V COMPOUND SEMICONDUCTORS BY THERMAL AND LASER-ASSISTED METALORGANIC CHEMICAL VAPOR DEPOSITION

by

Steven P. DenBaars

A Dissertation Presented to the

FACULTY OF THE GRADUATE SCHOOL

UNIVERSITY OF SOUTHERN CALIFORNIA

In Partial Fulfillment of the

Requirements for the Degree

DOCTOR OF PHILISOPHY

(Electrical Engineering)

October 1988

UNIVERSITY OF SOUTHERN CALIFORNIA
THE GRADUATE SCHOOL
UNIVERSITY PARK
LOS ANGELES, CALIFORNIA 90089

This dissertation, written by

Steven P. DenBaars

under the direction of h.i.s..... Dissertation Committee, and approved by all its members, has been presented to and accepted by The Graduate School, in partial fulfillment of requirements for the degree of

DOCTOR OF PHILOSOPHY

Patricia Salomon

Dean of Graduate Studies

Date October 19, 1988

DISSERTATION COMMITTEE

Chairperson

DEDICATION

I would like to dedicate this dissertation to my wife Leslie, and to my parents for all the support and encouragement they provided.

ACKNOWLEDGEMENTS

My deepest thanks are to my thesis advisor, Dr. P. Daniel Dapkus, for his constant support, inspiration, and ideas on the work presented here. Dr. Dapkus' enthusiastic attitude toward research has made graduate school an interesting and rewarding experience. I would also like to thank Dr. W. H. Steier and Dr. M. Gershenzon for serving as committee members and for the excellent classes they teach.

I am especially grateful to an excellent group of fellow graduate students. I would like to thank Dr. H. C. Lee and Dr. A. D. Danner for training me on the MOCVD reactor. For their support of my research efforts and friendship I would like to thank Chris Beyler, Qisheng Chen, Ken Dzurko, Ashan Hariz, Steve Hummel, Weon Jeong, Ben Maa, Dr. E. P. Menu, Jules Osinski, Dr. D. A. Sunderland, Majid Zandian, and Yao Zao.

I would like to thank my wife Leslie for all the support and encouragement. I would also like to acknowledge my parents and brothers for their support.

TABLE OF CONTENTS

LIST OF FIGURES

LIST OF TABLES

ABSTRACT

Atomic Layer Epitaxy (ALE) is a promising variation of conventional vapor phase epitaxy which achieves uniform growth of ultra-thin epitaxial layers by a self-limiting monolayer by monolayer deposition process. By employing a new regime of metalorganic chemical vapor deposition (MOCVD) growth, in which saturated surface reactions control the growth, it is possible to alternately deposit monolayers of column III and column V elements so that only one monolayer of the III-V compound semiconductor is deposited in every cycle of the deposition.

In this work, ALE growth of single crystal GaAs, as well as AlAs and GaAs/AlGaAs heterostructures and devices is demonstrated. We have been able to grow extremely uniform ultra-thin epitaxial layers and quantum wells (QWs) with thickness variations of less than one monolayer per cm over an entire sample in an optimized reactor using ALE. The observed dependence of the growth rate on temperature and trimethylgallium flux is modeled by first order adsorption kinetics utilizing measured reaction rate constants. The low temperature photoluminescence (PL) of ALE grown GaAs QW's exhibit narrow line intrinsic luminescence with linewidths comparable to the best reported values by conventional MOCVD. We have established for the first time that ALE can be hybridized with conventional MOCVD to grow device quality structures. This has been demonstrated by the operation for the first time of an injection laser with an active region grown by ALE.

Threshold densities as low as 380A/cm^2 have been achieved for these structures.

Laser assisted ALE (LALE) of GaAs and related materials has been accomplished by the use of a Argon laser during the trimethylgallium (TMGa) exposure cycle in a novel four chamber ALE reactor. The "fast writing" potential of LALE to selectively deposit GaAs at scan speeds of 4000μm/sec is demonstrated. We have employed a scanned laser beam with spot sizes as small as 30μm to deposit GaAs stripes on $Al_{0.3}Ga_{0.7}As$ surfaces. Laser assisted ALE of GaAs displays several very favorable characteristics such as perfect monolayer saturated growth over an order of magnitude TMGa pressure, and growth saturation over a range of laser power densities.

CHAPTER 1
INTRODUCTION TO ATOMIC LAYER EPITAXY

1.1. MOTIVATION

In recent years, there has been an increasing demand for higher speed and higher efficiency operation of electronic and opto-electronic devices. The III-V compound semiconductor system is the leading materials system in which to produce the next generation of high speed electronic and photonic devices. Heterostructure devices composed of III-V semiconductors not only have a significant speed advantage over silicon based devices,[1] but also possess the ability to be integrated with optical devices on the same chip. In addition, heterostructure devices exhibit several interesting and useful physical phenomenon due to the quantum size effect which can be obtained in these structures. For such devices as high electron mobility transistors (HEMTs), quantum well lasers and other heterostructure devices, control of epitaxial layer thicknesses to within a single atomic layer becomes extremely desirable for high-yield implementation. Currently, metalorganic chemical vapor deposition (MOCVD) and molecular beam epitaxy (MBE) are the two leading processes utilized to grow these sophisticated semiconductor structures. Both processes have demonstrated sophisticated heterostructure devices with 1-2 monolayer abrupt interfaces in various III-V semiconductor systems. However, each technique has its own

disadvantages and advantages.

Metalorganic chemical vapor deposition (MOCVD) is a non-equilibrium vapor phase growth technique which is typically operated at atmospheric pressure. The column III elements are transported to the growth reactor in the form of organometallic compounds, and the column V elements are supplied from gaseous hydride sources such as arsine and phosphine. The reactants are then simultaneously injected into the growth chamber where they thermally decompose in the hot boundary layer above the substrate and form single crystal layers. High quality materials and abrupt heterostructure devices have been grown by this technique. In addition, MOCVD shows the greatest promise for scale up to large area epitaxial growth for production of the next generation of electronic and opto-electronic devices owing to the economy and simplicity of the technique.

There are several inherent limitations of this growth technology. Because the growth rate is limited by diffusion of the column III reactant through the boundary layer, variations in layer thickness and compositional uniformity arise due to hydrodynamic fluctuations within the reactor. This dependence on hydrodynamics makes reactor design extremely crucial to both uniformity and scale. Currently, the best thickness uniformity achieved is ±1.5% across 4-cm diameter wafers in small research reactors.[2]

The other leading technology for III-V semiconductor deposition is a high vacuum evaporation process known as molecular beam epitaxy (MBE). In this process shutters shield the crystal from molecular beams

of the constituents and thin layers can then be grown by actuating these shutters.[3] This technique has made impressive advances in demonstrating sophisticated heterostructure devices with extremely abrupt heterointerfaces of 1 monolayer.[4] The main disadvantages of this technique has been the high cost of the equipment and it has proven to be extremely difficult and expensive to scale up this research technique to production capacities.[5]

Utilizing these growth techniques to fabricate new heterostructure devices requires the precise control of such growth parameters as: growth time, flux of sources, and growth temperature. The ability to produce extremely uniform epitaxial layers is very important to the implementation of circuits based on HEMT's for which slight deviations in the channel thickness lead to significant threshold voltage variations. Quantum well injection laser threshold current and emission wavelength are also sensitive to well width. The sensitivity of these devices to the layer thickness and doping provides a major motivation for the subject of this thesis. In addition, development of a low temperature deposition process would result in reduction of defect concentration and elimination of temperature driven impurity redistribution.

In this dissertation, we have sought to develop a growth technology in which uniform large area deposition of one monolayer of column III elements followed by the deposition of one monolayer of column V elements is achieved. Atomic Layer Epitaxy (ALE) is a new crystal growth technique which allows control of the growth process at the atomic level.[6,7] In contrast to conventional crystal growth, where the

reactive gaseous precursors arrive simultaneously at the substrate. ALE proceeds by separately exposing the semiconductor surface such that one monolayer of an element containing adsorbate is deposited per exposure. Layer growth proceeds by repetition of this alternate exposure cycle. Because it employs saturated surface reactions, ALE is expected to produce extremely uniform layers and be amenable to the growth of ultrathin layers. Therefore, atomic layer epitaxy can be considered the crystal growth process with the ultimate in control because it operates with a self-limiting monolayer deposition mechanism at low substrate temperatures. For III-V compounds, the use of a volatile molecule for the column III element is required to avoid clustering of the element on the surface. In this work we have achieved ALE by employing conventional MOCVD reactants trimethylgallium (TMGa) and arsine (AsH_3) as the reactants for the ALE growth of GaAs.

The ALE technique has achieved excellent results in the II-VI compound semiconductor system, and is currently used in the manufacturing of electroluminescent displays.[8] ALE films can be grown by making use of either large pressure differences in the vapor pressures of the II-VI compounds and their pure constituents, or by sequential surface exchange reactions between compound reactants which have high vapor pressures in comparison with the product film.

The ALE process can also be stimulated locally by photolytically controlling the surface reactions with laser radiation. In this work we demonstrate that laser assisted ALE (LALE) selectively deposits GaAs with a perfect 100% monolayer saturated growth rate over a range of

laser power densities and TMGa fluxes. We employ scan speeds of 4000μm/sec to deposit GaAs stripes as small as 30μm on $Al_{0.3}Ga_{0.7}As$ surfaces. This "fast writing" aspect of LALE has great potential for integrating opto-electronic and electronic devices on the same chip. All of the above advantages result in ALE and LALE being attractive technologies for the growth of heterostructure devices with critical layer requirements.

1.2. Basic Theory of Atomic Layer Epitaxy

1.2.1 Elemental Source ALE

Two different techniques have been discovered to yield atomic layer epitaxy in the II-VI semiconductor system.[9] The first technique utilizes elemental sources to achieve ALE, the second technique achieves monolayer growth from compound gas sources via a sequential surface exchange reactions. These two different methods are illustrated in figures 1 and 2. Method one (Elemental Source ALE) achieves ALE growth by making use of the large vapor pressure differences of the II-VI compound semiconductor compounds and their pure elemental constituents. Because of the low vapor pressure of column III metals at temperatures at which both the III-V bond and column V compounds are stable, self-limiting growth of III-V compounds is not thermodynamically possible using the elemental source method.

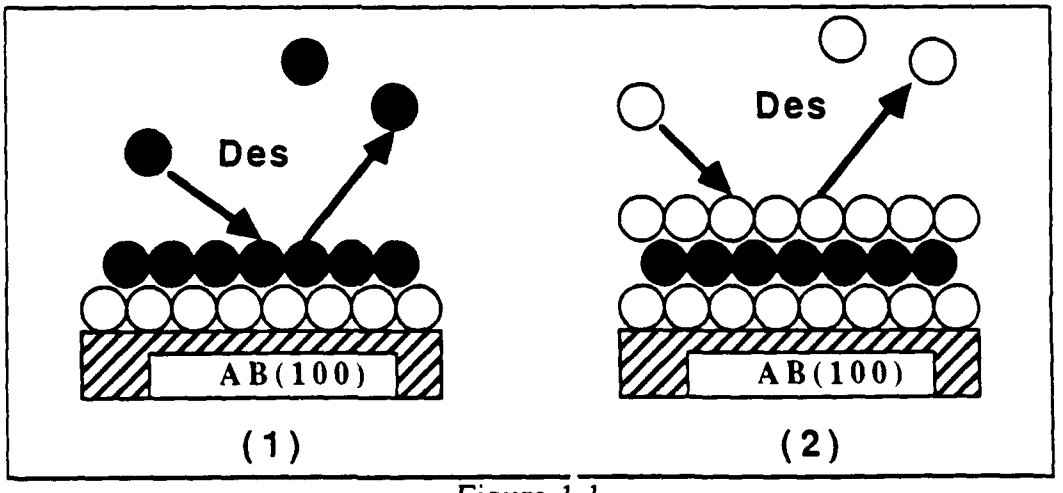

Figure 1.1
Film growth by the Elemental Source ALE method:(1) Excess incident A atoms evaporate, while A atoms that are bonded to underlying B atoms form stable surface with small vapor pressure.(2) First layer of injected B atoms are chemisorbed to the surface while excess B atoms evaporate.

1.2.2 Molecular Source ALE

Method two (Molecular Source ALE) utilizes surface exchange reactions between compound reactants which have high vapor pressures in comparison to the product film. This technique achieves self-limiting growth which can be attributed to the fact that the first gaseous layer interacts strongly with the substrate (chemisorption), and subsequent layers interact less strongly (physisorption), and will evaporate above a critical temperature. Thus by obtaining a monolayer of chemisorbed compound reactant a self-limiting crystal growth process can be obtain. The general reaction for ALE by a surface exchange reaction can be expressed as follows:

$$AX_{(v)} \text{----> } AX_{(ads)}$$
$$AX_{(ads)} + BY_{(v)} \text{----> } AB_{(s)} + XY \qquad (1.1)$$

For a self-limiting monolayer deposition process the time dependence of fractional surface coverage will be a function of both the rate of chemisorption on the unoccupied sites and the rate of desorption from the occupied sites. By using the following first order adsorption expression we can effectively describe the the ALE growth rate:

$$\frac{d\theta}{dt} = k_{ads}(1-\theta) - k_{des}(\theta) \qquad (1.2)$$

Where: Θ =fraction of occupied surface sites

k_{ads} =rate of impinging molecules adsorbed on surface

k_{des} =desorption rate of molecules from the occupied sites

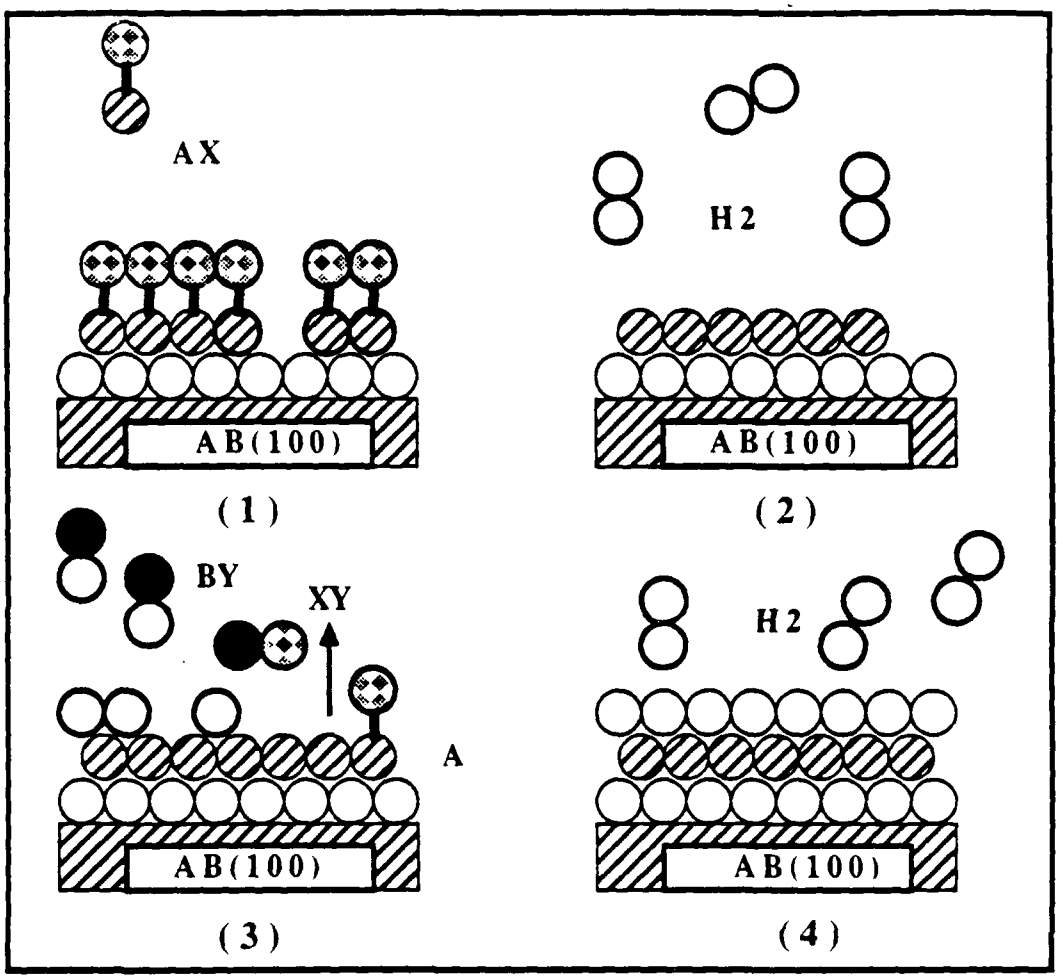

Figure 1.2
Method two (Gaseous Source ALE) utilizes surface exchange reactions between compound reactants: (1) one monolayer of AX gaseous precursor is chemisorbed on surface, excess AX molecules can only physisorb and evaporate off above a critical temperature, (2) reactor is purged with inert gas (H2), (3) precursor BY is injected and forms a complete monolayer by a surface exchange reaction, (4) reactor is purged in preparation for repeat of cycle.

1.3. Background Literature

1.3.1 ALE of II-VI Compound Semiconductors

The first research on ALE was done in the II-VI semiconductor system. The most widespread commercial application of ALE has been the growth of ZnS for use in AC electroluminescent display panels. Both amorphous and polycrystalline ZnS has been grown by using both types of ALE deposition techniques. $ZnCl_2$ and $Zn(CH_3COO)_2$ in conjunction with H_2S have been utilized to achieve ALE of ZnS in a chemical vapor deposition (CVD) system. After exposing the surfaces to ZnCl2, films were analyzed by Auger Electron Spectroscopy (AES) which identified chemisorped $ZnCl_2$. Surfaces were then exposed to H_2S, after which subsequent analysis revealed only a small amount of Cl. This indicates close to 100% completion of a surface exchange reaction. Reactions which govern the process are:

$$ZnCl_{2(v)} \text{-------} > ZnCl_{2(chemisorped)} \quad \{350°C\text{-}550°C\}$$

$$ZnCl_{2(chemisorped)} + H_2S_{(v)} \text{------} > ZnS_{(s)} + 2HCl \qquad (1.3)$$

$$Zn(CH_3COO)_2 + H_2S \text{ --> } ZnS + 2CH_3COOH \qquad \{250\text{--}350°C\} \quad (1.4)$$

Vacuum evaporation techniques utilizing elemental Zn and S

sources have also been successful in obtaining films of ZnS by ALE. The crystalline quality of the ZnS is found to be highly dependent on the growth temperature and the type of substrate.[10] In general the degree of crystalline perfection was found to increase with increasing temperature. Both cubic and hexagonal structure was found in the deposited films. The dislocation density of ZnS ALE films(10^{10} cm^{-2})[11] was found to be significantly lower than electron beam evaporated films (10^{11} cm^{-2}).

Single crystal CdTe has been grown on CdTe(111), CdTe(110) and GaAs(100) substrates. M. A. Herman et al.[12] have also utilized ALE to deposit CdTe films on CdTe(111)B substrates. Using the elemental source method they observed monolayer depositions that were highly dependent on the pause time separating the Cd and Te pulses. This was achieved in a high vacuum evaporation system with elemental Te and Cd sources. Elemental sources can be used here since both Cd and Te have relatively large vapor pressures in comparison to the single crystal CdTe at growth temperatures of 270°C. In this study it was determined crucial to accurately control the growth parameters since Cd and Te continue to re-evaporate and will form less then unity monolayer coverage. Therefore minimum pause durations of 0.5 seconds were found necessary to achieve good surface coverage. Typical growth conditions consisted of 1.0 second pulse of Cd and 2.5-2.8 second pulses of Te separated by 0.5 second delay times. The purge time ($\Delta\tau$) between Cd and Te pulses was shortened to achieve monolayer by monolayer deposition. This observed growth behavior could be explained by taking into account the temperature dependence of the evaporation rate relative to lower

temperatures with the following Arrhenius expression:

$$R(T_1) = R(T_0)\exp\left[\frac{E_a\left(\frac{1}{T_o} - \frac{1}{T_1}\right)}{k}\right] \qquad (1.3)$$

The fractional monolayer coverage "Θ" of CdTe can than be modeled by taken into account this evaporation rate and balancing it with the incoming flux of Cd atoms. This can be expressed by the following equation:

$$\theta = \frac{\left(\Phi_{Cd}\tau - R_{Cd}\Delta\tau\right)}{D_{Cd}} \qquad (1.4)$$

Where: R_{Cd} =Rate of Cd evaporating

D_{Cd}=Surface density of Cd needed for one monolayer

Φ_{Cd}=Incoming flux of Cd atoms

τ_{exp}=Exposure time

$\Delta\tau$=Purge time

1.3.2 ALE of III-V Compound Semiconductors

The first report of ALE in the III-V semiconductor system was reported by Nishizawa and co-workers in 1985.[13] Utilizing gaseous sources in a high vacuum MBE apparatus, Nishizawa observed saturated monolayer growth of GaAs. Monolayer film growth was obtained at relatively low substrate temperatures (450-500°C). A slow deposition rate of one atomic layer every 24 seconds was observed due to the inefficient cracking of the arsine in the high vacuum environment, thus comparatively long exposures of arsine are necessary. The deposited films were found to be heavily p-type with doping on the order of 10^{18} cm^{-3} and room temperature mobilities of around $100 cm^2/V \cdot sec$. Increasing the amount arsine injected into the reactor was found to substantially reduce the background doping, therefore improvements in the film quality are anticipated with optimization of the surface reaction of arsine. The addition of UV irradiation on the sample allowed single-crystal growth to occur at substrate temperatures in the range of 350°C. This is thought to be caused by either a photochemical effect or the fact that the migration length of admolecules is increased by photoirradiation as is the case for silicon epitaxy.[14]

ALE of GaAs using hydride VPE was reported by Usi et al.[15] Using a dual chamber growth system the substrate was alternately rotated between the GaCl flow and AsH_3. Monolayer saturated growth was observed over an order of magnitude of GaCl pressures. This is in contrast to the linear dependence of growth rate on GaCl pressure usually

observed in conventional VPE. Due to the long substrate transfer time the deposition rate was 60 seconds long for each monolayer. ALE was observed to occur over a wide range of temperatures with the hydride technique. Below 550°C all the deposited films were single crystal with good morphology and remarkably free of surface defects. No enhancement of layer thickness near the edge of windows opened in SiO_2 was observed in this ALE technique. Large thickness variations have been a problem in conventional VPE where the growth is diffusion limited, thus excess reactants diffusing across the SiO_2 mask enhance the growth rate near the edges of the window.

The first report of ALE in a atmospheric MOCVD reactor was by Bedair and Tischler[16] at North Carolina State University. The experimental setup consisted of rotating a susceptor between separated column III and column V gas streams. After exposure to each gas stream the recessed wafer is rotated past a fixed graphite edge assembly which effectively "shears the boundary layer," thus preventing any cross-mixing of the column III and column V gas stream. Saturated monolayer growth was observed at higher growth temperatures (560-650°C) than was observed by both Nishizawa[12] (460-500°C) and in the work reported here (445-500°C). Photoluminescence of ALE GaAs sandwiched between $GaAs_{0.67}P_{0.33}$ at 77K exhibited an intense band to band peak with a 11 meV linewidth. Tischler et al.[17] reported on ALE growth of InAs/GaAs single quantum well structures where the wells were only 2 and 4 monolayers thick. Photoluminescence from the quantum wells was found to be sharp, intense, and uniform across the sample with full widths at

half-maximum for the 2 and 4 monolayer wells of 12 and 17 meV, respectively.

1.3.3 Flow-rate Modulation Epitaxy

A variation of ALE is a process entitled Flow-rate Modulation Epitaxy (FME) which was reported by Kobayashi et al. in 1985.[18] This method is also based on alternating the gas flow of the column III and column V sources, however, a small amount of arsine is always injected into the reactor to suppress arsenic vacancies near the growing interface. To date, these workers have utilized triethylgallium (TEGa) for the column III gas source because it has a lower cracking temperature than TMGa.[19] In contrast to the p-type GaAs films previously reported in ALE films, the FME layers grown at 550°C were found to be n-type with carrier concentrations as low as $7x10^{14}cm^{-3}$ and mobilities of 42,000 $cm^2V^{-1}s^{-1}$ at 77 K. This is caused by the addition of a small amount of arsine during the column III cycle, since p-type films with low mobility resulted when the growth was performed without the small arsine supply. This drastic improvement in film quality is theorized to be due to either the suppression of arsenic vacancies near the growing interface or enhanced reaction of As-H with the surface adsorbed Ga ethyl complexes. However, since a small amount of arsine is supplied continuously the growth rate dependence on TEG flux observed in FME, as shown in figure 1.3, does not saturate completely at the monolayer level. This is in contrast to ALE using completely separated exposures of Ga and As compounds where complete saturation has been observed.

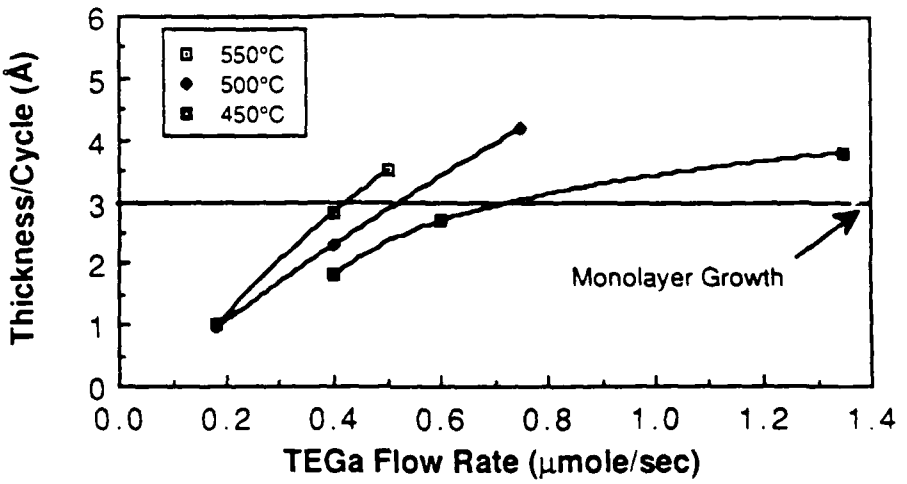

Figure 1.3.
Dependence of growth rate per cycle on TEGa in the FME method.

1.3.4 Laser-Assisted ALE

Laser assisted atomic layer epitaxy (LALE) of GaAs was first reported by A. Doi et al. in 1986.[20] In this method, modulation of both a CW Argon ion laser and the gas stream is performed. The laser irradiates the surface during Ga exposure at an intensity of 100-200W/cm^2. Utilizing laser irradiation a perfect self-limiting monolayer deposition mechanism was observed over two orders of magnitudes TMGa fluxes. The improved self-limiting nature of LALE in comparison to thermal ALE is theorized to be due to a photocatalytic effect. This is supported by the fact that for laser wavelengths below the band gap of GaAs such as the Nd:YAG laser (λ=1.06μm) perfect saturation is not achieved, whereas for two different wavelengths of the Argon ion laser above the band edge

(λ=514.5μm, 354μm) perfect monolayer saturated growth is observed. A desirable characteristic of selectively deposited GaAs by LALE is the flat-top profile of the deposit in spite of the Gaussian profile of the intensity of the laser beam. This is explained by the fact that the photocatalytic mechanism exhibits a saturation in growth rate as a function of laser power as shown in figure 1.4. This data also supports the theory the observed laser ALE deposition mechanism is not entirely a thermal effect, which would have exhibited a linear growth rate with power density, but rather a surface photocatalytic effect. In addition, the growth rate was found to be independent of temperature in the temperature region of 370-430°C which provides further proof that the growth mechanism involves a surface photoreaction.

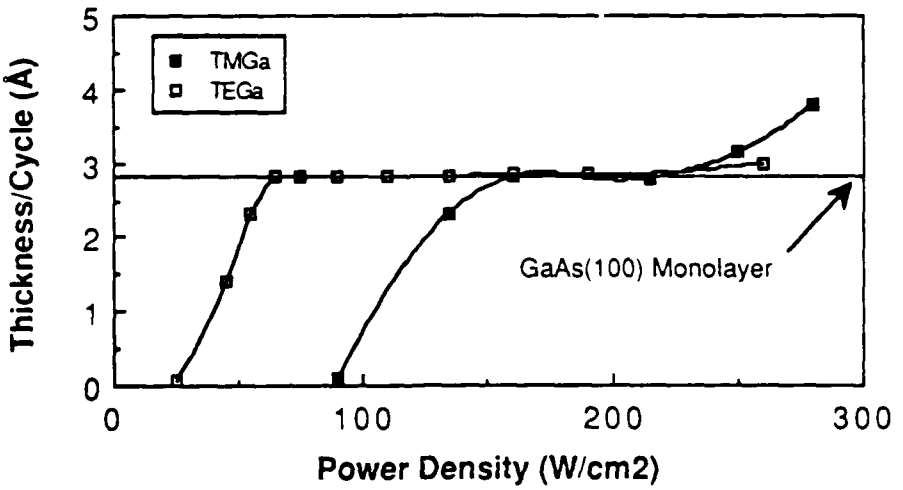

Figure 1.4.
Growth rate as a function of the laser power density in laser-assisted ALE for both TMGa and TEGa.[21]

A summary of all the growth rate data for thermal and laser-

assisted ALE to data is presented in figure 1.5. In comparison to other ALE methods laser-assisted ALE exhibits the best self-limiting growth mechanism. In thermally driven ALE there appears to be a window of conditions over which saturated growth is obtained for various reactor pressures, exposure times, and growth temperatures. For ALE in a high vacuum environment the growth appear to saturate at a rate slightly below a perfect monolayer per cycle because of inefficient cracking of arsine as Nishizawa observed.

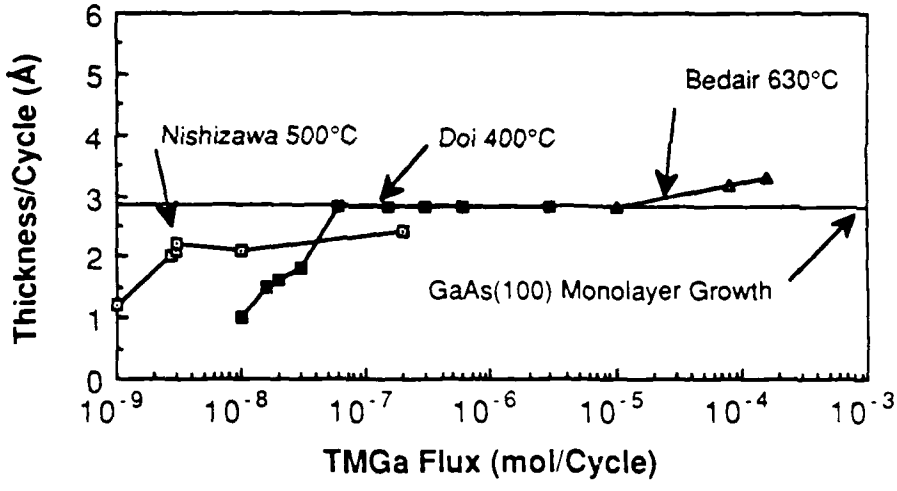

Figure 1.5.
Laser-assisted ALE demonstrates a perfect monolayer per cycle growth rate over a wide range of TMGa fluxes. Thermally driven ALE shows saturated growth over a smaller range of conditions.

1.4. Thesis Organization

This dissertation is organized so that the next two chapters provide the reader with insight into the epitaxial growth and reaction kinetics of conventional MOCVD, because ALE is a variation of this vapor phase epitaxial technique. The fourth chapter describes the experimental conditions, reactor design considerations to achieve ALE, and growth results achieved in thermally driven ALE. Chapter five provides theory and results on ALE grown quantum wells and heterostructure devices. Chapter six consist of photochemical theory and results of laser scanning to achieve laser assisted ALE of GaAs. Chapter seven provides future direction from this research effort on integrated opto-electronic devices and conclusions on the observed experimental results.

REFERENCES-CHAPTER 1

1 B. K. Gilbert, Gallium Arsenide Technology,(Howard W. Sams & Co., Inc., Indianapolis, IN, 1985) D. K. Ferry, ed., p.28.

2 J. J. Coleman and P. D. Dapkus, Gallium Arsenide Technology, (Howard W. Sams & Co., Inc., Indianapolis,IN, 1985) D. K. Ferry, ed., p.91.

3 R. Z. Bachrach, Crystal Growth, 2nd edition(Pergamon Press Ltd., London, 1980) B. R. Pamplin ed., pp. 221-271.

4 H. Kawai, I. Hase, K. Kaneko and N. Watanabe, J. Crystal Growth **68**, 508 (1984).

5 P. D. Dapkus, J. Crystal Growth **68**, 345 (1984).

6 M. Pessa, P. Huttunen, M. A. Herman, J. Appl. Phys. **54**, 6047 (1983).

7 M. Pessa, R. Makela, R. Sunotla, Appl. Phys. Lett. **38**, 131 (1980).

8 Y. Aoyagi, A. Doi, S. Iwai, S. Namba, J. Vac. Sci. Technol. **B5**, 1 460(1987).

9 M. Pessa, R. Makela, R. Suntola, Appl. Phys. Lett.**38**, 131 (1980)

10 V. P. Tanninen, M. Oikkoinen and T. Tuomi, Thin Solid Films **109**, 283 (1983).

11 C. H. L. Goodman and M. V. Pessa, J. Appl. Phys. **R65**, 60 (1986).

12 M. A. Herman, M. Vulli, and M. Pessa, J. Cryst. Growth **67**.339 (1985).

13 J. Nishizawa, H. Abe, T. Kurabyashi, J. Electrochem. Soc. **132**, 1197, (1985).

14 M. Kumagawa, H. Sunami, T. Terasaki, and J. Nishizawa, Japan J. Appl. Phys. **7**, 1332 (1968).

15 A. Usi and H. Sunakawa, Inst. Phys. Conf. Ser. No. **79**, 753 (1985).

16 M. A. Tischler,and S. M. Bedair, Appl. Phys. Lett. **48**, 1961 (1986).

17 M. A. Tischler, N. G. Anderson, and S. M. Bedair, Appl. Phys. Lett. **49**, 1199 (1986).

18 N. Kabayashi, T. Makimoto, and Y. Horikoshi, Jap. J. Appl. Phys. **24**, L962 (1985).

19 M. Yoshida, H. Watanabe, and F. Uesugi, J. Electrochem. Soc. **130**, 413 (1985).

20 A. Doi, Y. Aoyagi, S. Namba, Appl Phys. Lett. **48**, 1787, (1986).

21 Y. Aoyagi, A. Doi, S. Iwai, and S. Namba, J. Vac. Sci. Technol. **B5**(5),1460 (1987).

CHAPTER 2
EPITAXIAL GROWTH BY CONVENTIONAL METALORGANIC CHEMICAL VAPOR DEPOSITION

2.1 Introduction

In the past few years, metalorganic chemical vapor deposition (MOCVD) has evolved into the most promising technique for production of high speed electronic and opto-electronic devices. High purity materials[1] and monolayer abrupt heterojunctions[2] have been demonstrated by this technique. Because of the economy and simplicity of the technology, MOCVD is the most viable technique for scale up to large area epitaxial growth for commercial applications. MOCVD is a non-equilibrium vapor phase growth technique which is typically operated at pressures near atmospheric pressure. In this technique a metal alkyl, such as trimethylgallium (TMGa), is mixed in the vapor phase with a hydride, such as arsine (AsH_3), and the reactants are simultaneously injected into the growth chamber where they thermally decomposed to form single crystal layers.

The MOCVD technique originated from the early research of Manasevit,[3] who demonstrated demonstrated that triethylgallium (TEGa) and arsine deposited single crystal GaAs pyrolytically in an open tube reactor. Manasevit and co-workers[4,5,6] subsequently expanded the use of this technique for the growth of $GaAs_{1-y}P_y$, $GaAs_{1-}Sb_y$, and Al containing compounds. Seki et al.[7] demonstrated that high quality GaAs

could be obtained by MOCVD by growing films with n-type background doping of $7x10^{13}$ cm^{-3} and mobilities of μ_{77}=120,000$cm^2V^{-1}s^{-1}$. Bass[8,9] demonstrated the first devices by implementing MOCVD material in field effect transistors (FETs) and photocathode applications. An important milestone in the development of MOCVD was the demonstration of high performance solar cells and double heterostructure lasers by Dupuis and Dapkus.[10,11] This work firmly established that MOCVD could produce high-quality AlGaAs films with excellent optical properties necessary for semiconductor laser applications.

2.2 System Design

The overall MOCVD system consists of five major components: source materials, gas handling, reactor chamber, heating system, and exhaust. Only the first three items will be discussed in this section since they are the most pertinent to this work. Figure 2.1 presents a simplified schematic diagram of the components which constitute the MOCVD system employed in this study.

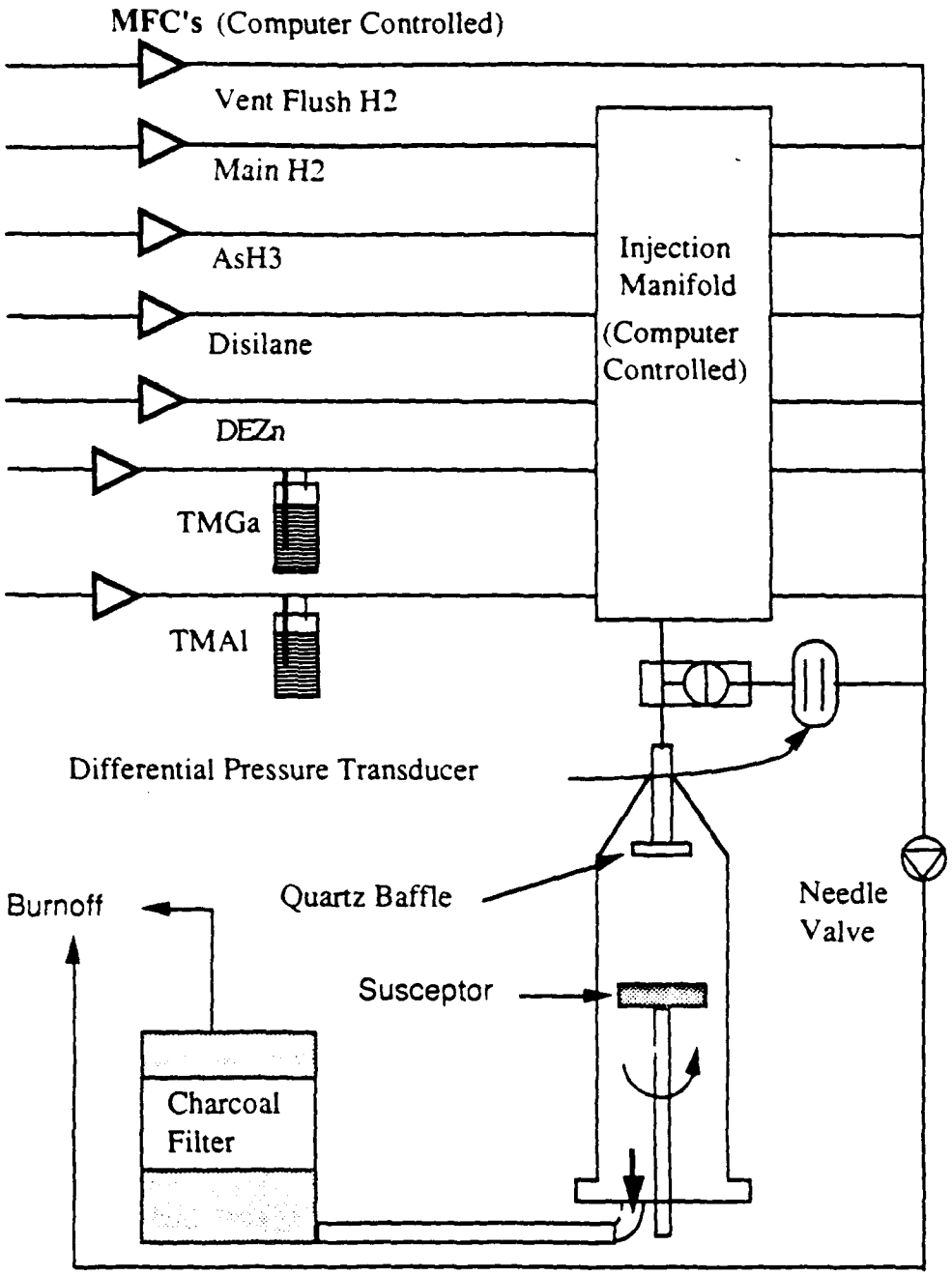

Figure 2.1.
Schematic of conventional MOCVD system employed in this study.

2.2.1 Source Material

Organometallic (OM) sources, such as TMGa and trimethylaluminum (TMAl), provide the group III elements. The OM sources are volatile liquids or solids which are kept in temperature controlled baths to insure a constant equilibrium vapor pressure. The OM sources are transported to the reactor in the vapor phase by flowing pure H_2 through the liquid or over the solid. The amount of the column III precursor transported to the reactor is accurately controlled by precision electronic mass flow controllers to within ±0.5 standard cubic centimeter per minute (SCCM).[12]

Group V elements are supplied from gaseous hydride sources such as arsine (AsH_3) and phosphine (PH_3). Typically, dilute mixtures of 10% AsH_3 in H_2 are contained in high pressure cylinders which incorporate flow-limiting valves for emergency shut-off. On-site purification of the hydride sources is an important concern in the MOCVD process. Both oxygen and water vapor are present in the high pressure gas cylinders at a level of several parts per million (ppm). In this work purification of AsH_3 is achieved by both a molecular sieve which adsorbs water, and a Li-impregnated resin. The proprietary Li-impregnated resin (ATM Technology Part #3010300T) removes both H_2O and O_2 to levels lower than 10 parts per billion (ppb) by an exothermic exchange reaction.[13]

High purity hydrogen (99.999%) is used as the primary carrier gas. A palladium cell hydrogen purifier and an oxygen remover are employed

to obtain the high level of purity necessary for state-of-the-art GaAs quality.

2.2.2 Gas Handling

The gas handling system is designed to deliver accurately measured amounts of pure reactants to the growth chamber. Precision control of the gas flow rates is achieved by electronic mass flow controllers (MFC), manufactured by Tylan Corp. or Unit Instruments, Inc. The design also transports the reactants to the growth chamber without any gas concentration transients due to pressure imbalances or flow changes by incorporating pressure sensors and auxiliary flow balances lines. The gas injection manifold consists of a series of fast gas switching valves employed in a vent/run configuration. An important point to note in figure 2.1 is the addition of pressure transducer between the vent and run lines; this eliminates gas concentration fluctuations resulting from pressure imbalances. Growth is initiated by switching the column III precursors from the vent to run line. An equal flow of hydrogen is switched from the run to the vent line instantaneously to eliminate any pressure surges. Computer controlled (Apple II) switching of the valves enables sharp transitions in the gas composition in the reactor. This allows the MOCVD technique to achieve the monolayer compositional transitions necessary for sophisticated heterostructure devices.

2.2.3 Reactor Design

The most common reactor chamber designs are the vertical and horizontal configurations. In the vertical design reactants are injected through the top. Typically, the substrate is held flat on a rotating silicon carbide coated graphite susceptor which is perpendicular to the gas flow direction. Heating is accomplished by radio frequency (RF) induction, and temperature monitoring is accomplished by either an infrared pyrometer or a thermocouple. The low gas velocities employed in our conventional MOCVD reactor (2-4 cm/sec) promote laminar flow conditions. However, convection currents do occur in this design and the flow pattern directly above the wafer is not well understood. The addition of a quartz disc baffle at the gas inlet promotes uniform gas distribution.

The horizontal design utilizes a susceptor which is situated approximately parallel to the gas flow direction. Minimal convection currents and highly laminar gas flow conditions exists in the horizontal reactors.[14] Uniform growth can be achieved only after precise tilting of the susceptor to eliminate reactant depletion along the flow direction. Heating in this design can be accomplished by either RF induction or infrared heating from quartz-halogen lamps.

2.3 Basic Reaction Chemistry

The exact chemical pathways operative in the MOCVD process are not yet clearly understood. The basic reaction most commonly used to

describe the growth of the compound semiconductor GaAs by MOCVD is as follows:

$$Ga(CH_3)_{3(v)} + AsH_{3(v)} \text{---> } GaAs_{(s)} + 3CH_{4(v)} \qquad (2.1)$$

This balanced expression ignores the fact that the specific reaction path and reactive species are largely unknown. A more likely reaction pathway leading to growth of the GaAs epitaxial layers involves the homogeneous decomposition of TMGa as was reported in an earlier study. [15,16]

$$Ga(CH_3)_{3(v)} + 3/2H_{2(v)} \text{---> } Ga_{(v)} + 3CH_{4(v)} \qquad (2.3)$$

Arsine is thought to decompose heterogeneously to yield As_4 at normal growth temperatures

$$2AsH_{3(s/v)} \text{----> } 1/2As_{4(v)} + 3H_{2(v)} \qquad (2.4)$$

Therefore the growth of GaAs which probably occurs at the solid vapor interface could be expressed as follows:

$$Ga_{(s/v)} + 1/4As_{4(s/v)} \text{---> } GaAs_{(s)} \qquad (2.5)$$

However, the level of understanding of the growth process is inadequate from a scientific point of view. The most difficult topic, and certainly the least developed, is the area of the kinetics of the process and growth

mechanisms occurring at the solid/vapor interface during MOCVD growth. This subject is discussed in detail in Chapter 3.

Most researchers have optimized their MOCVD reactors by empirical studies of external parameters such as growth temperature, V/III ratio, substrate tilt and mass flow rates. However, these studies yield little information about the mechanistic steps which eventually lead to epitaxial growth.

These studies have identified three region of growth: mass transport limited, desorption and surface kinetically limited regimes. As shown in figure 2.1, kinetics of surface reactions dominate the growth in the low temperature regime. Conventional MOCVD is usually performed in the mass transport limited regime which occurs over a wide temperature range (500°C-800°C). At high temperatures desorption of arsenic begins to limit the growth and a decrease in the growth rate becomes evident.

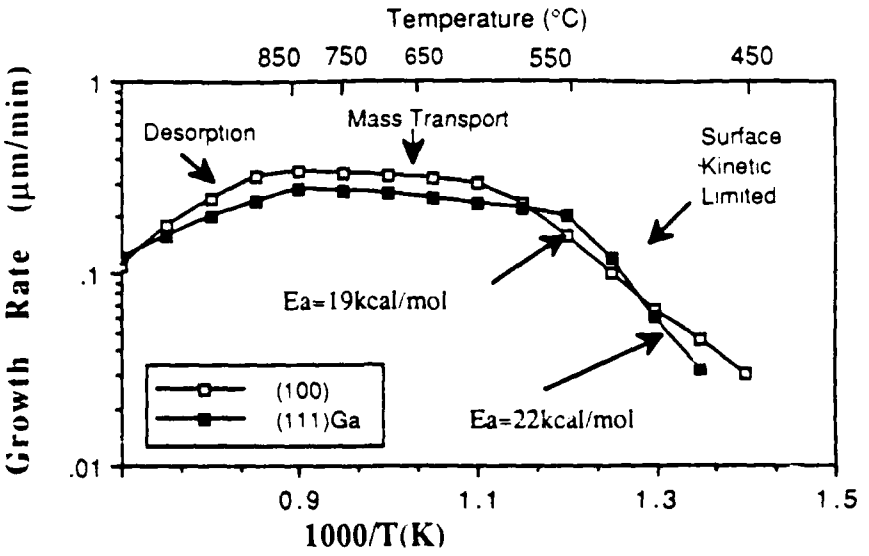

Figure 2.2.
Growth rate versus reciprocal temperature for epitaxial layers on (100) and (111)Ga oriented GaAs substrates, from Reep and Ghandi.[17]

2.3.1 Mass Transport Limited Regime

In this temperature region, 550-850°C, growth is limited by mass transport of the column III reactant to the growing interface. Because the diffusion process is slightly temperature dependent, there exists a slight increase in the growth rate in this temperature range as shown in figure 2.2. From Fick's law we can describe the flux of column III elements toward the substrate in the mass transport limited regime as:

$$J_{Ga} = \frac{D_{Ga}\left(P^{o}_{Ga} - P_{Ga}\right)}{\delta_b RT} \qquad (2.6)$$

where δ_b is the boundary layer thickness, D_{Ga} the diffusion coefficient for Ga in the vapor phase, P^o_{Ga} is the input gas stream partial pressure of TMGa, and P_{Ga} is partial pressure at the gas-solid interface. For temperatures above 550°C, the metal alkyl pyrolysis efficiency is unity, then we can assume $P^o_{Ga} \approx P_{TMGa}$. By noting the partial pressure of Ga at the interface is small in comparison to the input concentration of TMGa ($P_{TMGa} >> P_{Ga}$), we can then express the column III flux at the interface as:

$$J_{Ga} = \frac{D_{Ga} P_{TMGa}}{\delta_b RT} \tag{2.7}$$

From equation 2.7, we can see that control of the growth rate is easily obtained by controlling the number of moles of metal alkyls injected into the reactor. Precise control of the growth rate is then achieved by utilizing accurate electronic mass-flow controllers which control the flow through the metal alkyl bubblers. As shown in figure 2.3, the growth rate of GaAs in our reactor is directly proportional to the flow rate through the TMGa bubbler .

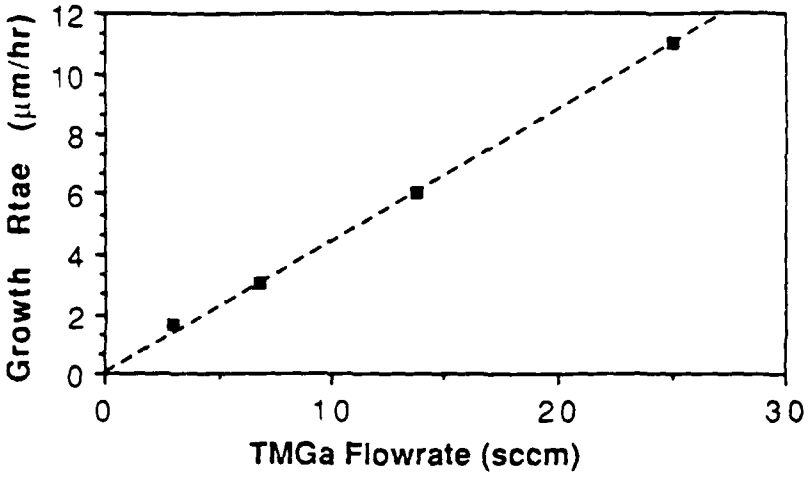

Figure 2.3
Growth rate as a function of TMGa flowrate shows linear dependence in the mass transport limited regime (T_{growth} =750°C).

2.3.2 Surface Kinetic Limited

In the temperature regime 300-550°C, the kinetics of surface reactions dominate the growth. Reep and Ghandi[17] theorized that the growth process is dominated by adsorption and decomposition of arsine at the growing interface. This view is supported by the fact that the activation energy for the heterogeneous decomposition of arsine on single crystal GaAs(100) surfaces of 18kcal/mol that we have previously reported,[15] is approximately equal to the activation energy of 19kcal/mol observed for growth on the GaAs(100) orientation. However, the presence of TMGa still plays an important role since the growth rate is still strongly influenced by the partial pressure of TMGa in the reactor.

2.3.3 Desorption Limited

The high temperature region where the growth rate begins to decrease is classified as the desorption limited regime. Several factors may cause the observed drop in the growth rate. One view is that desorption of Ga from the surface limits the growth rate at these temperatures. Desorption of As_2 or As_4 may also reduce the growth rate in this high temperature regime. Pre-deposition of the reactants on the reactor sidewalls is yet another mechanism which can limit growth at these temperatures.[18]

2.4 Hydrodynamic Concerns

2.4.1 Boundary Layer Effects

The flow dynamics and temperature gradients occurring near the hot susceptor play an important role in the growth process. Two flow regimes develop in a horizontal reactor.[19] A low-velocity boundary layer develops next to the susceptor. Flow is laminar, and steep thermal and concentration gradients exist in this region. The second is the mixed flow regime in which flow is turbulent and relatively flat concentration and temperature gradients exist. Figure 2.4 of a reactor tube cross-section illustrates the boundary layer and mixed flow zones

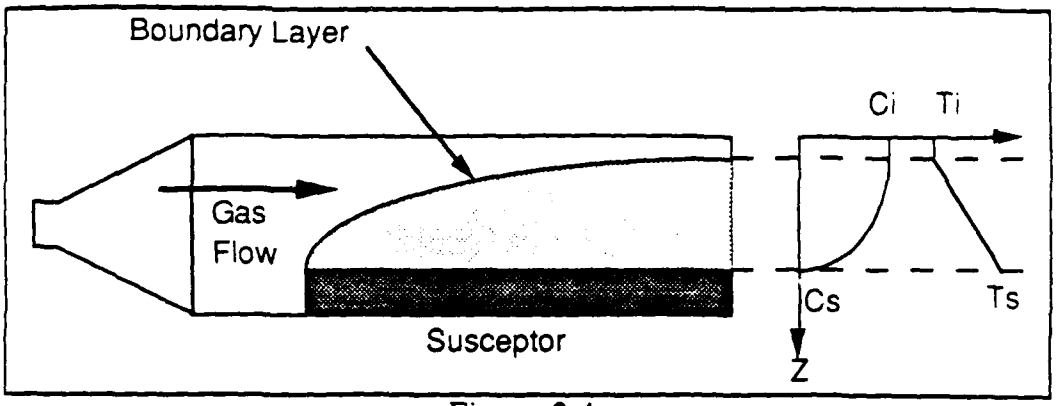

Figure 2.4.
Schematic illustration of boundary layer in a horizontal MOCVD reactor. Note temperature and concentration profiles in the boundary layer (modified from Berkman et al.).[21]

Transport of the precursors to the growing interface is controlled by diffusion through the boundary layer zone above the wafer. The reactant concentration decreases along the direction of flow because of consumption by the growth. Berkman et al.[20] have developed a detailed model which accurately predicts mass transport in a horizontal cold wall reactor. For a flat susceptor, their model projects an exponential decrease in the growth rate along the flow direction

Growth in our horizontal MOCVD reactor exhibits the predicted gas phase depletion behavior. Figure 2.5 displays the severe decrease in the layer thickness along the flow direction. Data was taken by measuring the photoluminescence emission energy of the quantum well as a function of wafer position with a tightly focussed laser spot. Well thicknesses were then estimated from a Kronig-Penney model of expected emission energies. This data illustrates the inherent uniformity disadvantage of conventional MOCVD. As we will demonstrate in

Chapter 5, extremely uniform quantum wells can be grown by ALE because it employs a self-limiting deposition mechanism.

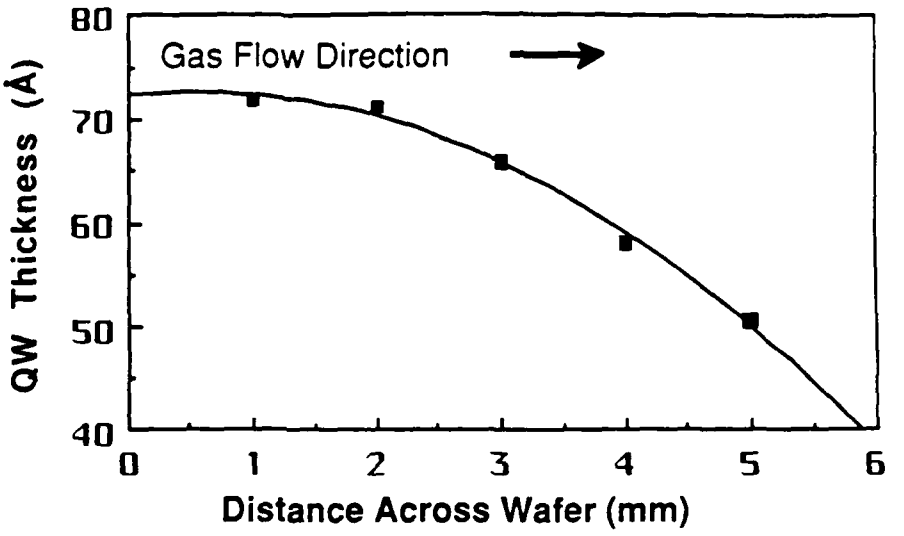

Figure 2.5
QW thickness versus wafer position on sample grown in conventional horizontal MOCVD reactor. Deposition was performed on a flat susceptor to exemplify the gas depletion effect.

By optimizing the hydrodynamic design of the reactor, improvements in the uniformity of the crystal growth can be achieved. Berkman's model predicts that the exponential variation can be minimized by tilting the susceptor at a unique angle (θ_C).

$$\sin(\theta_c) = \left(\frac{2D_o}{h_c v_o}\right)\left[\frac{T_a}{T_o}\right]^{0.88} \tag{2.8}$$

where D_o is the diffusion coefficient of the precursor molecule measured at the inlet temperature T_o. T_a is the average temperature in the boundary

layer, h_c is the channel height above the susceptor, and V_o is the initial gas velocity.

Several factors need to be taken into account to achieve uniform growth. As shown in equation 2.8, temperature effects the critical angle needed for uniform growth. Therefore growing layers at different temperatures requires readjustment of several of the process parameters. The total gas-flow rate should be optimized since it affects the complex nature of the boundary layer. Rotation of the susceptor also improves the uniformity of the epitaxial layer. These hydrodynamic concerns become magnified when MOCVD is scaled-up for commercial applications.

2.4.2 Compositional Control

For the growth of AlGaAs the solid composition is found to be proportional to the flux ratio of Al and Ga at the growing interface. Since the diffusion coefficients of Al and Ga are approximately equal, composition control of $Al_xGa_{1-x}As$ is achieved by linear adjustment of the molar flows of the column III sources. Data in figure 2.6 illustrates this simple relation of composition in the solid phase to mole fraction in the gas phase. This simple relation is described by the following equation:

$$X_{Al} = \frac{MF_{Al}}{\left(MF_{Al} + MF_{Ga}\right)} \tag{2.9}$$

This equation illustrates one of the greatest assets of the MOCVD growth process, that being the distribution coefficient is essentially unity. This

makes the growth of Al-In compounds possible, which is in contrast to liquid phase epitaxy (LPE) where the growth of Al-In compounds are impossible because of the large liquid distribution coefficient.[20]

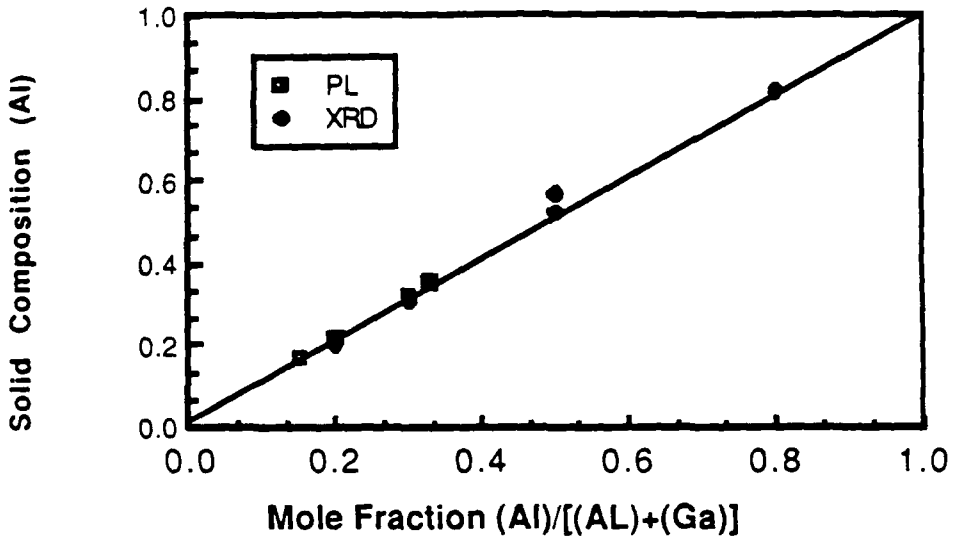

Figure 2.6
Compositional control in MOCVD is achieved by linear adjustment of the molar fraction of the constituents. X-ray Diffraction determined composition data is from H. C. Lee.[21]

2.5 Doping in MOCVD

2.5.1 p-Type Doping

A Group II impurity occupying a group-III sub-lattice position will create a hole in the lattice and therefore cause p-type doping. The standard group-II p-dopant used in MOCVD is Zn from either DMZn or DEZn precursors. For our MOCVD system, we selected DEZn as the source of p-doping. Dopant incorporation exhibits a temperature activated dependence of electrically active zinc into the lattice. For our

studies, we observe an activation energy of 1.8eV. The dopant concentration will also depend on the mole fraction of Zn to Ga injected into the reactor. DEZn is reported to have a sublinear dependence on the mole fraction.[22] For our reactor, we also observed a sublinear dependence of doping on the mole fraction.[23] Equation 2.10 predicts the doping incorporation of electrically active Zn in GaAs for our MOCVD reactor taking into account these factors. This equation is valid for doping in the range of $6x10^{16}$-$7x10^{18}$ cm^{-3} at temperatures between 650-800°C.

$$p = 1.13 \times 10^{29}\left[\exp\left(-\frac{1.8eV}{kT}\right)\right]\left\{\frac{MF_{Zn}}{MF_{Ga}}\right\}^{0.85} \qquad (2.10)$$

A drawback to using Zn as a dopant is its high diffusivity at typical growth temperatures. Carbon is an ideal p-type dopant since it has a very low diffusivity value even at high concentration.[24] Recently, Bhat et al.[25] have utilized ALE to grow a carbon doped p-type base in a heterojunction bipolar transistor. They have determined that high carbon doping could be achieved by proper control of the ALE injection sequence and growth temperature.

2.5.2 n-Type Doping

Silicon is utilized as the n-type dopant source in our MOCVD system. Si was selected because of its low vapor pressure and low diffusion coefficient to preserve abrupt doping profiles. Disilane was

selected as the Si source because of its has an efficient cracking pattern with no temperature dependence. However, for our system we observed a significant dependence of incorporation rate on the temperature.[26] This is believed to be caused by the decomposition of disilane into silane in our source bottle.

2.6 Conclusions

This chapter reviews the basic concepts underlying the conventional MOCVD growth process. Although MOCVD processes are not the main topic of this dissertation, the process serves as the base technology upon which we have built our work in ALE. In addition, the shortcomings of the process provide some of the motivation for our work. In particular understanding the surface reaction kinetics of MOCVD precursors, and obtaining uniform growth motivate the need for studying ALE.

REFERENCES-CHAPTER 2

1 S. K. Shastry, S. Zemon, D. G. Kenneson, G. Lambert, Appl. Phys. Lett. **52**, 150 (1988).

2 S. J. Jeng, C. M. Wayman, G. Costrini, and J. J. Coleman, Materials Lettters **2**, 359 (1984).

3 H. M. Manasevit, Appl. Phys. Lett. **12**, 156 (1968).

4 H. M. Manasevit and W. I. Simpson, J. Electrochem. Soc. **116**, 1725 (1969).

5 H. M. Manasevit, J. Electrochem. Soc. **118**, 647 (1971).

6 H. M. Manasevit and K. L. Hess, J. Electrochem. Soc. **126**, 2031 (1979).

7 Y. Seki, K. Tanno, K. Lida, and E. Ichiki, J. Electrochem. Soc. **122**, 1108 (1975).

8 S. J. Bass, J. Crystal Growth **31**, 172 (1975).

9 S. J. Bass, J. Crystal Growth **44**, 29 (1978).

10 R. D. Dupuis, P. D. Dapkus, R. D. Yingling, and L. A. Moudy, Appl. Phys. Lett., **31**, 201 (1977).

11 R. D. Dupuis and P. D. Dapkus, Appl. Phys. Lett., **32**, 472 (1978).

12 Unit Instuments, Inc. Orange, California, Sales Brochure (1986).

13 Advanced Technology Materials, Stamford, Conn.,Technical Sheet (1987).

14 L.J. Giling, J. de Physique, **C5**, 235 (1982).

15 S. P. DenBaars, B. Y. Maa, P. D. Dapkus, A. D. Danner, H. C. Lee, J. Crystal Growth, **77**, 188, (1986).

16 J. Nishizawa, H. Abe and T. Kurabayashi, J. Electrochem. Soc. **132**, 1197 (1985).

17 D. H. Reep and S. K. Ghandi, J. Electrochem. Soc. **130**, 675 (1983).

18 W. Richter, "Physics of Metal-Organic Chemical Vapour Deposition," Festkorperprobleme XXVI (Pergamon Press, New York, 1986).

19 S. Berkman, V. S. Ban, and N. Goldsmith, Heterojunction Semiconductors for Electronic Devices, G. W. Cullen and C. C. Wang, eds., (Springer-Verlag, Berlin. 1979) p. 264.

20 J. S. Yuan, C. C. Hsu,, R. M. Cohen, and G. B. Stringfellow, J. Appl. Phys., **57**, 1380 (1985).

21 H. C. Lee, PhD. Dissertation, University of Southern California, (1987) p.106.

22 V. Aebi, C. B. Cooper, R. L. Moon, and R. R. Saxena, J. Crystal Growth , **55**, 517 (1981).

23 A. D. Danner, PhD. Dissertation, University of Southern California (1987) p.74.

24 N. Kobayashi, T. Makimoto, and Y. Horikoshi, Appl. Phys. Lett, **50**, 1435 (1987).

25 R. Bhat, J. R. Hayes, E. Colas, and R. Esagui, IEEE Electron Device Lett., **9**, 442 (1988).

26 A. D. Danner, PhD. Dissertation, University of Southern California (1987) p.72.

CHAPTER 3
REACTION KINETICS STUDY OF METALORGANIC CHEMICAL VAPOR DEPOSITION

3.1 Introduction

To achieve atomic level control of the MOCVD process a study of the reaction kinetics involved in the thermal decomposition of metalorganic precursors would be invaluable. Currently, the understanding of the kinetics and mechanisms of gas phase and surface reactions operative in the MOCVD process is limited. Thermodynamics predicts that every closed isolated system will approach an equilibrium state, in which its properties are independent of time. The second law of thermodynamics can estimate the amount of driving force for epitaxy. For the equation typically used to describe the MOCVD process, thermodynamics tell us that the reaction is very exothermic and spontaneous even at room temperature.

$$Ga(CH_3)_3 + AsH_3 \rightarrow GaAs + 3CH_4 \qquad \Delta H^o_f = -83 kcal/mole \qquad (3.1)$$

However, thermodynamics is incapable of telling us anything about the chemical pathways or time required to obtain equilibrium. These problems can be solved by applying chemical kinetics, which predict the

time varying properties of chemical systems. Kinetics are not fast enough to establish equilibrium in the MOCVD process, therefore MOCVD is classified as a non-equilibrium growth technique.

In order to help elucidate critical reaction pathways in MOCVD we have applied an "ex-situ" sampled gas Infrared Spectroscopy (IR) setup to study the thermochemical kinetics. Through the use of this analysis we have been able to effectively measure decomposition reaction rates of gaseous precursors utilized in MOCVD. The homogeneous rates of decomposition are measured whenever possible. In some instances, surface catalytic reactions are dominant and the effect of the surface chemistry on the decomposition is described. These studies allow us to determine separately the homogeneous and heterogeneous reaction rates and to determine the catalytic reactivity of various surfaces and gaseous species. Rate constants measured for these decomposition processes can than be extrapolated to the case of ALE growth in chapter four to explain the observed growth behavior.

3.2 Reaction Kinetics

3.2.1 MOCVD Kinetic Steps

The growth rate in MOCVD is determined by the slowest process in a series of reactions leading to deposition. Figure 3.1 illustrates some of the plausible reaction pathways which lead to the epitaxial growth of GaAs. Gas phase reactants must diffuse through the boundary layer where several reaction pathways are possible. Pyrolysis of TMGa in the gas phase may provide the source of Ga atoms needed for crystal growth.

Alternatively, the formation of an adduct between TMGa and AsH_3 may be the mechanism for GaAs growth. Another reaction mechanism might occur is the surface reaction of adsorbed gallium monomethyl ($GaCH_3$) with arsenic hydride (AsH) to release methane (CH_4).

$$GaCH_{3(ads)} + AsH_{(s/v)} \dashrightarrow GaAs_{(s)} + CH_{4(v)} \qquad (3.2)$$

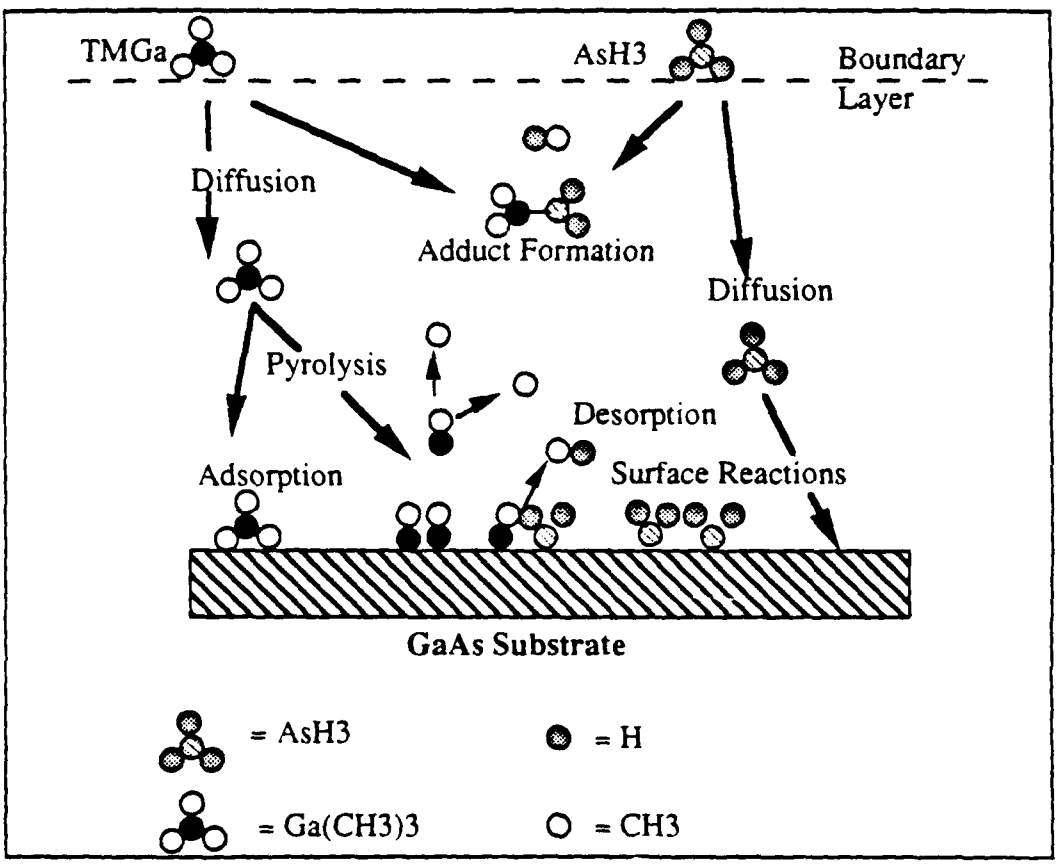

Figure 3.1
Schematic diagram illustrating some of the possible kinetic steps occurring in an MOCVD reactor.

3.2.2 Theory of Thermochemical Kinetics

The most useful quantitative model for describing reaction kinetics is the "activated complex theory" (ACT), also known as the "transition-state theory (TST) of rate processes."[1] In order for a unimolecular reaction to occur, the reacting molecule must obtain sufficient internal energy to break the necessary bond. For a gas phase reaction this "activation" energy may be accumulated by a sequence of "atypical" collisions with average molecules in the gas. The reaction-coordinate - energy diagram shown in figure 3.2 is useful for illustrating the kinetic process. The solid curve is the potential energy of the molecule corresponding to zero kinetic energy for that reaction coordinate. The light horizontal lines suggest the different vibrational levels of the molecule. The energy of the average molecule will be E^{o}_{A}, while E^{*}_{A} is the energy of the average reacting molecule . Note that at any finite temperature, the average reacting molecule is not precisely at the top of the energy barrier but significantly above it. The activation energy for the reaction of A-->B is given as E^{*}_{1} in the figure.

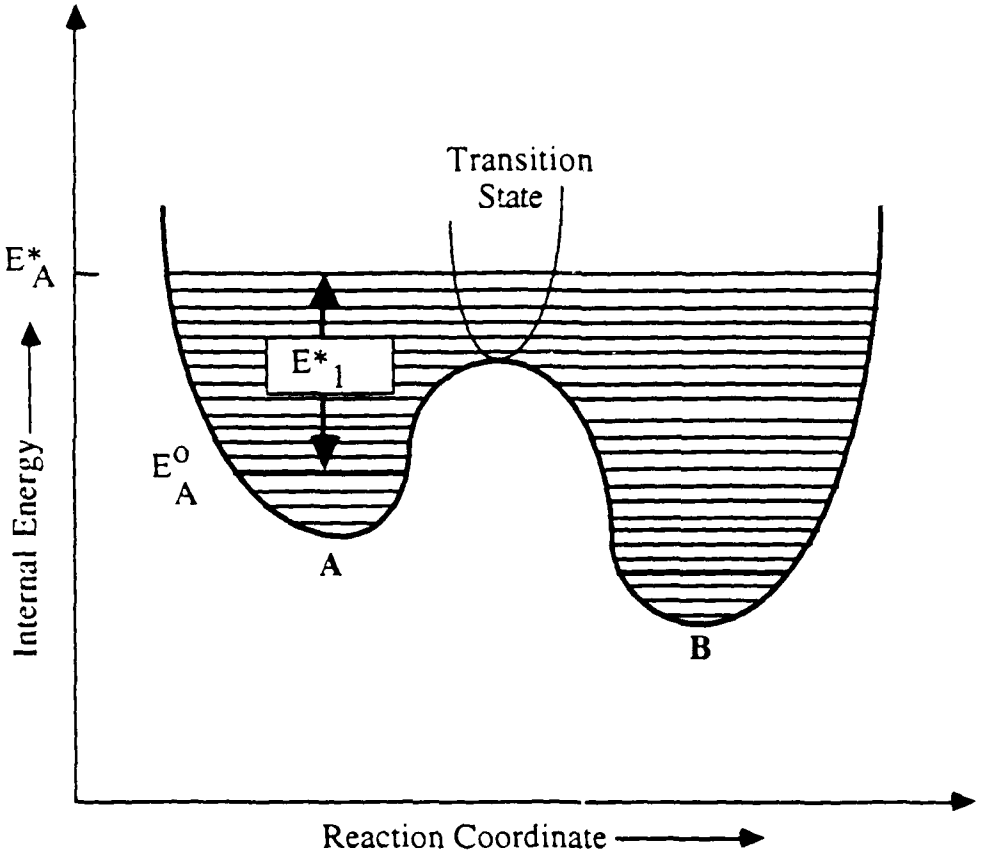

Figure 3.2 Energy-reaction coordinate diagram for simple fission of molecule A-->B (after Benson).[2]

To illustrate the fission of a complex metalorganic molecule such as $Ga(CH_3)_3$, lets first consider the simple, unimolecular fission of a molecule AB.

$$AB \leftrightarrow AB^* \leftrightarrow A + B \qquad (3.3)$$

Where AB* is a molecule that has obtain enough internal energy to be in the transition state and can therefore decompose into A and B. The first

order rate constant for the decomposition of AB, k_{AB}, can be related to the activation energy of the process by the Arrhenius equation:

$$k_{AB} = A * exp\left(-\frac{E_a}{RT}\right) \tag{3.4}$$

Where E_a is the activation energy, R is the ideal gas constant, A is the frequency factor, and T is the reaction temperature.

We now introduce thermodynamic formalism to demonstrate the relation between the activation energy and the dissociative bond strength. From S.W. Benson,[3] the rate constant can also be expressed as:

$$k_{AB} = \left(\frac{kT}{h}\right) K_{AB}^{*} \tag{3.5}$$

where K_{AB}^* is the equilibrium rate constant of the transition state species for motion across the barrier, h is Planck's constant, and k is Boltzmann's constant. The free-energy change for the transition state reactant is related to the rate constant by:

$$\Delta G^* = -RT \ln(K_{AB}^*) \tag{3.6}$$

By definition :

$$\Delta G^* = \Delta H^* - T\Delta S^* \tag{3.7}$$

We can then express the rate constant for the decomposition of AB as:

$$k_{AB} = \left[\frac{kT}{h}\right]\exp\left(\frac{\Delta S_{AB}^{*}}{R}\right)\exp\left(-\frac{\Delta H_{AB}^{*}}{RT}\right) \qquad (3.8)$$

Comparing equation 3.4 to the thermodynamic formalism of the rate constant, equation 3.8, we can see that the dissociative bond enthalpy is related to the activation energy by:

$$E_a = \Delta H_{AB}^{*} + RT_m \qquad (3.9)$$

where T_m is the mean temperature of experiment. For our experiments the RT_m contribution is typically small (1-2kcal/mol). We can also identify the relation between the frequency factor "A", and the entropy of dissociation as follows:

$$A = \left(\frac{ekT_m}{h}\right)\exp\left(\frac{\Delta S_{AB}^{*}}{R}\right) \qquad (3.10)$$

Several of the metalorganic precursors, such as TMGa, are believed to decompose by unimolecular gas phase reactions.[4] Therefore, if we can measure the reaction rates and activation energy for such processes we can measure the dissociative bond strengths for homogeneous gas phase reactions such as the fission of methyl groups from TMGa:

$Ga(CH_3)_3 \rightarrow Ga(CH_3)_2 + CH_3$ $\quad k_{TMGa}$ (3.11)

$Ga(CH_3)_2 \rightarrow Ga(CH_3) + CH_3$ $\quad k_{DMGa}$ (3.12)

$Ga(CH_3) \rightarrow Ga + CH_3$ $\quad k_{MMGa}$ (3.13)

3.3 Experimental Setup

The decomposition of AsH_3 and TMGa was measured by flowing a mixture of H_2 and the desired reactant through a heated quartz tube 5.0 cm in diameter inserted in a furnace with confined and well controlled hot zone 12.5 cm long. Figure 3.3 illustrates the experimental setup used in this study of MOCVD reaction kinetics. The concentration of reactants at various temperatures was measured by sampling a portion of the gas at the exit end of the hot zone and using infrared absorption spectroscopy to measure the absorption coefficient for known vibrational transitions of the molecules under study. In some cases, reactive surfaces such as GaAs wafers were inserted into the reactor to determine their effect on the decomposition of the reactants. Eight 2 inch GaAs (100) wafers were installed in such a way as to insure that most of the gas stream would interact with before exiting the hot zone, see figure 3.4. The absolute concentration of reactants was determined from the known vapor pressure of TMGa, the H_2 flows, and from the manufacture's analysis of AsH_3 concentration. The evolution of CH_4 from the decomposition of TMGa was measured and calibrated relative to a commercial standard.

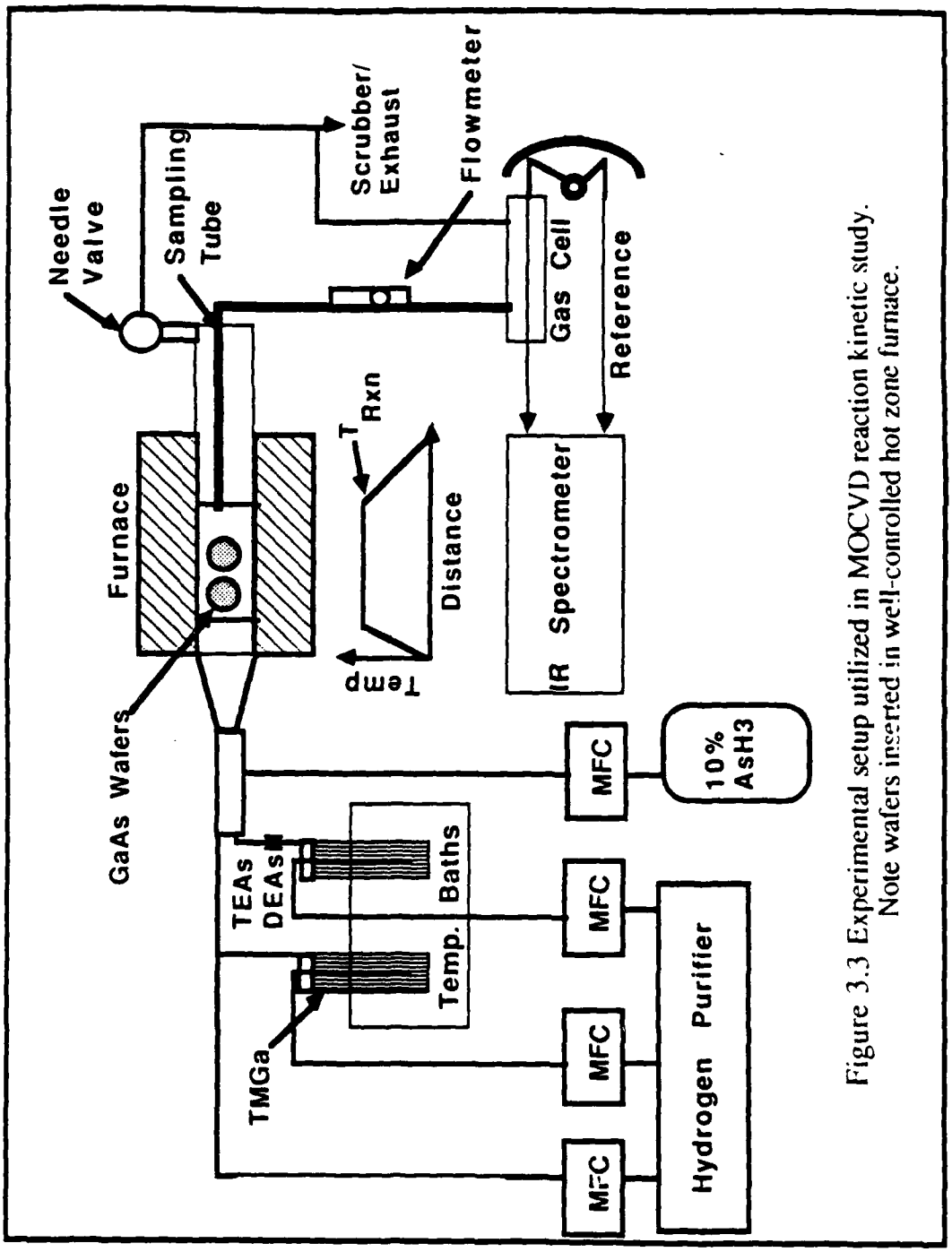

Figure 3.3 Experimental setup utilized in MOCVD reaction kinetic study. Note wafers inserted in well-controlled hot zone furnace.

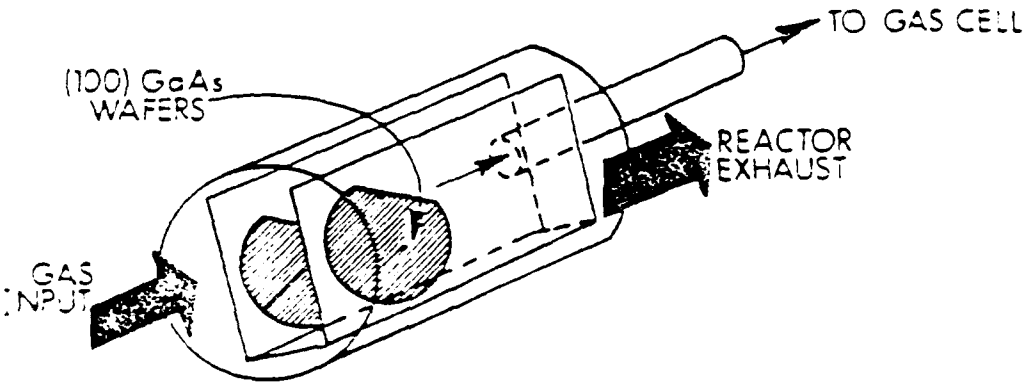

Figure 3.4
GaAs wafers are arranged in reactangular quartz boat to insure maximum maximum interaction with sampled gas stream.

3.4. Sampled Gas IR Spectroscopy $TMGa/AsH_3/H_2$

3.4.1 IR Spectra $TMGa/AsH_3/H_2$

The infrared absorption spectra of $TMGa/H_2$ mixtures sampled from a flowing gas stream have been examined in detail at a variety of temperatures. The gas mixture was passed through the hot zone at an average gas velocity of 1.25 cm/sec. Figure 3.5 shows the room temperature spectra of TMGa which exhibits peaks at ~ 580, ~700, ~1200, and ~2900 cm^{-1}. We have monitored the features at 1200 and 580 cm^{-1} that are associated with the C-H vibrational mode and the Ga-C stretching mode respectively,[5] to determine the change in TMGa concentration. Above 400°C the spectra show additional features at 1304 and 3014 cm^{-1} that are associated with CH_4 vibrational modes.

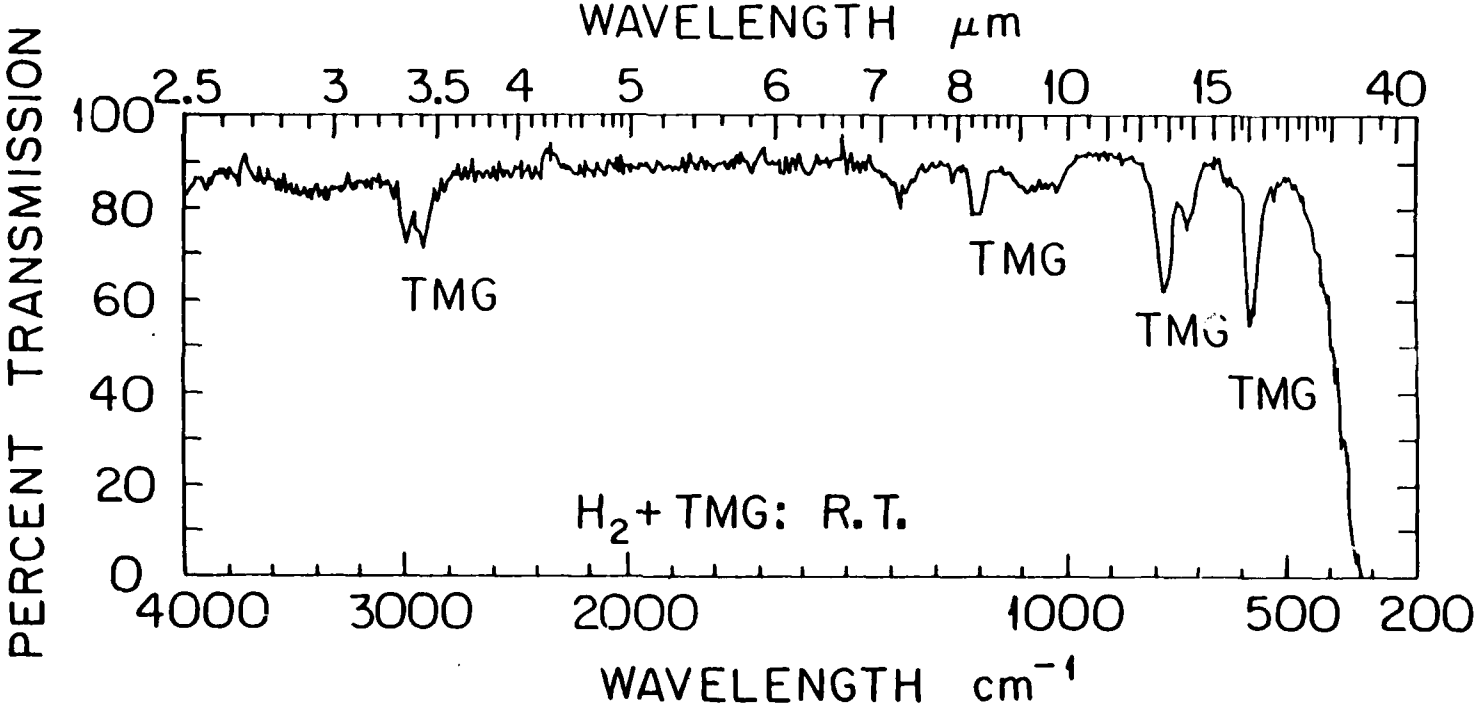

Figure 3.5
Room temperature IR spectrum of TMGa.

The relative concentration of reactants is obtained from the transmission spectra by the use of Beer's law:

$$T = T_o e^{(-abc)} \tag{3.14}$$

where: T_o is the baseline transmission, a is the absorptivity of the molecule at a specified wavelength ($moles^{-1}\ cm^{-1}$), b is the path length of the cell (10 cm), and c is the molar concentration of the reactant. By measuring the input and output IR transmission spectra, we can determine the final reactant concentration relative to the initial concentration:

$$\frac{C_f}{C_i} = \frac{\ln\left(\frac{T_o}{T_f}\right)}{\ln\left(\frac{T_o}{T_i}\right)} \tag{3.15}$$

Figure 3.6 shows the dependence of the TMGa concentration upon the temperature of the hot zone. Note that the relative concentration is unchanged up to a temperature of 380°C and decreases above 400°C to zero at ~460°C. The decomposition curves for TMGa in quartz tube with and without GaAs wafers in the hot zone show only a small difference.

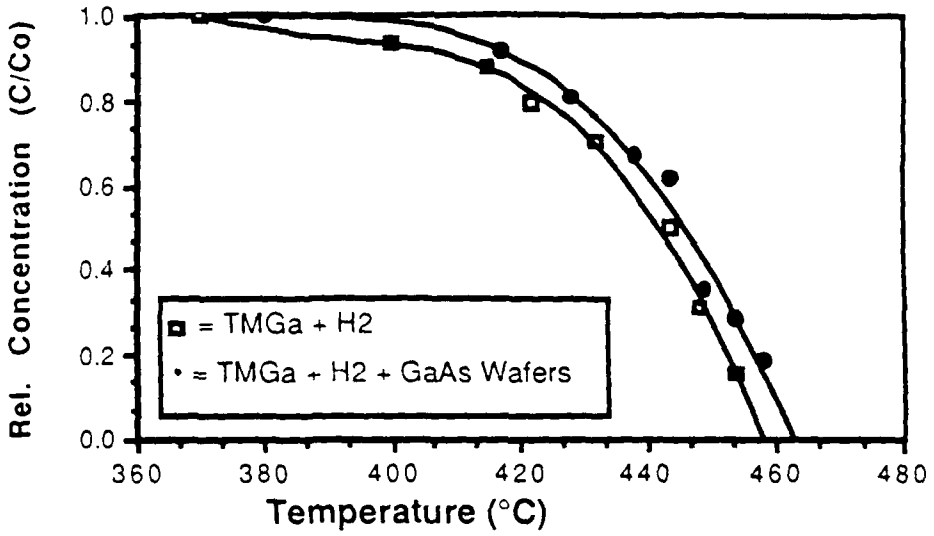

Figure 3.6
Relative concentration of TMGa in H_2 at various temperatures.

We have also measure the evolution of CH_4 from the decomposition of TMGa. Figure 3.7 shows the temperature dependence of this evolution for several different gas mixtures. In all cases the formation of CH_4 coincides with the onset of TMGa decomposition. The evolution of CH_4 continues up to ~500°C at which temperature it saturates. We have calibrated the concentration relative to a commercially prepared mixture and find that in all cases the CH_4 concentration saturates at CH_4 = 3 TMGa.

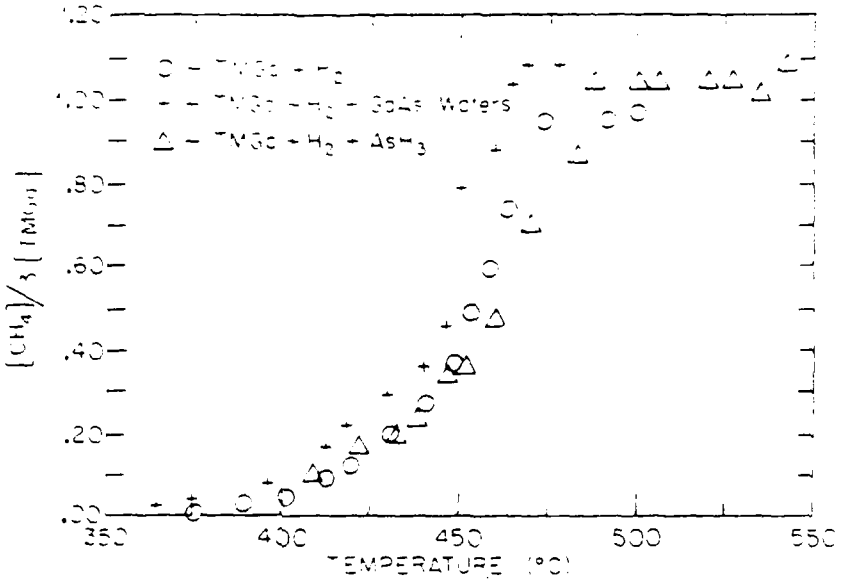

Figure 3.7
Evolution of methane from pyrolysis of TMGa.

Infrared spectra of AsH_3/H_2 and $AsH_3/TMGa/H_2$ mixtures have also been examined at various gas temperatures. Spectral features are observed at 880-1050 and 1950-2300cm^{-1} that are related to AsH_3 vibrational modes. The appearance of peak at 2080 cm^{-1} is observed upon the addition of TMGa to the AsH_3/H_2 system. Nishizawa et al.[6] have also observed the appearance of this unknown peak. We believe this to indicate the formation of a organoarsenic compound in the gas phase. This is based upon examination of the IR spectrum for diethylarsenic hydride (DEAsH) which exhibits a red shifted As-H vibrational peak also at 2080cm^{-1}, see figure 3.11 presented later in this chapter.

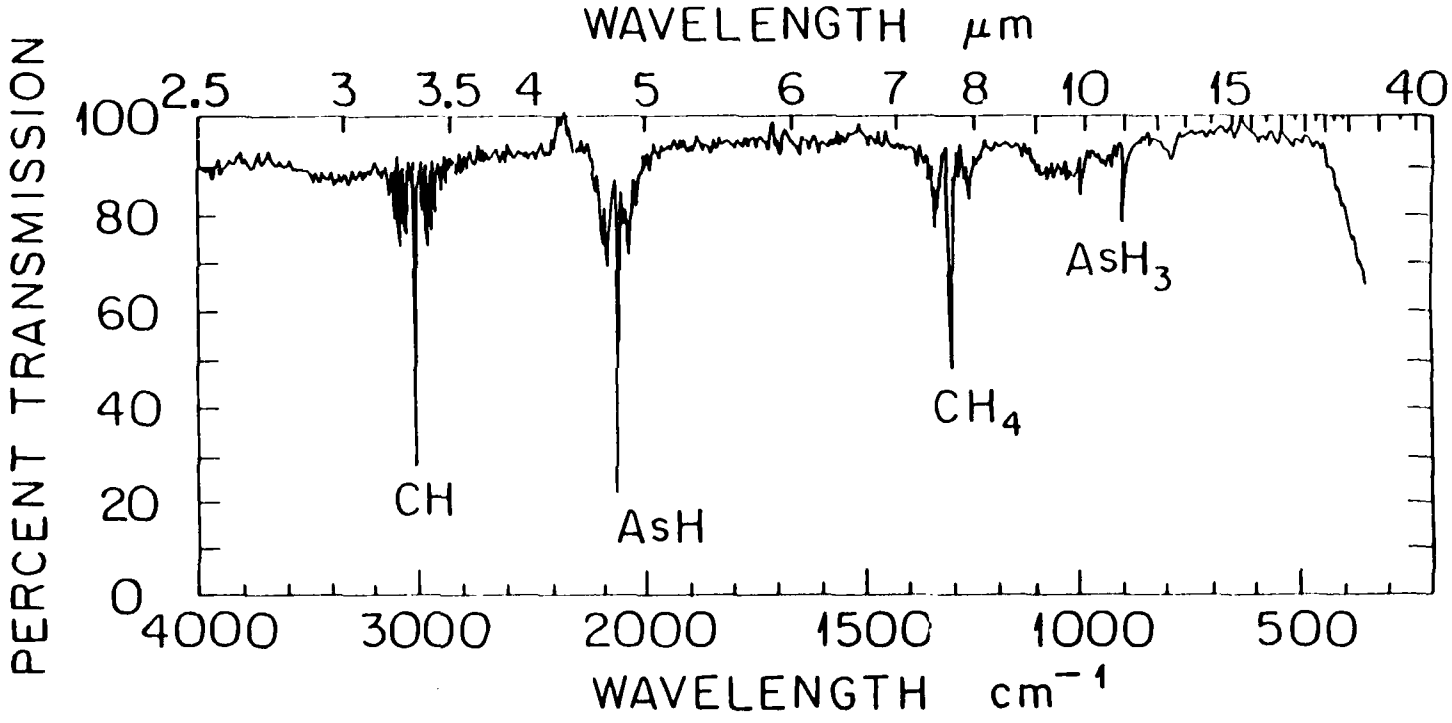

Figure 3.8
IR spectrum of AsH3/TMGa/H2 MOCVDsystem at 500°C.

We monitor the feature at 2112 cm^{-1} to determine the concentration of AsH_3 in heated mixtures. Figure 3.9 shows the variation with temperature of the AsH_3 concentration measured in this way. Note the gradual decrease in AsH_3 concentration with increasing temperature The concentration of AsH_3 in H_2 is strongly affected by the nature of the surfaces in the reactor, as is indicated by the difference between the decomposition curve obtained in a clean quartz reactor and that obtained when GaAs wafers are present in the reaction zone. The rate of decomposition of AsH_3 was also enhanced by the presence of Ga wall deposits and nonstoichiometric Ga:As wall deposits. The presence of TMGa in the gas phase also increases the rate of AsH_3 decomposition, the rate increasing with the TMGa concentration as shown in figure 3.9 In this case it is not possible to separately determine the role of gas phase reactions from those occurring on the reactor walls due to Ga:As deposits that inevitably occur.

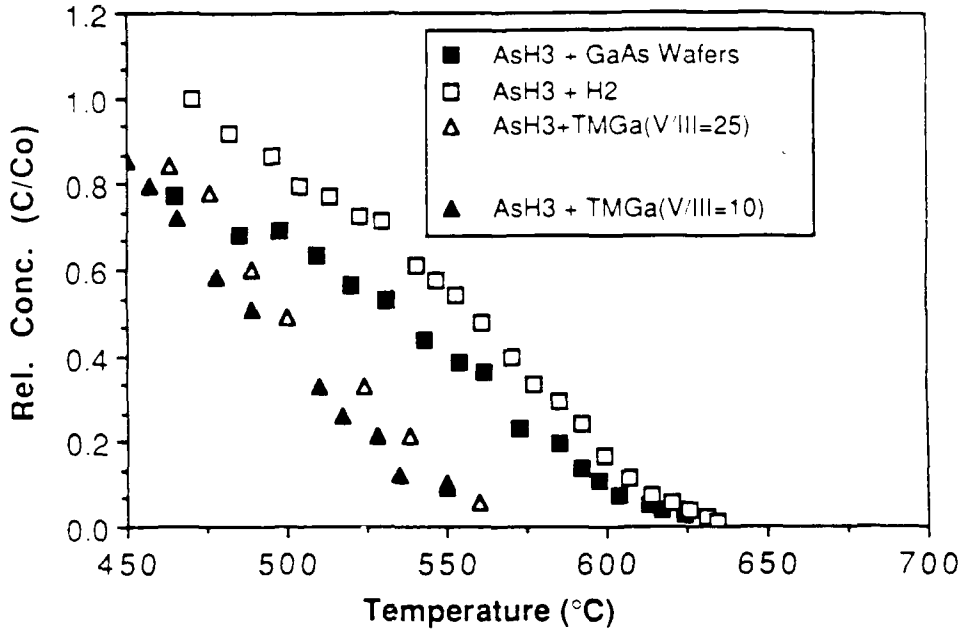

Figure 3.9
Relative concentration of AsH_3 in H_2 at various temperatures and for several different reactor conditions. Note the strong effect of the surfaces on AsH_3 decomposition.

3.4.2 Activation Energies

The data of figures 3.6-9 can provide further insight into the reaction processes occurring in an MOCVD reactor. Yoshida et al.[4] have shown that the decomposition of TMGa is a first order reaction. The kinetics for this decomposition process can be described by:

$$\frac{dC}{dt} = -kC \tag{3.16}$$

where C is the concentration of the reactant and k is a rate constant of the Arrhenius form:

$$k = A \exp\left(-\frac{E_a}{RT}\right) \tag{3.17}$$

A has the units of sec^{-1} and E_a is the activation energy for the process. As derived in section 3.2.2. for a homogeneous unimolecular process E_a will reflect the dissociative bond strength of the Ga-C bond in TMGa. We determine k by integrating equation 3.16:

$$\int_{C_o}^{C_f}\left(\frac{dC}{C}\right) = -\int_{0}^{\Delta t} k\,dt \tag{3.18}$$

where Δt is the contact time in the reactor hot zone. This leads to the following expression for the effective reaction rate constant:

$$k = \frac{\ln\left(\frac{C_o}{C_f}\right)}{\Delta t} \tag{3.19}$$

From equation 3.17 we can deduce that a logarithmic plot of k versus 1/T will yield the activation energy for the process under study.

$$E_a = \frac{\partial \ln(k)}{\partial\left(\frac{1}{RT}\right)} \tag{3.20}$$

Figure 3.10 shows a plot of ln k versus 1/T for the decomposition of TMGa in hydrogen. The slope of the straight line fit to the data of

figure 3.8 yields an activation energy of E_a = 58 kcal/mol for this process and E_O = 62 kcal/mol for decomposition in the presence of GaAs wafers. It is not known whether the difference in activation energy observed in these two cases is significant or merely a measure of experimental error. Both activation energies are comparable to the activation energy for the loss of one methyl group from TMGa that was measured by Jacko and Price[7] (59.5 kcal/mol) which is an approximate measure of the dissociative bond enthalpy for the first methyl group on $(CH_3)_3Ga$, i.e. $DH((CH_3)_2Ga\text{-}CH_3)$.

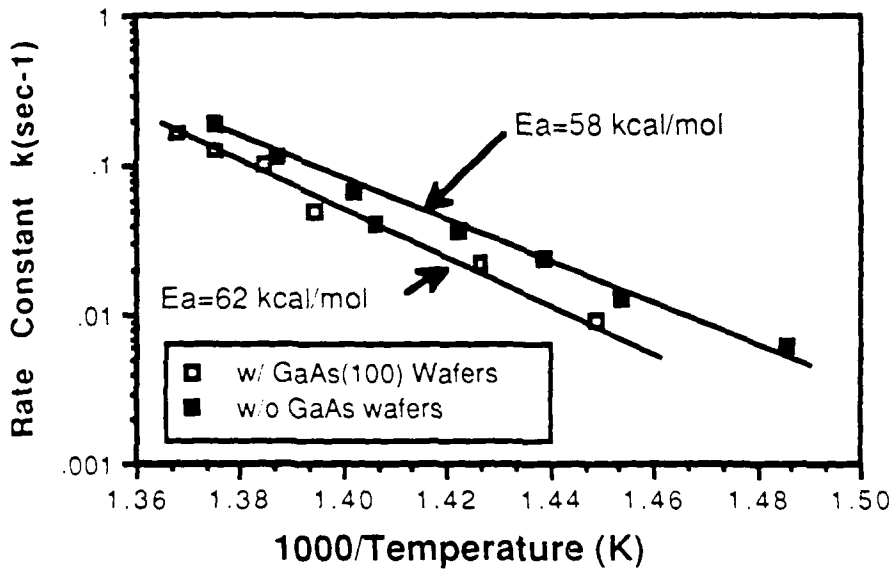

Figure 3.10
Effective decomposition rate constant versus reciprocal temperature for the decomposition of TMGa.

Jacko and Price observed no more than two CH_4 molecules for each TMGa molecule decomposed at any temperature in their studies with a

tolulene carrier. The data of figure. 3.7 can be further analyzed to yield information related to the decomposition path of TMGa H_2 mixtures. In figure 3.11 we plot the ratio of the CH_4 present at each temperature to the TMGa concentration loss (TMGa) due to decomposition at that temperature. This ratio gives a measure of the number of methyl groups lost from the TMGa in the decomposition process. For low temperatures, where there is quantifiable loss of TMGa, the ratio $R = CH_4/\Delta TMGa = 2$, indicates that more than one methyl group is lost from the TMGa prior to sampling of the gas. We have observed a range of values for this low temperature ratio, R, e.g. $1.7 \leq R \leq 2.0$. These data suggest suggest that the loss of the first methyl group from the TMGa is followed promptly by the loss of a second methyl group at a rate that exceeds our current measurement ability. At temperatures above 460°C we consistently observe three methane molecules for each decomposed TMGa molecule. This observation suggests that, contrary to the results of Jacko and Price, all methyl radicals are removed from TMGa in H_2 at temperatures above 500°C.

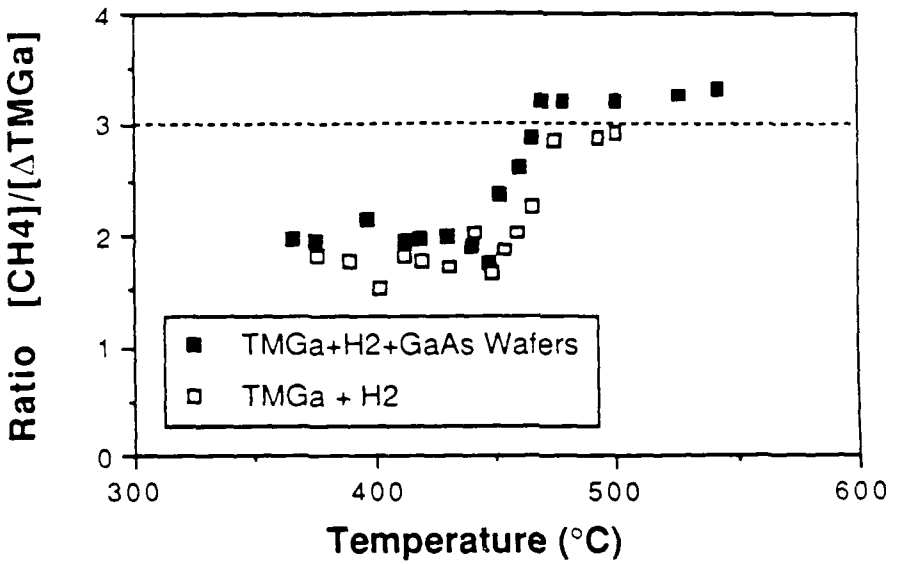

Figure 3.11
Ratio of evolved CH4 concentration to change in concentration of TMGa
The low temperature value of R is 2.0, while above 500°C,R~3

It appears that the fission of methyl groups on TMGa occurs in stages. The first group is removed by homogeneous reactions. This is suggested by the relative insensitivity of the reaction rate constant and its temperature variation to reactor surfaces and deposits. The loss of the second methyl group cannot be measured by our current experimental arrangement. The variation of R at low temperature for different runs and conditions suggests that factors other than homogeneous reaction can play a role.

We are not able to reliably extract the reaction rates for the loss of the second and third methyl group. However, the rate of loss of the

second methyl group is at least as large as that for the first methyl group. The sharp transition between the temperature region where the two and three methyl groups are lost suggests a high activation energy for this process. A more accurate determination of the rate constants than is possible with the current apparatus is required to assess the degree of decomposition of TMGa in the boundary layer of a typical MOCVD reactor.

The decomposition of AsH_3 in H_2 is characterized by an activation energy of 34 kcal/mol when analyzed as a first order reaction, see figure. 3.12. This activation energy is somewhat larger than that determined by Tamaru[8] (23 kcal/mol). In Tarmaru's work, however, the decomposition was carried out on coherent arsenic and antimony surfaces at very low temperatures. Our data suggest that AsH_3 decomposition is largely surface catalyzed. This is indicated by the sensitivity of decomposition rate to the surface preparation and wall deposits. An example of the effect of GaAs surfaces on the rate of decomposition of AsH_3 is also shown in figure 3.12. The activation energy for the process is 18 kcal/mol in the temperature range below ~ 530°C when GaAs surfaces are present and increases above 530°C to the value determined for homogeneous or quartz decomposition (34 kcal/mol). This transition suggests that homogeneous or quartz catalyzed decomposition dominates at temperatures above 530°C in our experiments.

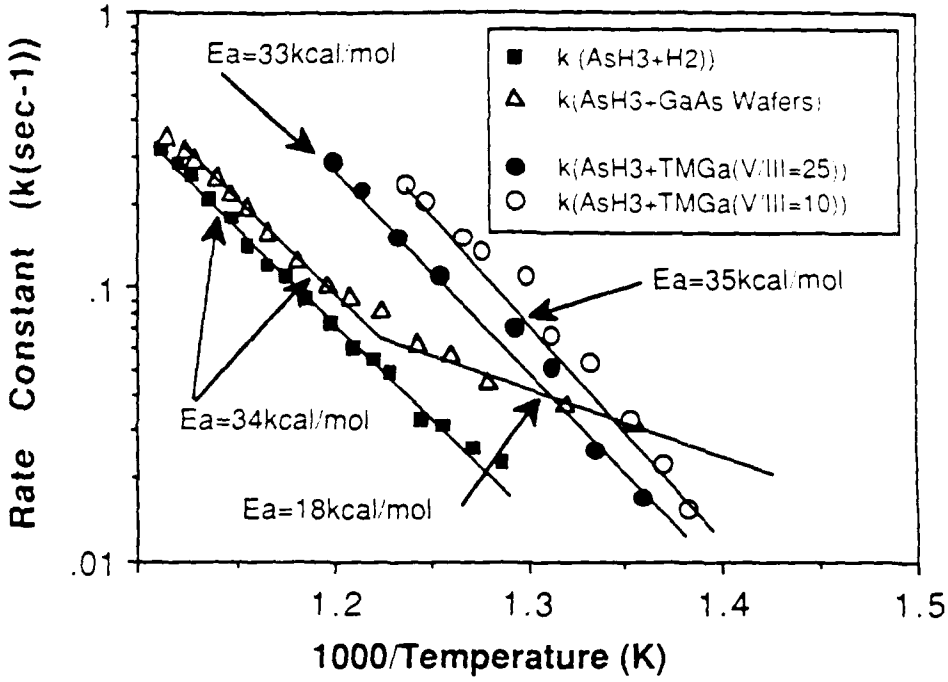

Figure 3.12
Effective rate constant for decomposition of arsine in H_2, H_2 + TMGa, and H_2 with GaAs (100) wafers present.

The presence of TMGa in the reactor greatly enhances the rate of decomposition of AsH_3, but does not substantially alter the activation energy of the process. A complete explanation for this is not possible at present. The implication for the growth of GaAs however is that TMGa promotes the decomposition of AsH_3 at temperatures well below normal growth temperature. Clearly this process dominates the decomposition of arsine for most MOCVD growth conditions.

3.5 Sampled Gas IR Spectroscopy DEAsH/TEAs

In order to achieve thermally driven ALE of III-V compounds a low decomposition temperature source of arsenic would be beneficial. Also, reducing the safety hazards associated with arsine gas by development of high purity organometallic group V sources would be of considerable importance to growth of gallium arsenide by MOCVD. The use of liquid organometallic arsenic sources would reduce the toxic hazard and handling problems associated with high pressure arsine gas cylinders. The group V hydrides also have slow decomposition rates and require high temperatures for pyrolysis. Thus, large excesses of arsine are required to obtain good epitaxial growth. In contrast, group V organometallics sources might potentially decompose at temperatures allowing a more stoichiometric mixture in the gas phase at "normal" growth temperatures or they may allow reduced temperature growth to eliminate temperature driven diffusion of dopants. These benefits have led to the investigation of alternative arsenic sources to replace arsine.[9,10,11,12] However, little is currently understood about the basic chemical reactions operative in the MOCVD growth of GaAs with these new organoarsenic sources.

In this study we present data on the reaction mechanisms and rates of decomposition of the organometallic V sources triethylarsenic (TEAs) and diethylarsine (DEAsH) in a hydrogen carrier gas. In addition, the catalytic reactivity of single crystal GaAs surfaces on the decomposition of the gaseous reactants is also studied.

3.5.1 IR Spectra DEAsH/TEAs

The infrared absorption spectra of DEAsH/H_2, and TEAs H_2 mixtures sampled from a flowing gas stream have been examined in detail at various temperatures. The room temperature spectra of DEAsH and TEAs is shown in figure 3.13 and figure 3.14 respectively. For our current experiments we have monitored the IR absorption peaks at 2980, 2080, 955 and 585cm^{-1}, which correspond to the C-H, As-H vibrational modes and the C=C, As-C stretching modes, respectively.[5] It is of interest to note that the As-H vibrational mode in the DEAsH molecule is located at 2080cm^{-1}, which is red shifted with respect to its value of 2122cm^{-1} in the arsine molecule. Based upon this observation we conclude that the appearance of an unknown peak at 2080cm^{-1} previously observed in decomposition studies of the TMGa/AsH_3 system[6] is likely to be caused by the formation of an intermediate organoarsenic compound. These compounds may play a role in conventional MOVPE growth of GaAs.

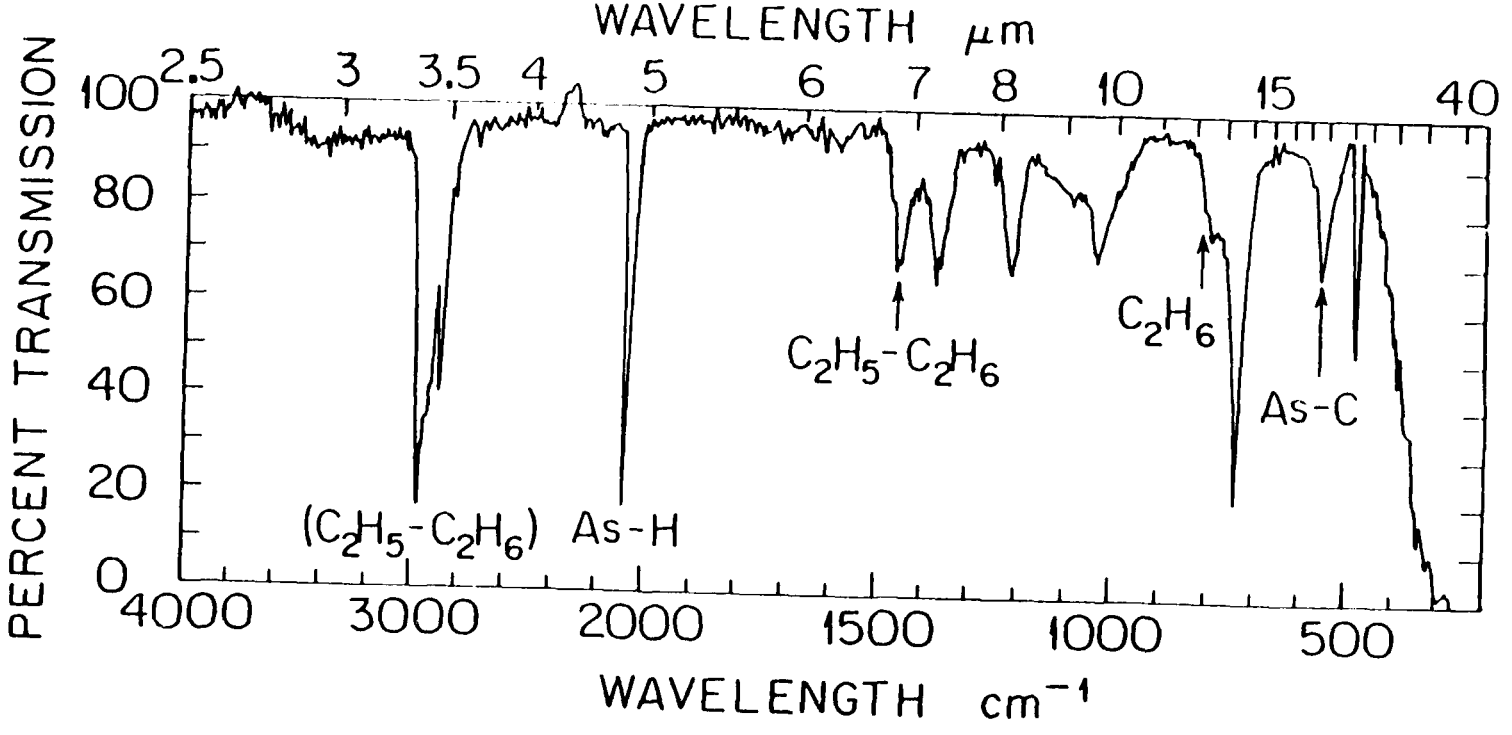

Figure 3.13
Infrared absorption spectrum of diethylarsine at room temperature.

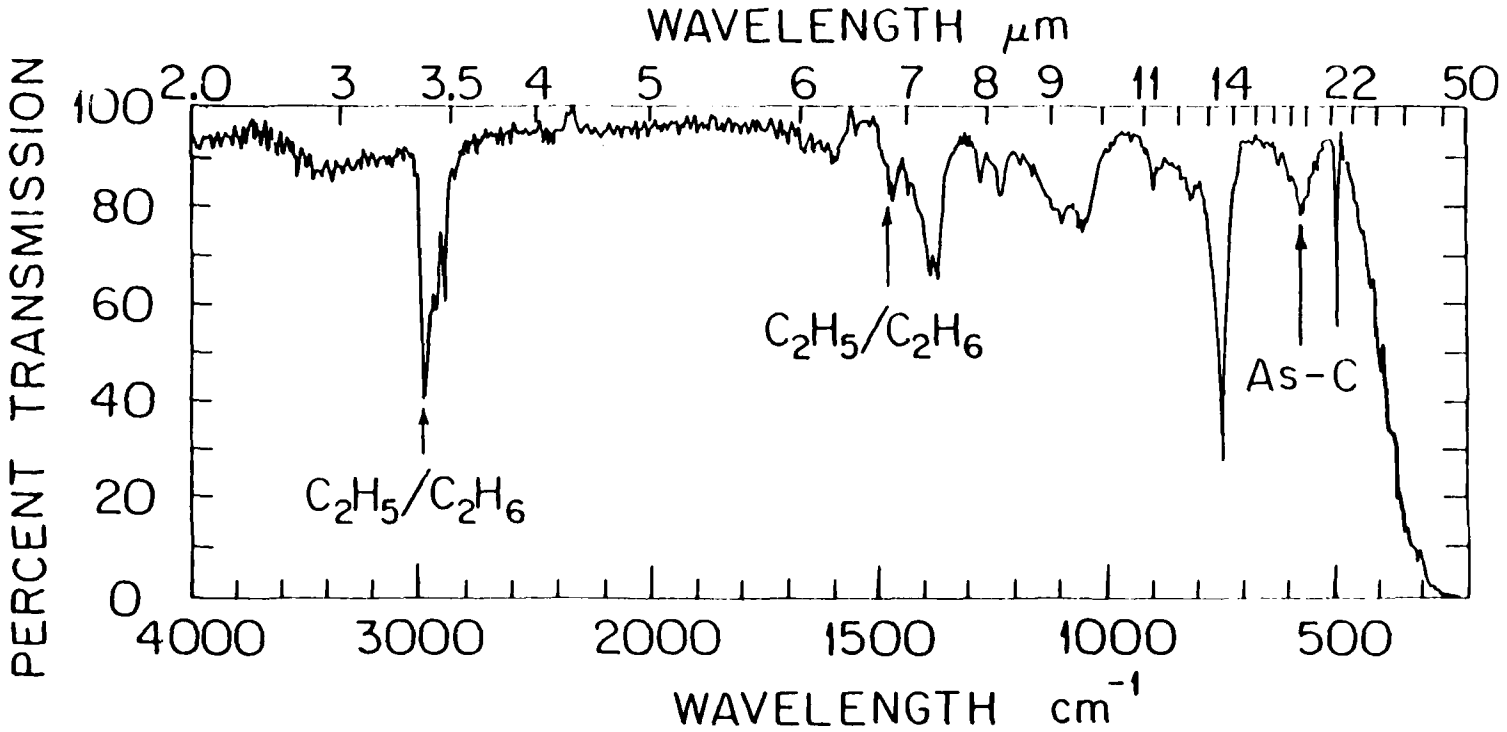

Figure 3.14
Infrared absorption spectrum of triethylarsenic at room temperature

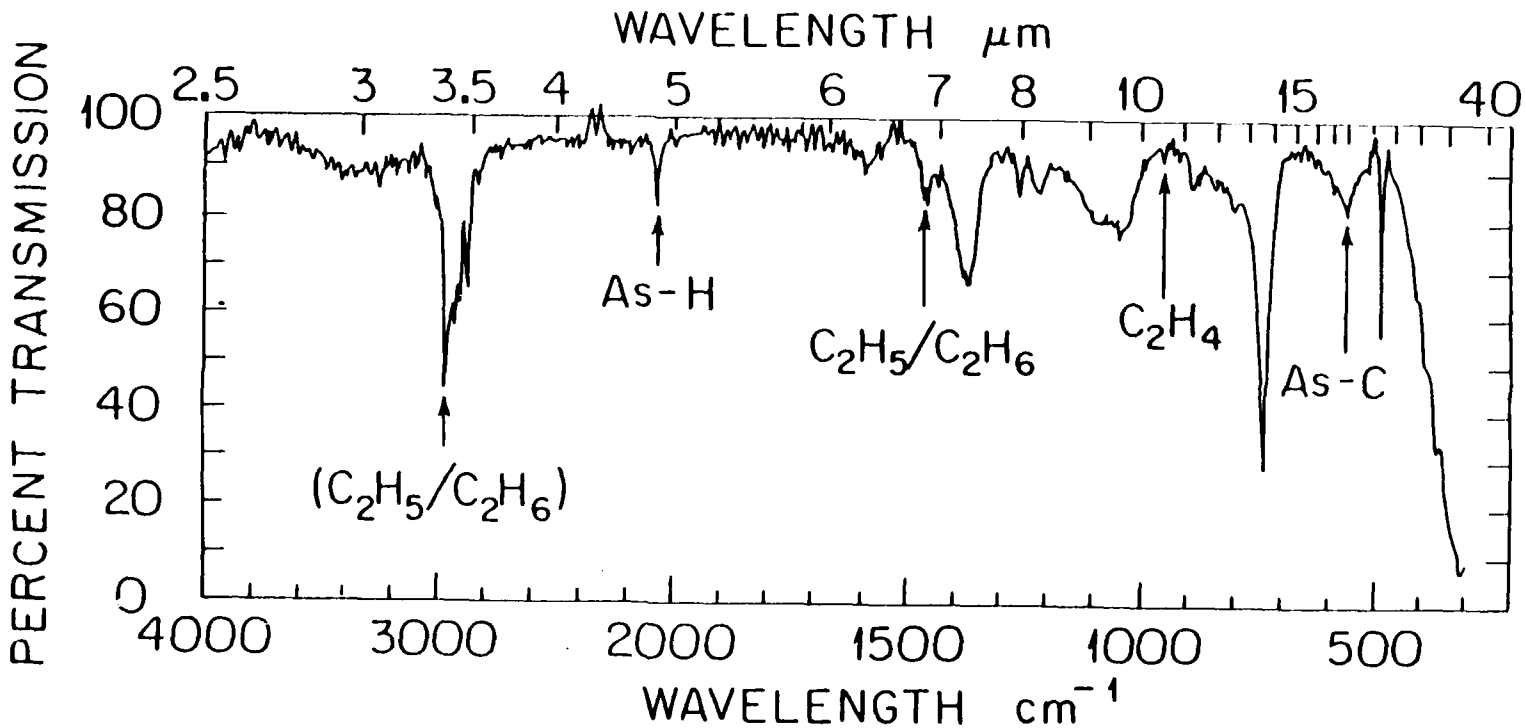

Figure 3.15
Triethylarsenic spectrum at 410°C, note appearance of diethylarsine peak at 2080cm-1.

3.5.2 DEAs/TEAs Reaction Mechanism

Upon thermally decomposing the DEAsH, ethane (C_2H_6) and ethylene (C_2H_4) are observed to be the main reaction products. In addition, a small quantity of arsine at 2122cm^{-1} was observed to be produced at temperatures exceeding 440°C. From infrared spectral analysis it was determined that the pyrolysis of DEAsH begins at 400°C and is virtually complete at 460°C. In a hydrogen carrier stream the decomposition reaction for DEAsH appears to be:

$$(C_2H_5)_2AsH \text{ ------> } 1/2As_2 + (2-x)C_2H_6 + xC_2H_4 \qquad (3.21)$$

The value of x for this reaction can not be quantitatively determined since the absolute vapor pressure of DEAsH at 20°C is unknown.

Triethylarsenic shows a different reaction pathway, which interestingly enough yields DEAsH as an intermediate reaction product in the temperature range of 350-430° C. Figure 3.15 shows an infrared absorption spectrum of TEAs taken at 410°C, note the appearance of the As-H vibrational mode at 2080cm^{-1}. A ß-hydride elimination mechanism is the most likely reaction pathway that explains the formation of DEAsH from the thermal decomposition of TEAs. This can be described by the following expression:

$$(C_2H_5)_3As \text{---> } (C_2H_5)_2AsH + C_2H_4 \text{ (350-430°C)} \qquad (3.22)$$

Figure 3.16 shows the relative concentration of the gaseous species as a function of temperature in the hot zone. Since the vapor pressure of DEAsH is not known, the concentration of DEAsH was estimated by taking the IR absorptivity at the As-H vibrational frequency to be 1/3 of the value for the arsine molecule. Note that the evolution of DEAsH increases until a temperature of 430°C at which point the rate of decomposition of DEAsH exceeds the rate of its formation from the decomposition of TEAs. On account of the overlap in the ethyl and ethane IR absorption peaks the relative concentration of C_2H_6 is not plotted.

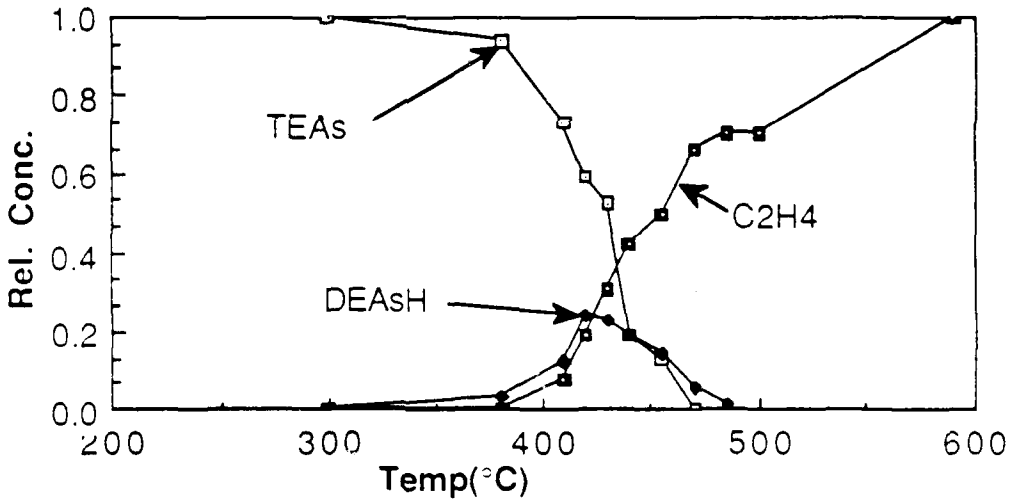

Figure 3.16.
Relative concentration of triethylarsenic, diethylarsine and ethylene and as a function of temperature.

The addition of GaAs(100) wafers to the hot zone has been found to catalyze the decomposition of both DEAsH and TEAs. As shown in figure

3.17 the relative rates of decomposition of both DEAsH and TEAs at 430°C are 3 times greater with GaAs surfaces in the hot zone. In addition, the slopes of the decomposition curves are steeper upon the addition of GaAs wafers which is indicative of a different activation energy for the process.

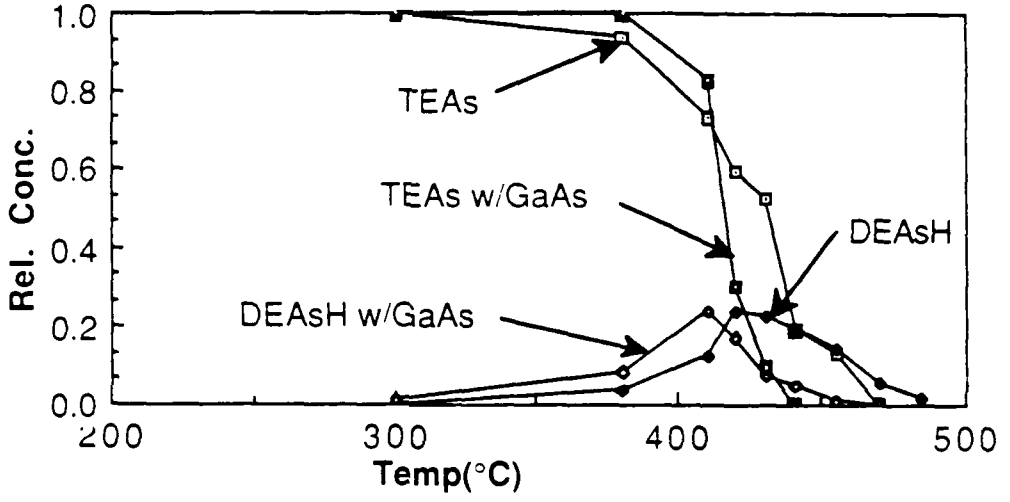

Figure 3.17
Effect of GaAs(100) surfaces on the pyrolysis of TEAs and DEAsH.

3.5.3 DEAsH/TEAs Activation Energies

For the simple uncatalyzed pyrolysis of DEAsH and TEAs we model the decomposition by first order reaction kinetics. As shown in figure 3.18, an activation energy of 43.3kcal/mole was measured for the decomposition rate of TEAs. This was determined by monitoring the As-

C stretching frequency (565cm^{-1}) in the TEAs molecule. The decomposition of DEAsH exhibited a significantly lower activation energy of 20.6kcal/mole for the As-H vibrational frequency(2080cm-1), see figure 3.19. The activation energy for the decomposition of DEAsH is significantly lower than the As-H bond strengths[13] in AsH_3, similar to results of earlier studies on the decomposition of AsH_3.[14]

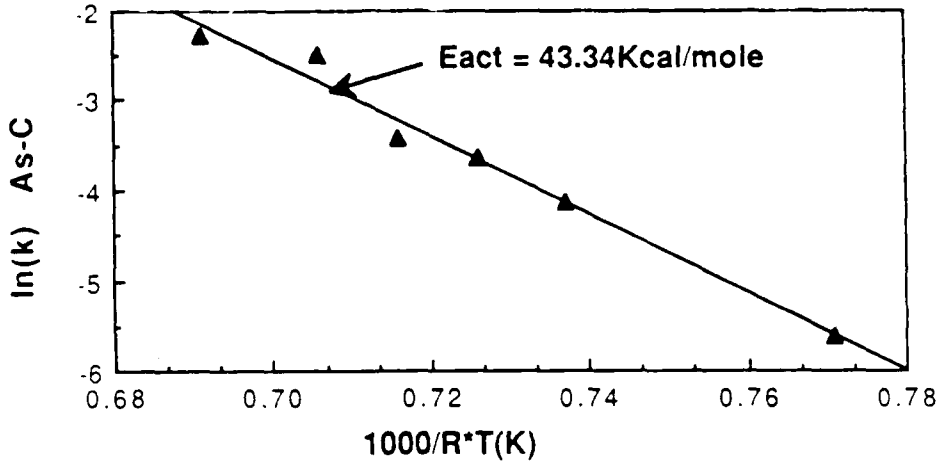

Figure 3.18.
Reaction rate of triethylarsenic plotted against inverse temperature times ideal gas constant yields activation energy of decomposition process.

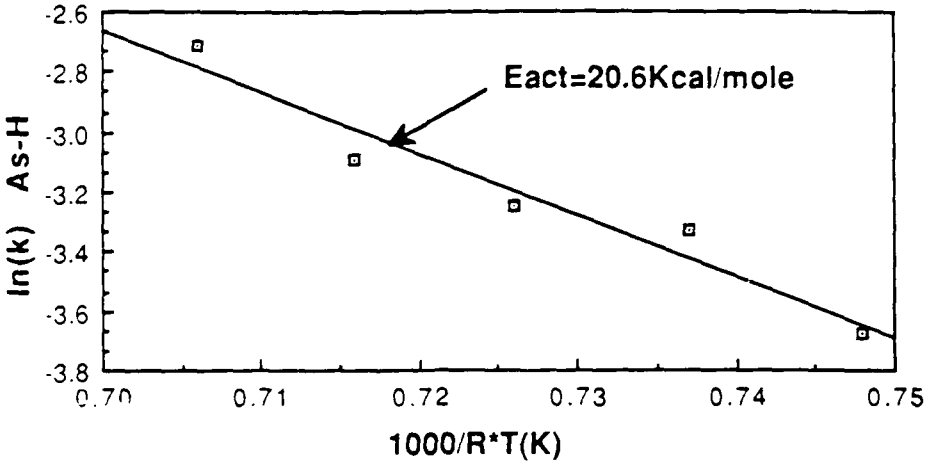

Figure 3.19.
Reaction rate of diethylarsine as a function of inverse temperature.

Table 3.1 Rate Constants for DEAsH/TEAs Decomposition

$k = A \exp[-E_a/RT]$		
	$\log_{10}A(sec^{-1})$	E_{act}(kcal/mol)
TEAs/H2	12.1	43.4
DEAsH	5.1	20.6

3.5.4 TEAs Decomposition Kinetics Model

By using the effective reaction rate constants shown in Table 3.1, we can generate a kinetic model which supports the experimentally observed evolution of DEAsH and C_2H_4 from the decomposition of TEAs by a β-hydride elimination mechanism. The temperature dependence of the relative concentration of TEAs(C_f/C_o) at a fixed contact time is shown

in figure 3.20, in which both the line representing the kinetic model equation 3.23 and experimentally measured points are shown.

$$TEAs\left(\frac{C_f}{C_o}\right) = \exp(-k_1\tau) \qquad (3.23)$$

If we assume that all the TEAs decomposes to form DEAsH then the relative amount evolved should be$(1-C_f/C_O)$. By using the effective rate constant for the decomposition of DEAsH observed separately in the DEAsH experiment we can write the following kinetic expression for the final DEAsH concentration observed:

$$DEAsH\left(\frac{C_f}{C_o}\right) = [1 - \exp(-k_1\tau)] * \exp(-k_2\tau) \qquad (3.24)$$

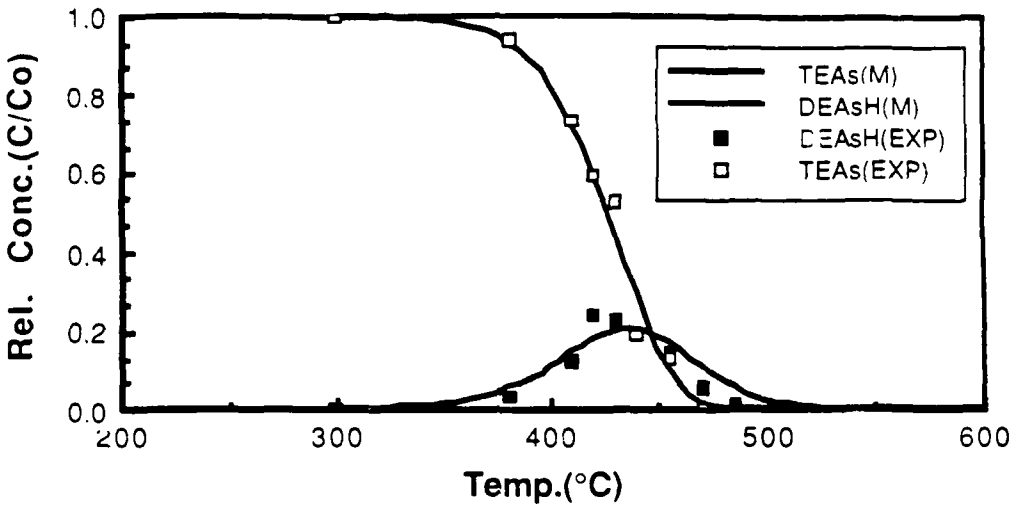

Figure 3.20.
Fit of reaction kinetics model to the experimentally observed relative concentrations of TEAs and DEAsH.

As shown in Fig. 3.20, there is an excellent fit of the experimental data to the kinetic model. This supports the conclusion that the predominant mechanism for TEAs decomposition is β-hydride elimination resulting in the formation of DEAsH and ethylene. Consequently, it appears that DEAsH is the more stable organoarsenic molecule.

This is also supported by the experimental observation that upon the addition of trimethylgallium (TMGa) to gas stream a low volatility liquid adduct forms with TEAs. but not with DEAsH. The formation of the TEAs/TMGa adduct has required heating of reactor lines to 120°C in

order to obtain successful GaAs growth.[15] The use of DEAsH in MOCVD growth has yielded reasonably high purity GaAs with n-type background free carrier concentrations as low as $3x10^{14}cm^{-3}$ and 77K mobility of $64,600cm^2/(V \cdot sec)$. On the basis of our studies and previous work, we conclude that DEAsH is a most promising arsine replacement. In addition, the As to hydrogen bond in DEAsH may play an important role in reducing the carbon incorporation in GaAs by hydrogenolysis of the methyl groups from TMGa. This view is supported by the work of R. Bhat[16] who observed high p-type background GaAs layers when elemental arsenic was substituted for arsine.

3.6 Summary

By using sampled gas infrared absorption spectroscopy we have been able to effectively measure the decomposition rates for the $TMGa/AsH_3/H_2$ system. Table 3.2 summarizes first order rate constant for the MOCVD process. The pyrolysis of TMGa was found to occur in stages, with the first two methyl groups releasing in the 350-450°C range. It is not definite that all stages of alkyl elimination are homogeneous. However, the rate of decomposition is not enhanced by wall deposits of GaAs substrates for the TMGa partial pressure and reactor pressure examined. The only gas phase by product of the decomposition observed is CH_4. Arsine decomposition on the other hand is strongly catalyzed by wall deposits, GaAs surfaces, and gaseous mixtures with TMGa. The activation energy for AsH_3 decomposition is reduced for the reactor at the GaAs surface. We emphasize that these catalytic reactions play an

important role in the MOCVD growth of GaAs and must be taken into account when modeling a large scale reactor.

Thermal decomposition of TEAs in H_2 occurs via a ß-hydride elimination mechanism, producing DEAsH and C_2H_4 as the organic by-products. Thermal decomposition of DEAsH was observed to produce predominantly C_2H_6 , C_2H_4 and a small quantity of arsine. Both DEAsH and TEAs decomposition was discovered to be catalyzed by the addition of single crystal GaAs(100) surfaces to the reactor. Since DEAsH does not form an adduct with TMGa, whereas TEAs does, DEAsH is concluded to be the more attractive group V alternative source

Table 3.2 Rate Constants for TMGa/AsH_3 Decomposition

k= A exp[-E_a/RT]		
	$\log_{10}$A(sec^{-1})	E_{act}(kcal/mol)
TMGa/H_2	16.64	58
TMGa w/GaAs	18.12	62
AsH_3/H_2	7.55	34
AsH_3/H_2/GaAs	3.72	18 (T<530°C)
AsH_3/TMGa (10:1)	8.86	35 (T>530°C)
AsH_3/TMGa (25:1)	8.13	33

REFERENCES-CHAPTER 3

1 I. R. Levine, Physical Chemistry, (McGraw-Hill Publ. Co.,New York, 1978) p. 771.

2 S. W. Benson, Thermochemical Kinetics , 2nd Ed, (John Wiley & Sons, New York, 1976) p. 17.

3 S. W. Benson, Thermochemical Kinetics , 2nd Ed, (John Wiley & Sons, New York, 1976) p. 85.

4 M. Yoshida, H. Watanabe, and F. Uesugi, J. Electrochem. Soc. **130**, 413 (1985).

5 M.R. Leys and H. Veenvliet, J. Crystal Growth, **55**, 145 (1981).

6 J. Nishizawa and T. Kurabayashi, J. Electrochem. Soc. **130**, 413 (1983).

7 M. G. Jacko, and S. J. W. Price, Can. J. Chem. **41**, 1560 (1963).

8 K. Tamura, J. Phys. Chem. **59**, 777 (1955).

9 P. Lee, D. McKenna, D. Kapur and K.F. Jensen, J. Crystal Growth. **77**,120 (1986).

10 W.T. Tsang, Appl. Phys. Lett. **45**,1234 (1984).

11 R. Bhat, M.A. Koza, and B.J. Skromme, Appl. Phys. Lett. **50**, 1194 (1987).

12 D.M. Speckman and J.P. Wendt, Appl. Phys. Lett. **50**, 676 (1987).

13 S.R. Gunn, Inorg. Chem., **11**, 796 (1972).

14 S.P. DenBaars, B.Y. Maa, P.D. Dapkus, A.D. Danner and H.C. Lee, J. Crystal Growth.**77**, 188 (1986).

15 K. Tamaru, J. Phys. Chem. **59**, 777 (1955).

16 R. Bhat, J. Electron. Mater. **14**, 433 (1985).

CHAPTER 4
ATOMIC LAYER EPITAXY BY THERMALLY DRIVEN METALORGANIC CHEMICAL VAPOR DEPOSITION

4.1 Introduction

As described in the first chapter, the Atomic Layer Epitaxy (ALE) process is a stepwise deposition process in which alternate monolayers of each constituent element in the compound are deposited using a self-limiting surface reaction mechanism. By employing a new regime of MOCVD growth, in which saturated surface reactions control the growth, it is possible to alternately deposit monolayers of column III and column V elements so that only one monolayer of the III-V compound semiconductor is deposited in every cycle of the deposition. Extremely uniform films can be deposited by repetition of this alternate exposure cycle. For III-V compounds, the use of a volatile molecule for the column III element is required to avoid clustering of the element on the surface. In this study, we employ conventional MOCVD reactants trimethylgallium (TMGa), trimethylaluminum (TMAl), and arsine (AsH_3) as the ALE reactants for the growth of GaAs, AlAs and AlGaAs. We describe the kinetics of thermally driven ALE growth using these reactants in both H_2 and N_2 ambients in the temperature range 445°C - 500°C. We further demonstrate that this technique can be integrated with the existing technological base of conventional MOCVD. Hybrid structures are grown by utilizing ALE for the layers of critical thickness

control and thicker layers by MOCVD. In order to integrate the two technologies several design considerations must be addressed. This chapter describes the ALE system employed in this work, saturated growth results, and kinetic growth model.

4.2 Design of ALE Reactor

ALE was performed in a modified atmospheric MOCVD reactor system. The system was designed to allow fast transitions between the column III and column V gas sources with a minimum of intermixing. Figure 4.1 shows a schematic of the modified vent/run MOCVD system which is equipped with a pressure balanced injection manifold to eliminate gas concentration fluctuations. The reactor vessel is a small volume rectangular tube which is water-cooled on the top surface to promote laminar gas flow. The average gas residence time in this reactor design is only 0.5 seconds at the high flowrates employed in this work (35cm/sec). The recessed graphite susceptor lies flush with the adjacent bottom quartz wall insuring minimal gas turbulence along the leading edge. The small residence time growth chamber allowed alternate exposures of the substrate to be achieved by a pulsed gas injection method. In this method, ALE of GaAs, AlAs, and AlGaAs is achieved by using conventional MOCVD precursors in a four step gas injection sequence at low growth temperatures.

The use of variable growth temperature in a run allowed us to grow the best quality GaAs/AlGaAs heterostructure by a hybridization of ALE and conventional MOCVD. By using an infrared heating assembly rapid

and conventional MOCVD. By using an infrared heating assembly rapid changes in the growth temperature were possible. The highest quality AlGaAs is grown by conventional MOCVD at 750°C.[1] The temperature is then lowered to the surface controlled growth regime (445-500°C) where the quantum well active regions are grown by ALE.

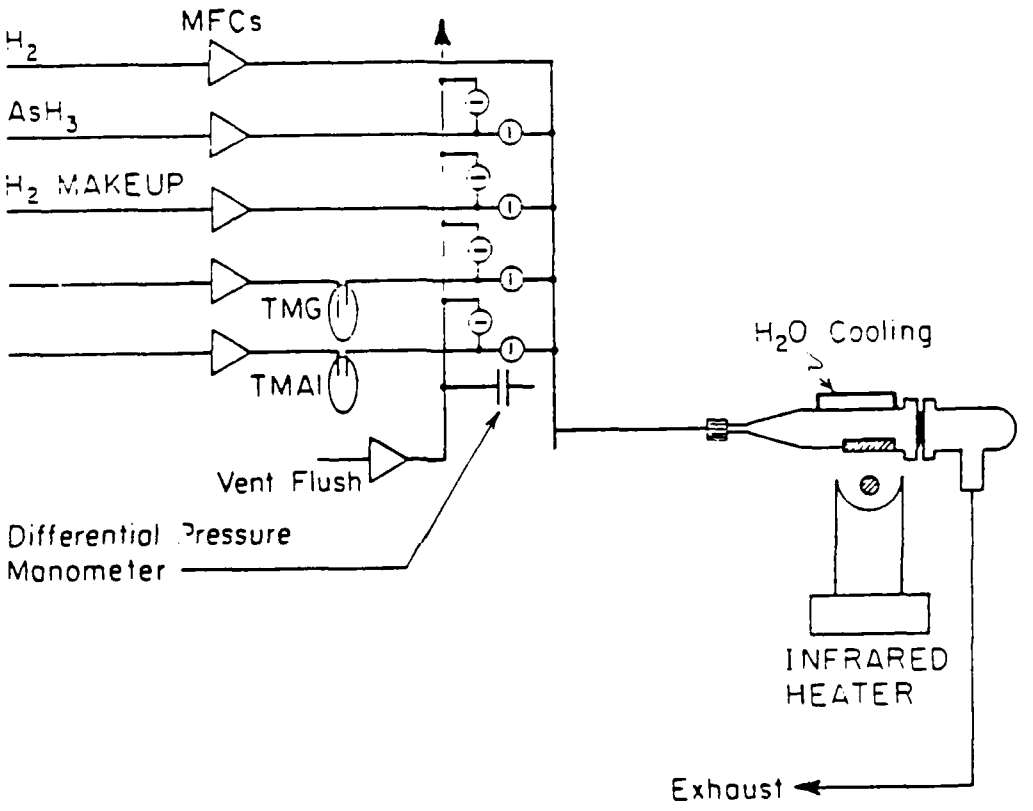

Figure 4.1
Schematic of fast gas switching ALE system. Note pressure-balancing of vent/run lines to minimize gas phase mixing of gaseous precursors.

4.3. Experimental Procedure

Both undoped and Si-doped GaAs, orientated (100)±0.5°, are used as substrates. The cleaning procedure consists of a 5 minute heated bath in separate beakers of trichloroethane(1,1,1), acetone, and methanol. Following a 5 minute 18MΩ deionized (DI) water rinse, the sample is etched in a 3:1:1 (H_2SO_4: H_2O_2:H_2O) solution for 3 minutes to remove polish damage and surface oxides. Finally, the sample is given a 10-minute 18MΩ DI water rinse and then blown dry with filtered nitrogen.

The sample is then loaded onto a graphite susceptor in the horizontal reactor. The quartz chamber is connected to the system with glass-to-metal seals via ultra-Torr O-ring fittings (Cajon, Inc.). The reactor is pumped down to 75 millitorr and back-filled twice with ultra-pure hydrogen to eliminate residual oxygen from the system. After a 1/2 hour hydrogen purge, the sample is heated to 750°C under a arsine overpressure to remove surface oxides. The temperature is monitored with a Alumel-Chromel type K thermocouple (Omega Inc), which is sheathed in a quartz feedthrough. Calibration of the surface temperature on the graphite susceptor is performed at the Al-Si eutectic point (577°C). This is accomplished by monitoring the transition in the surface reflection pattern of 1000Å Al dots on a Si substrate with a He-Ne laser beam.

Growth is initiated by switching the group III metalorganic from the vent line to the run line. Typically, a 5000Å GaAs buffer and 1-2μm AlGaAs layer are grown by conventional MOCVD at 750°C. The thick AlGaAs layer insures that the only luminescence from the subsequent

ALE GaAs layers would be observed. The reactor temperature is then lowered to the surface kinetically controlled growth regime, 500°C or lower. The small thermal mass of the thin graphite susceptor in conjunction with the infrared heating lamp allows rapid 300°C temperature changes with stability after only 3 minutes. ALE layers are then grown by a four step pulsed gas injection method.

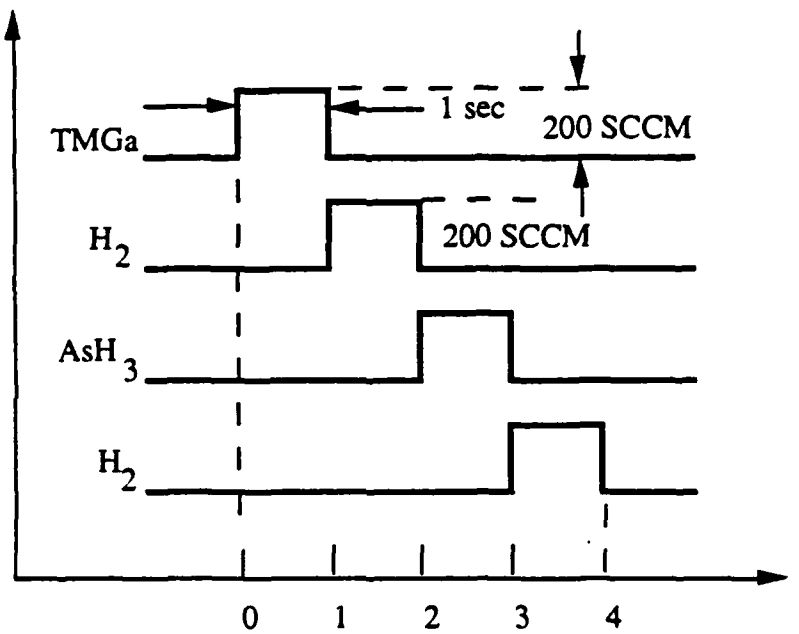

Figure 4.2
Pulsed injection time sequence in four step ALE growth process

As shown in Figure 4.2, the ALE growth sequence consists of a one second pulse of arsine, a one second pure hydrogen purge, a one second pulse of TMGa or TMAl, and a final one second purge of hydrogen.

Since the average gas residence time in the growth chamber is only 0.5 seconds at the high gas flow velocities employed in this work, minimal gas phase mixing of the precursors will occur. This has been confirmed by the observation that longer hydrogen purge times did not change the deposited film thickness.

The effect of several growth variables on the ALE process was studied by growing quantum wells under various ALE conditions with the wells separated by 1 μm MOCVD-grown AlGaAs barriers. The photoluminescence (PL) from each well could be analyzed to determine material's quality and well thickness. For the Argon ion laser excitation wavelength (514nm) utilized in this study the 1/e absorption depth is shorter than 1μm, therefore only photoluminescence (PL) emission from the uppermost quantum well is observed. The typical five single quantum well sample (SQW) sample is shown in Figure 4.3. After obtaining PL from the top well, the sample is then etched with a calibrated etch to within 1000Å of the next quantum well. The etched consisted of a H_2O:H_2O_2:H_2SO_4 mixture in a 80:8:1 ratio. Calibration was confirmed by a surface profiliometer accurate to within 50Å. Utilizing this measurement technique five SQWs of varying growth parameters could be analyzed on the same sample produced in a single run. Layer thicknesses were estimated from peak emission wavelength expected from a Kronig-Penney model of QW emission energies. A complete explanation of the QW emission energy model along with a detailed study of the PL from the ALE QWs is presented in Chapter 5. Accuracy of the

layer thickness determined in this way was confirmed by cleaved corner TEM.

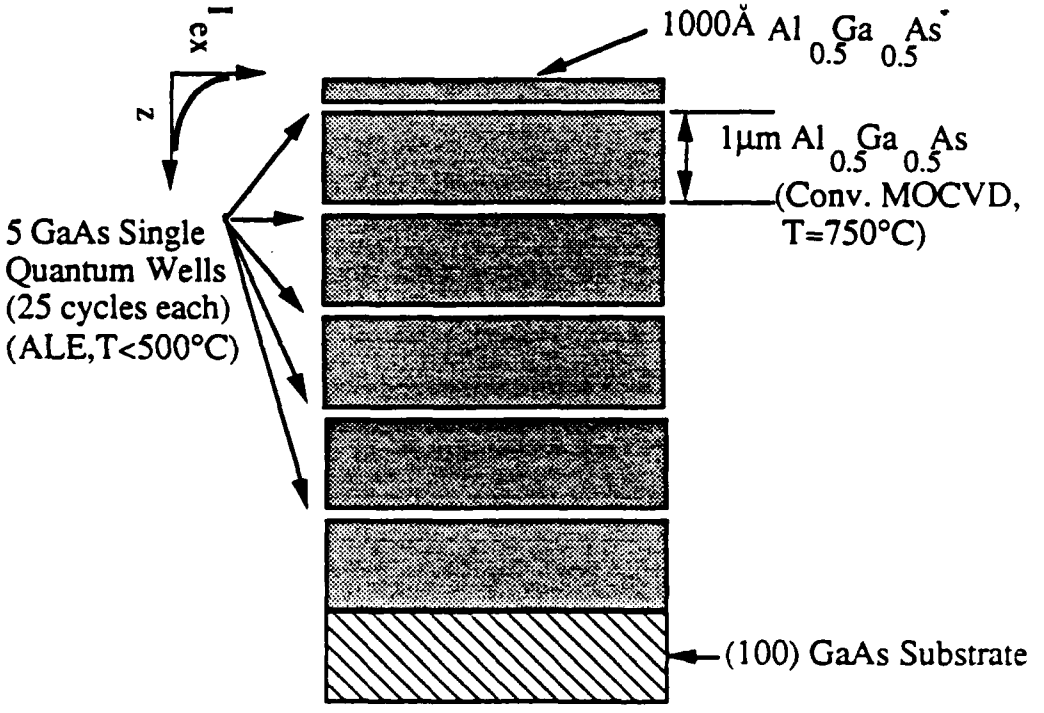

Figure 4.3
Hybrid ALE GaAs/AlGaAs single quantum well sample. Note 1μm thick AlGaAs cladding regions allow separation of PL from the individually grown ALE GaAs quantum wells

4.4 Growth and Characterization

4.4.1 ALE Growth Results

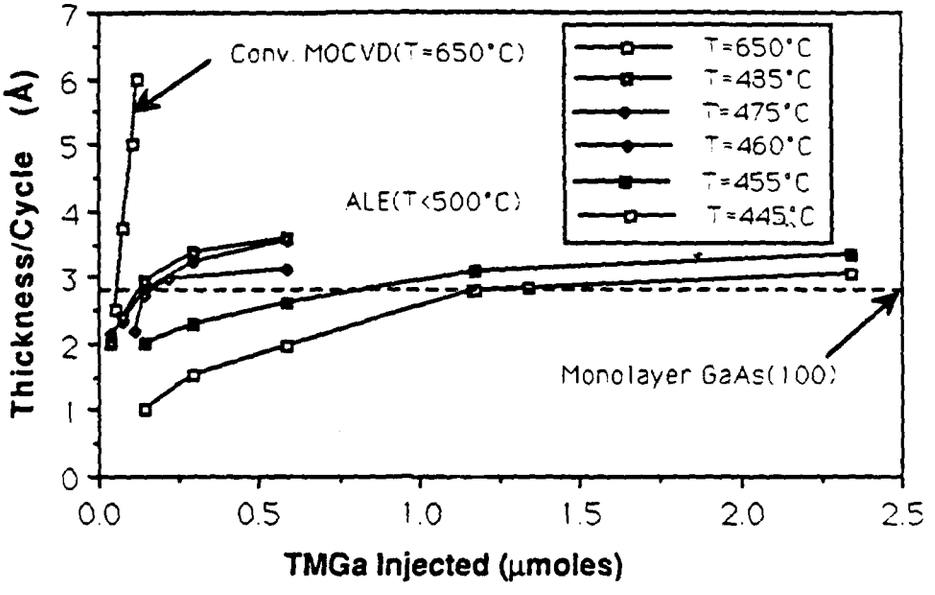

Figure. 4.4.
Comparison of growth rate of GaAs grown utilizing ALE growth regime and conventional MOCVD

Saturated monolayer growth of GaAs has been achieved under conditions where surface reactions dominate the deposition of gallium and arsenic adsorbates. In contrast to conventional MOCVD, in which the growth rate is directly proportional to the TMGa flux in the diffusion controlled regime, the ALE growth rate is strongly sublinear in its dependence on both TMGa and arsine as shown in figures 4.4 and 4.5. The conventional MOCVD data shown in figure 4.4 has been normalized to the same delivery rate as the ALE data to illustrate this point. It is evident that at low temperatures, gas phase reaction rates decrease and

surface kinetics control the growth rate. Note that the growth rate increases linearly with the reactant volume injected during the cycle up to a critical value near one monolayer and then saturates The chemisorption of a Ga methyl species is proposed to explain this saturation with TMGa exposure over the temperature range 445°C-485°C. The fact that the deposited film thicknesses slightly exceed the ideal one monolayer per cycle deposition rate is thought to be caused by the deposition of involatile atomic gallium or incomplete flushing of the reactor. The strong saturation with arsine exposure shown in figure 4.5 indicates that the arsine is not limiting the growth rate and the Ga deposition step is responsible for the non-ideal saturation of figure 4.4.

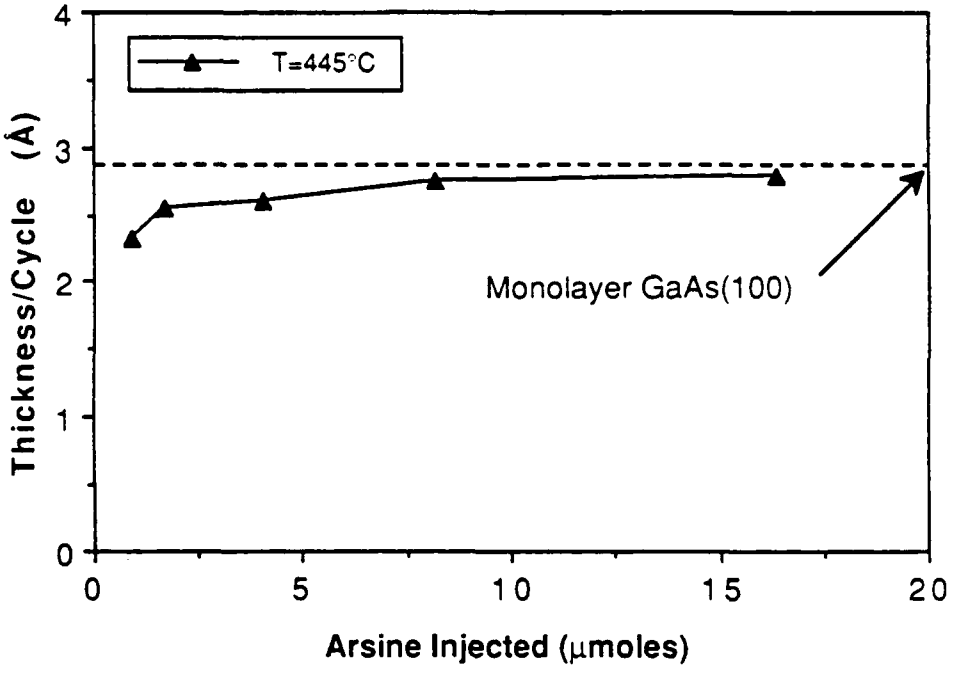

Figure 4.5 .
Growth rate of ALE GaAs layers as a function of arsine injected into reactor.

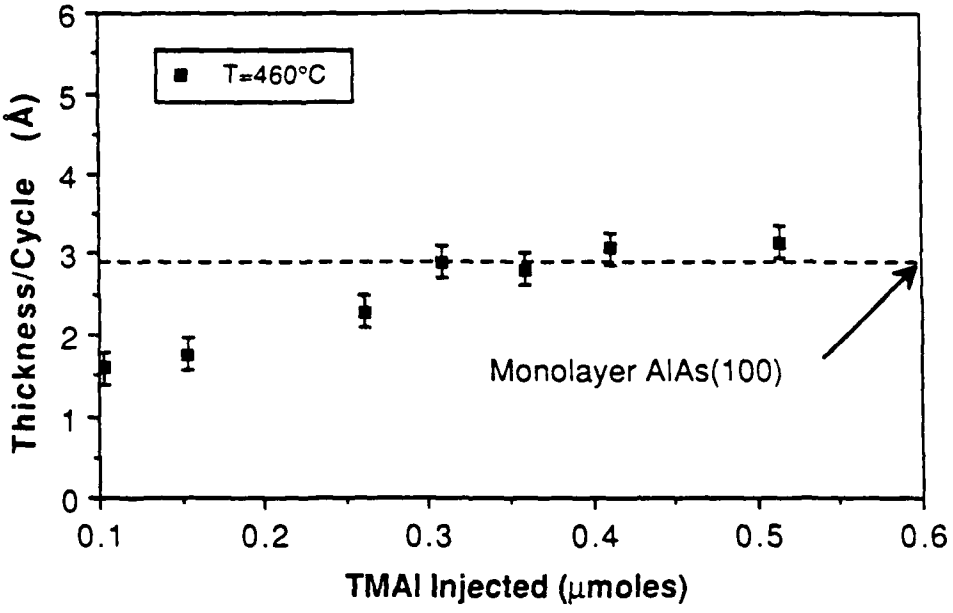

Figure 4.6
Growth rate of AlAs layers grown under ALE conditions as a function of TMAl injected into the reactor.

Deposition of AlAs by ALE also demonstrates a monolayer saturation growth regime as shown by the dependence of growth rate on reactant flux as shown in figure 4.6. Note that the ALE growth rate of AlAs at 460°C saturates at slightly higher TMAl quantities than does GaAs using TMGa at the same temperature. We believe that this is most likely due to the lower decomposition rate constant of TMAl. This suggests that partial gas phase or surface decomposition of TMAl also plays an important role in achieving ALE growth. This is supported by the fact that TMAl is a dimer in the gas phase and one would expect that less TMAl

is needed for saturated growth. ALE of AlGaAs was also achieved by pulsed introduction of the gaseous precursors. Room temperature photoluminescence from both thick AlGaAs ALE layers and quantum wells in which the AlGaAs barrier is also grown by ALE has been studied. The data display the expected behavior, however, low temperature luminescence of ALE AlGaAs exhibits extrinsic luminescence indicating that further optimization of the deposition process is needed for ternary growth.

4.4.2 Digital Growth Nature

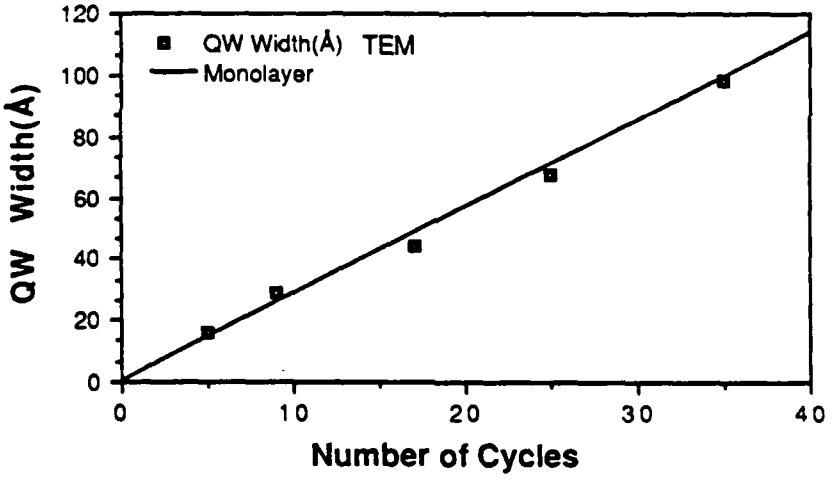

Figure 4.7.
Film thickness dependence on number of ALE deposition cycles demonstrates "digital" nature of ALE growth process.

The "digital"nature of the ALE growth process is best illustrated by the dependence of deposited film thickness on the number of deposition cycles as shown in figure 4.7 where the solid line corresponds to perfect

monolayer deposition per cycle. Layer thickness measurements for this illustration were performed by cleaved corner TEM which is accurate to within 10% at the magnification used. Under the conditions identified in figures 4.4 and 4.5, the grown thickness becomes relatively insensitive to the source gas pressure and the total thickness is determined solely by the number of ALE cycles. Therefore, in comparison with molecular beam epitaxy (MBE) and MOCVD, ALE can be considered a "digital process" since it does not require the precise control of such analog parameters as growth time and reactant flux.

4.4.3 Thickness Uniformity

Excellent layer thickness uniformity is one of the inherent advantages expected from using the self-limiting monolayer growth mechanism in the ALE process. We have realized excellent QW thickness uniformities through the use of the ALE deposition process. Figure 4.8 shows the spatial variation in the ALE GaAs quantum well thickness as a function of distance along the gas flow direction. The QW width variation across the wafer was measured by focusing the excitation laser to a 300μm diameter spot and measuring the peak emission energy shift as function of spot position. A quantum well grown by conventional MOCVD on the same untilted susceptor exhibited a 20-30% variation in layer thickness due to the gas depletion of TMGa along the gas flow direction. This figure demonstrates the inherent benefits to uniformity that the surface saturated growth mechanism operative in the ALE

process affords. Therefore, ALE liberates the crystal growth process from the hydrodynamic concerns that plague conventional MOCVD reactor designs. This is of particularly importance in the mass-production of multiple wafers with good uniformity.

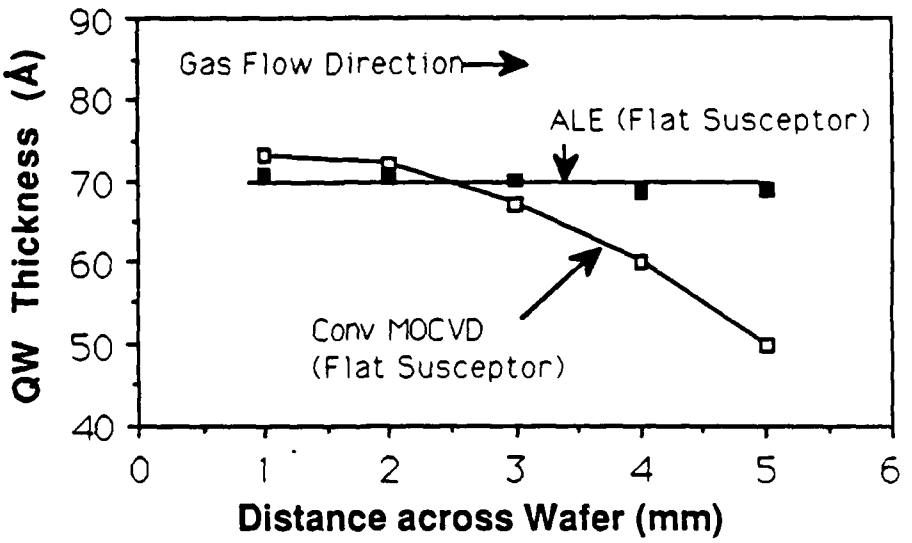

Figure 4.8
QW thickness versus wafer position for quantum wells grown by conventional MOCVD and ALE.

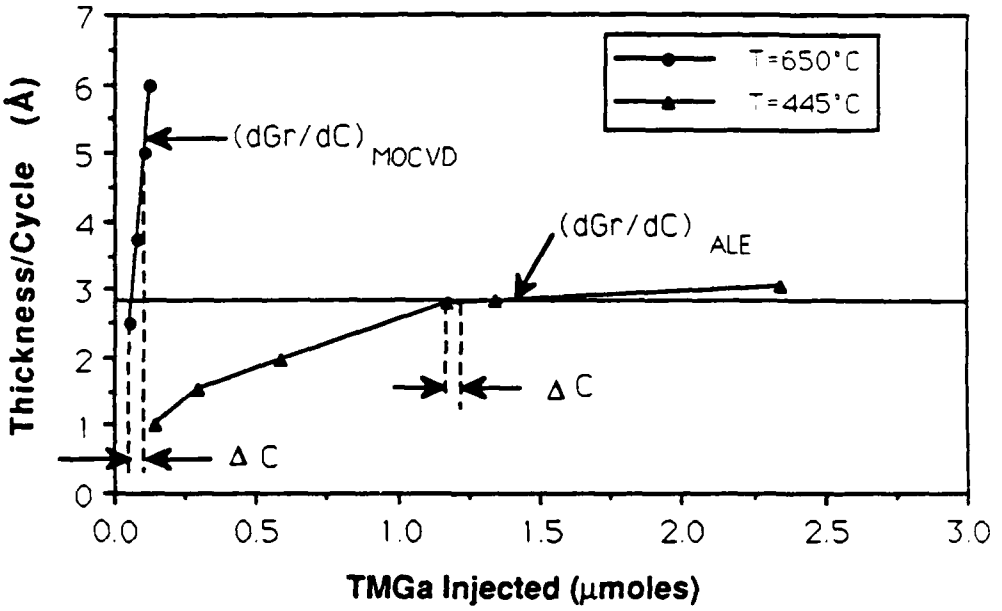

Figure 4.9
The saturated growth mechanism operative in ALE makes the growth rate relatively insensitive to concentration fluctuations.

The excellent thickness uniformities obtainable from ALE, in comparison to conventional MOCVD, can be further explained by analysis of the growth data. As shown in figure 4.9 the slope of the growth rate versus TMGa injected, (dG_r/dC_{TMGa}), gives a measure of sensitivity of the process to concentration changes. From this graph we can deduce that the ALE process is 230 times less sensitive to concentration fluctuations than conventional MOCVD. For a given gas concentration difference "ΔC" caused by the gas depletion effect along the gas flow direction we can calculate the corresponding thickness uniformity by the following equation:

$$\left(\frac{\Delta T}{T}\right) = \left(\frac{\Delta C\left(\frac{\partial G_r}{\partial C}\right)}{G_r}\right) \qquad (4.1)$$

From figure 4.9 we can determine the sensitivity of the growth rate to reactant concentration:

$$\left(\frac{\partial G_r}{\partial C}\right)_{MOCVD} = \frac{57.5A}{\mu moles}$$

$$\left(\frac{\partial G_r}{\partial C}\right)_{ALE} \approx \frac{0.25A}{\mu moles}$$

For a gas concentration depletion of just 0.02μmoles this results in 32.9% thickness change across the wafer for conventional MOCVD. In contrast, for the same concentration fluctuation ALE will theoretically yield excellent uniformity control with a thickness variation of **just 0.14%**!

4.4.4 Cleaved Corner TEM

Epitaxial layer thickness measurements of the GaAs quantum wells are made by transmission electron microscopy (TEM) analysis of the freshly cleaved single crystal corner and photoluminescence emission energy from the individual wells. Utilizing the natural (110) cleavage planes in GaAs, it is possible to obtain an extremely sharp corner, the thinnest portion of which can be penetrated by the electrons. Thus by orienting the edge of the sample at 45° with respect to the electron beam, a thin area exists near the corner allowing TEM analysis of layers in the cross section. Figure 4.10 illustrates the geometry of the TEM imaging conditions. This is relatively new technique,[1] which eliminates the time consuming sample preparation usually required for TEM evaluation of semiconductor layer thickness measurements. Evaluation by corner TEM and photoluminescence results confirm that the ALE growth process is controlled at the atomic level. Analysis of ALE AlAs films was performed by cleaved corner TEM, SEM and angle lapping measurements of thicker layers.

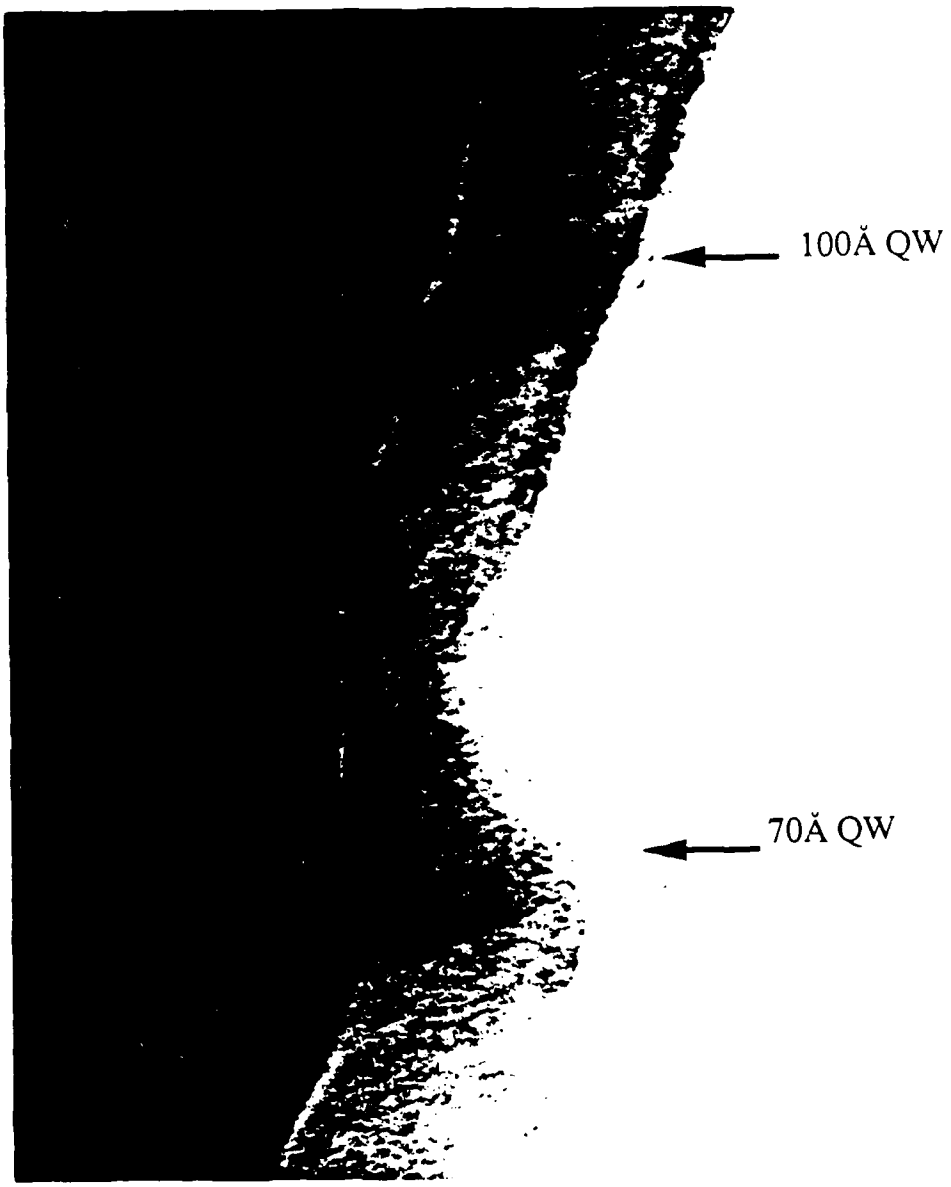

Figure 4.10
Cleaved-corner transmission electron micrograph of two ALE grown GaAs quantum wells (MAG=1,200kX)

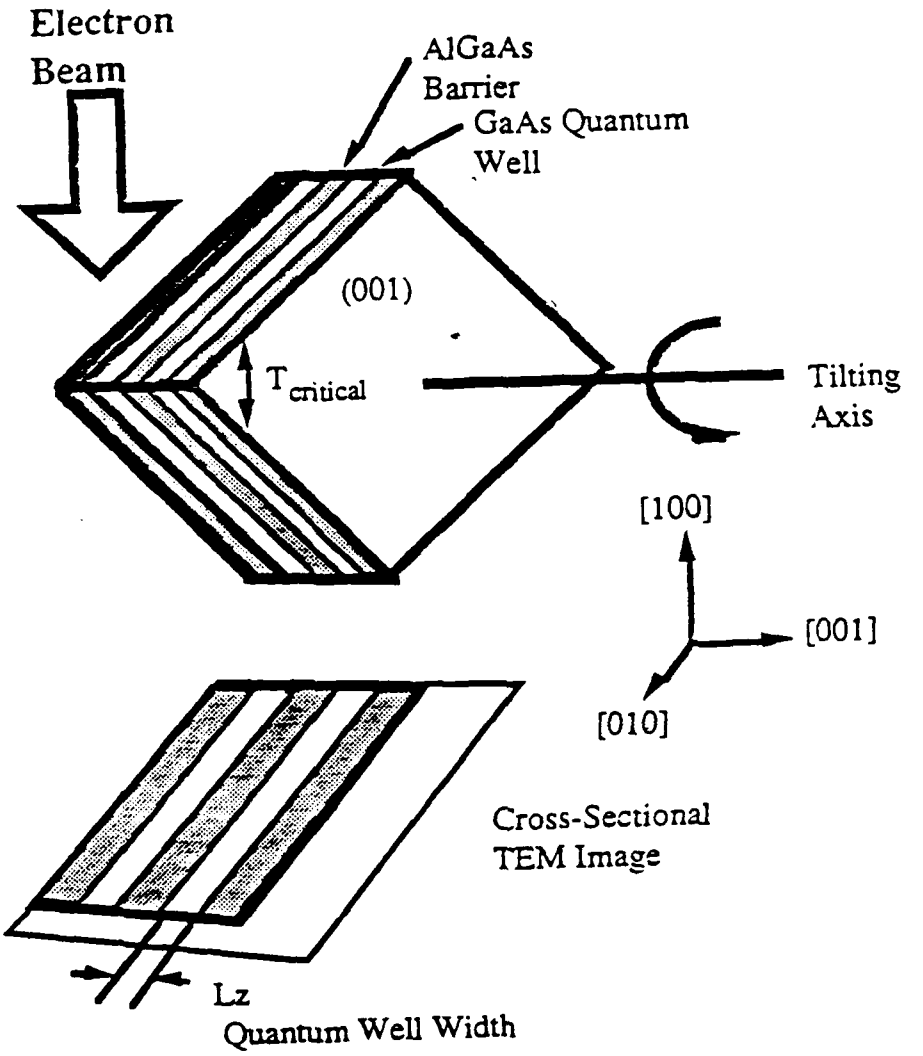

Figure 4.11
Schematic illustration of geometry of imaging conditions utilized in cleaved-corner TEM evaluation of GaAs/AlGaAs sample (modified from Kakibayashi et al.).[2]

4.4.5 SEM Evaluation of ALE layer thickness

Scanning Electron Microscopy has been used to verify the monolayer deposition nature of the ALE process. Accurate SEM measurements can be made by growing thick ALE GaAs and AlAs layers 1000-1500Å thick, and confining them between AlGaAs or GaAs for contrast. Figure 4.12 shows a typical structure consisting of three ALE AlAs with GaAs cladding regions, in which the ALE layers are grown under varying TMAl fluxes. In this structure, each layer was grown at 460°C with twice the TMAl flux of the layer preceding it. For fluxes above the critical amount, the layer thickness saturate at the expected monolayer deposited thickness of 1500Å for 530 cycles

4.4.6 Morphology ALE GaAs

The surface morphology of GaAs grown by ALE is smooth with mirror-like surfaces. Figure 4.13 shows the surface of a 1 micron GaAs sample grown by ALE at 460°C. The defect on the left side is typical of our conventional grown GaAs and is thought to be cause by a defect or particulate matter at the interface between the grown layer and susceptor. The smoothness of the surface surrounding the defect provide evidence that Ga is not balling up on the surface. If the growth temperature is too high, we violate the conditions under which the surface saturation growth mechanism dominates; therefore, deposition of involatile gallium occurs and we observe dendritic growth. Figure 4.14 shows an SEM of dendritic growth occurring on a sample grown by ALE at 540°C

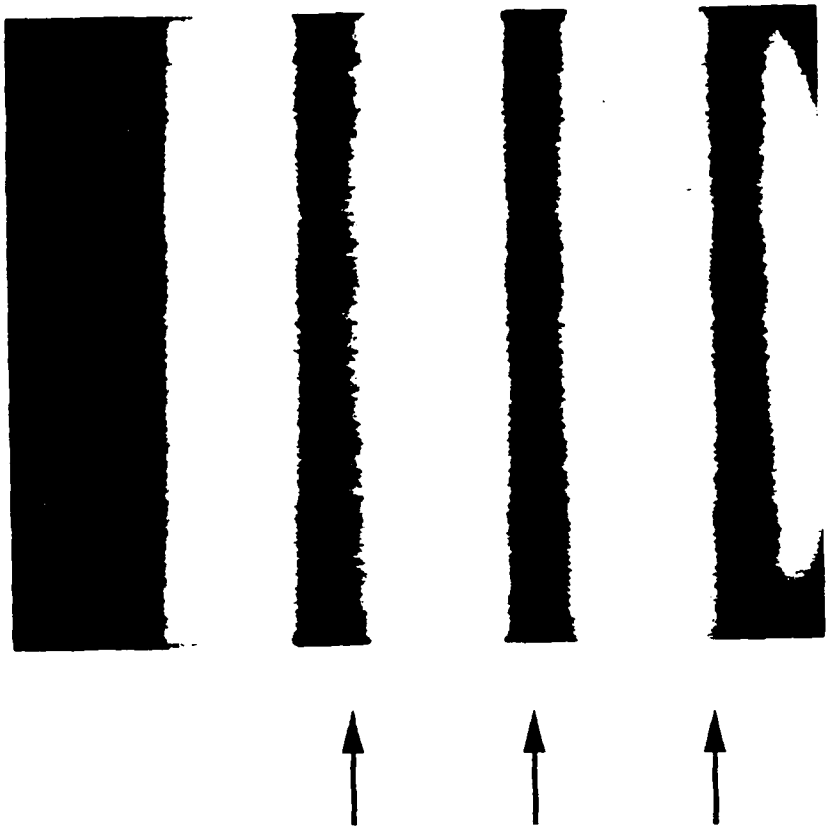

Figure 4.12
SEM micrograph of 3 ALE AlAs layers with GaAs cladding regions.
Each layer is grown with twice the TMAl flux of the layer preceding it.
(MAG=56kX)

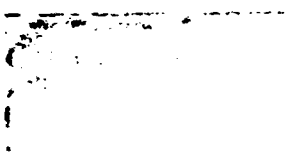

Figure 4.13
Smooth surface morphology of 1μm thick GaAs grown
by ALE at 460°C.

Figure 4.14
Surface morphology of ALE layers grown above 500°C exhibit dendritic growth indicative of excess Ga (SEM 5kX).

4.4.7 Electrical Characterization

In order to perform electrical characterization of the epitaxial layers at least 1μm of material is needed to compensate for the depletion depth created by the electric field from the ohmic contacts. Because of the slow growth rate in ALE (0.71Å/sec), only a few thick samples were grown for electrical characterization. These samples required 3533 ALE cycles and took approximately 4 hours to grow. Hall measurements at room temperature and 77K were performed on 1 μm thick ALE GaAs layers using the Van der Pauw technique.[2] Ohmic contact was made to these samples by alloying Indium-Zinc (99%In-1%Zn) dots. As listed in Table 4.1, all ALE layers exhibit high p-type background carrier concentrations with low mobilities. This high p-type background doping has been observed in all the previous studies of ALE GaAs.[3,4] Methyl radicals adsorbed on As sites are thought to lead to p-type doping in MOCVD.[5] Therefore, incompletion of the surface reaction between the gallium methyl adsorbate and arsine would lead to the p-type doping observed in ALE films.

Recently Colas et al.[6] have obtained significantly lower background doping, n-type $3x10^{15}cm^{-3}$, and higher mobility values of 35,000 $cm^2/V{\cdot}s$ at 77K. The highest mobility samples were found to be grown by using 1/2 monolayer surface coverage of the column III source and no purge after the arsine exposure step. They explain their results by noting that carbon incorporation depends on the effective V/III ratio at the surface. In conventional MOCVD it is well established that an

increase in the V/III ratio results in a decrease in carbon incorporation.[7] Therefore, if no purge follows the arsine step there will be minimal arsine desorption and the V/III ratio is at its peak. These results indicate that with further optimization, the ALE process could possibly grow high purity GaAs. Rather than focussing on electrical properties of ALE, we have elected to optimize ALE for the growth of ultrathin quantum well layers and incorporate these layers in devices. As we will demonstrate in the next two chapters high quality quantum wells and heterostructure devices can be grown by ALE.

Table 4.1 Electrical characteristics of ALE GaAs.

Growth Temperature	Carrier Conc.	Mobility
460°C	$1x10^{17}cm^{-3}$	$240cm^2/V{\cdot}s(300K)$
		$940cm^2/V{\cdot}s(77K)$
500°C	$3x10^{18}cm^{-3}$	$110cm^2/V{\cdot}s(300K)$
		$480cm^2/V{\cdot}s(77K)$

4.4.8 Optical Properties

Strong intense photoluminescence (PL) is observed from the ALE GaAs layers at both room temperature and 4.8K. A cw Argon ion laser (λ=514nm) was used as the excitation source with power densities in the 10-1000mW/cm^2 range. As shown in figure 4.15, low temperature PL spectra exhibits an intense free exciton (FX) peak at 8180Å and impurity related luminescence which can be attributed to carbon. The luminescence intensity observed from ALE GaAs films is approximately equal to that from conventional grown GaAs films at equal excitation powers. This demonstrates that ALE GaAs has good optical efficiency and is not dominated by non-radiative recombination. Therefore, optical devices incorporating ALE layers should exhibit good characteristics.

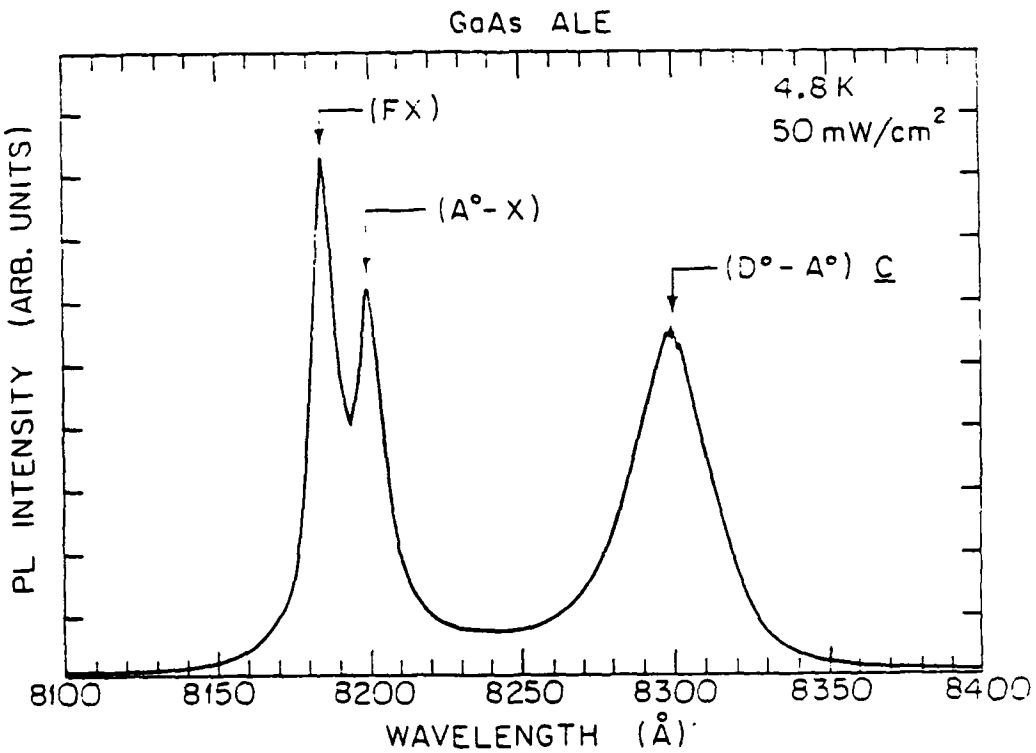

Figure 4.15
Low temperature photoluminescence of ALE GaAs exhibits intense free exciton peak and donor to acceptor (carbon) peak.

4.5 ALE GROWTH MODEL

4.5.1 Proposed ALE Reaction Model

We propose that the self-limiting mechanism operative in the ALE process consists of the partial decomposition of trimethylgallium followed by the chemisorption of the gallium adsorbate on arsenic sites. The most plausible series of reactions occurring in the ALE process are as follows:

$$Ga(CH_3)_{3(v)} \rightarrow Ga(CH_3)_2 + CH_{3(v)} \quad (4.2)$$

$$Ga(CH_3)_{2(v)} \rightarrow Ga(CH_3) + CH_{3(v)} \quad (4.3)$$

$$Ga(CH_3)_{(\text{chem. ads.})\text{As site}} + AsH_{3(s/v)} \rightarrow GaAs_{(s)} + CH_{4(v)} + H_{2(v)} \quad (4.4)$$

This view is supported by our experimental observations along with the recent research of several other groups. Upon injecting arsine onto a gallium adsorbate saturated surface, Nishizawa et al.[8] observe the release of methane into the vapor phase. In another study,[9] ALE growth is observed to occur on the arsenic terminated (111)B plane, but no growth was observed on the gallium terminated (111)A plane. Therefore, the gallium methyl complex may adsorb on arsenic atoms but it does not adsorb on Ga atoms at the surface. In Chapter 3, data was presented which indicated that TMGa decomposes in two stages. In the first stage, which occurred in the temperature range 380°C - 440°C in the decomposition experiments, TMGa sequentially loses two methyl radicals in rapid succession. The third methyl radical is lost only in the second

stage at higher temperatures to release atomic Ga. Thus it is likely that the partial gas or surface phase decomposition of TMGa in H_2 at the temperatures and times employed here (1 sec) for ALE will result in the formation of CH_3Ga. The saturated monolayer growth we have observed suggests that the adsorbed species must retain some of the organic radicals to remain volatile enough to allow only one monolayer to be chemisorbed and avoid the deposition of excess Ga. This is confirmed by the fact that other researchers observe the formation of Ga droplets at higher temperatures.[10] Therefore we conclude that CH_3Ga is the surface adsorbed species in our experiments. Figure 4.16 illustrates the surface reactions which we believe lead to the self-limiting growth observed in the ALE process.

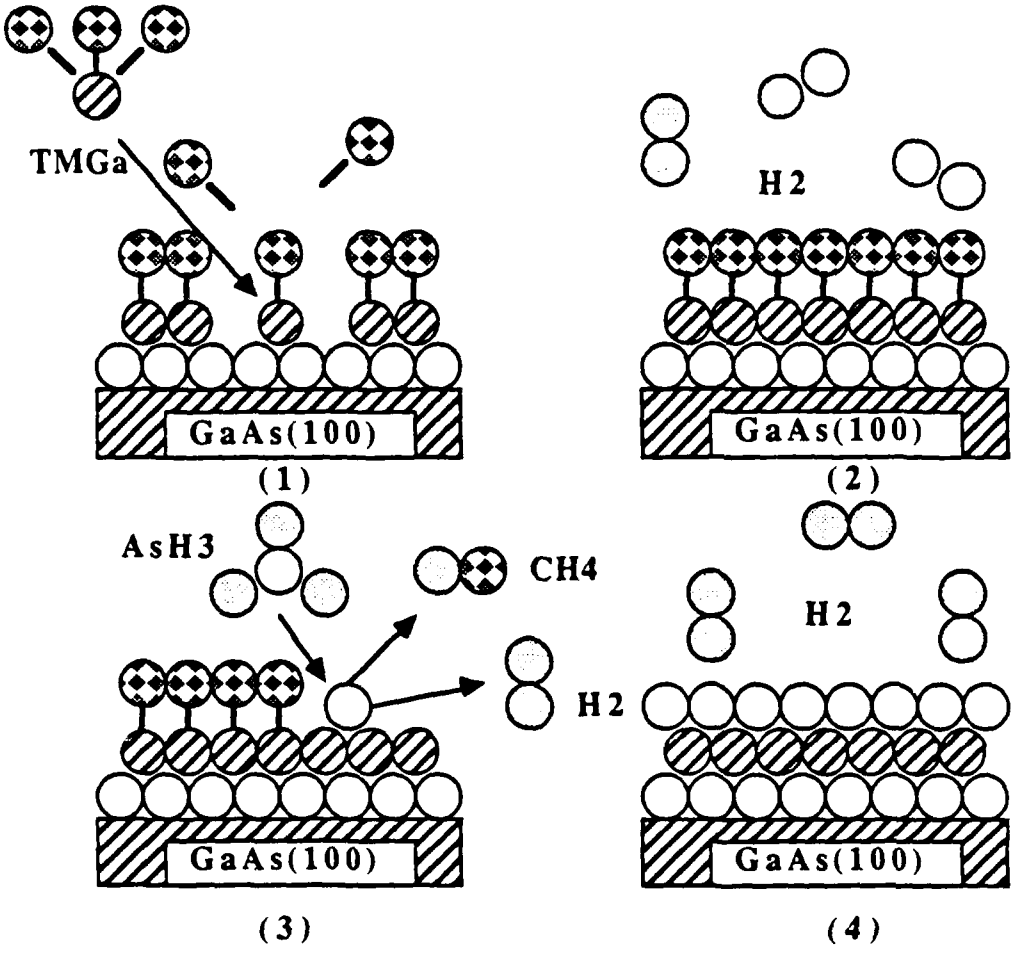

Figure 4.16
Schematic illustration of the growth model showing Gallium-methyl radicals chemisorbed on the surface. Layer growth is completed by the surface reaction of AsH_3 with the gallium adsorbate.

4.5.2 Calculated Surface Coverages

To achieve atomic layer epitaxy the deposited number of atoms should be approximately equal to the surface density in the plane of interest. The surface density of atoms in the (100) plane of GaAs is

$6.26x10^{14}$ atoms/cm^2. Using Fick's equation for flux through the boundary layer, equation 2.7 Chapter 2, we can get a measure of the excess surface coverage of TMGa on the GaAs surface The amount of surface coverage "Θ" can then be estimated by divided the flux of molecules to the surface by the surface site density. As shown in Table 4.2, the surface densities of TMGa provided for observed perfect monolayer coverages (Θ=1), are in excess of the available surface sites at all the temperatures over which saturated growth was observed. Therefore, it appears that a temperature activated process is necessary to drive the chemisorption of a gallium adsorbate.

Table 4.2 Excess Surface Coverages(Θ)

Temp. (°C)	TMGa Injected for Θ=1	TMGa Flux	Surface Coverage Θ
485	0.13μmoles	$5.38x10^{16}$molecules/cm^2 sec	1.3
460	0.26μmoles	$1.08x10^{17}$molecules/cm^2 sec	2.6
445	1.3μmoles	$5.40x10^{17}$molecules/cm^2 sec	13

Further evidence of a temperature driven adsorption process is the fact that the actual number of collision of the TMGa molecule with each surface site yields an even greater value of excess surface saturation. The impinging collision rate "R_i" of molecules on the surface can be determined from the average speed of the molecules in the gas phase and the number density of TMGa. If we assume that the thermal energy of the gas is equal to the total kinetic energy of all moving particles, then the

impinging rate of molecules on a planer surface at any given temperature T_m can be expressed as:[11]

$$R_i = \frac{N_g}{4}\sqrt{\frac{8kT_m}{\pi M}} \tag{4.5}$$

where: N_g is the gas phase density of column III molecules/cm^3, M is the molecular weight of the column III source, T_m the mean reactor temperature. The amount of excess collisions per site "#Θ" is then given by the impinging rate R_i time the exposure time "τ", divided by the surface site density N_S.

$$\#\theta = \frac{R_i \tau}{N_s} \tag{4.6}$$

For the partial pressures of TMGa utilized in our study the number of excess collisions for each surface site is from 800-8000. Thus it is obvious that the ALE process is not limited by simply the supply of available reactant, but rather by kinetics of the surface adsorption process.

4.5.3 Kinetic Models of ALE Process

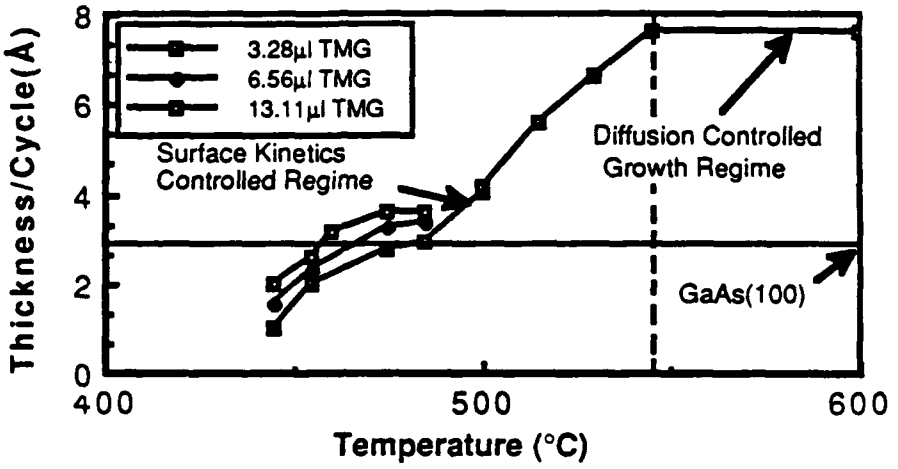

Figure 4.17
Effect of temperature on growth rate in surface reaction controlled ALE growth regime.

4.5.3.1 ALE Growth Model 1

The observation of increasing surface coverage with increasing temperatures is contrary to normal adsorption models. When the species is physisorbed on the surface, the temperature dependence of Θ is controlled by the rate of desorption, k_{des}, and $d\Theta/dt$ decreases with increasing temperature. The data of figure 4.17 show the opposite trend. This indicates that the adsorbed species are chemisorbed and that rate of adsorption, k_{ads}, controls the temperature dependence of Θ.This trend is

illustrated in figure 4.17. Therefore, we expect that k_{ads} will be dependent upon some gas phase or surface reaction that is more strongly activated than the surface desorption process.

We propose that a two process model occurs in thermally driven atomic layer epitaxy. The first step is the thermal decomposition of TMGa which generates gallium methyl radicals. The second step is the adsorption of the reactive species, which saturates with increasing partial pressures because of the limited adsorption sites. We assume that the diffusive flux of the adsorbate is proportional to the reactant concentration in the gas phase, C_{TMGa} (atoms/cm^3), proportional to the gas phase or surface reaction rate that produces the adsorbate, k_g (sec^{-1}), and proportional to the diffusion distance which we take to be the boundary layer, δ (cm). The effective adsorption is given by

$$k_{ads} = \frac{\delta \, k_{TMGa} C_{TMGa}}{N_s} \tag{4.7}$$

where N_S is the atomic surface site density in cm^{-2}.

The saturated ALE growth data from figures 4.4-4.6, along with the observed temperature dependence, can be qualitatively explained by a first order adsorption model which takes into account the temperature activated generation of a gallium adsorbate. We describe the rate of

surface coverage ($d\Theta/dt$) as the difference between a surface adsorption rate, k_{ads}, and a surface desorption rate, k_{des}.

$$\frac{d\theta}{dt} = k_{ads}(1 - \theta) - k_{des}(\theta) \tag{4.8}$$

Integration leads to a simple Langmuir adsorption isotherm for the surface coverage.

$$\theta = \left(\frac{k_{ads}}{k_{ads} + k_{des}} \right) \left[1 - \exp\left[- \left(k_{ads} + k_{des} \right) t \right] \right] \tag{4.9}$$

where both k_{ads} and k_{des} are functions of temperature.

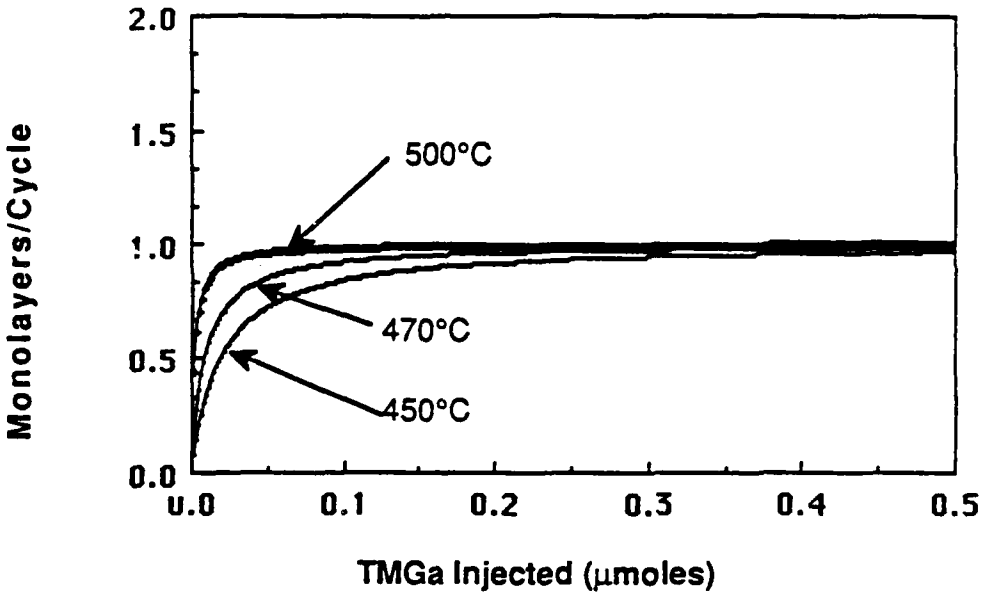

Figure 4.18
First order model predicts self-limiting growth in the same temperature range as observed experimentally.

Figure 4.18 shows the computer generated curves for the first order adsorption model. Using the measured rate constant for removal of the first methyl group from TMGa presented in Chapter 3, we observe that the model predicts self-limiting growth in the same time and temperature range as was observed experimentally. However, a more accurate model should take into account the non-ideal saturation observed experimentally.

4.5.3.2 ALE Growth Model 2

To account for the observed deviation from perfect monolayer growth we introduce a rate expression (k_{Ga}) which predicts the amount of involatile Ga produced by the pyrolysis of monomethylgallium. The rate of deposited Ga will be independent of surface coverage since it has a low vapor pressure and can not evaporate as readily as the gallium methyl complex. The first order adsorption model is then corrected to the following expression:

$$\frac{d\theta}{dt} = k_{ads}(1 - \theta) - k_{des}(\theta) + k_{Ga} \tag{4.10}$$

Where:

$$k_{Ga} = \frac{\left(\delta\, k_{MM} C_{MM}\right)}{N_s} \tag{4.11}$$

k_{Ga} utilizes the activation energy (-77.5 kcal/mole) required for the removal of the third methyl radical from TMGa which determined by Jacko and Price.[12] The frequency factor"A" for the rate constant k_{MM} in hydrogen was estimated by setting the relative concentration of the third methyl group to 99% at 460°C, as was observed in figure 3.9. Integration of equation 4.11 leads to the following adsorption isotherm for the surface coverage (See Appendix A for Integration).

$$\theta = \left(\frac{k_{Ga} + k_{ads}}{k_{ads} + k_{des}}\right)\left[1 - \exp\left[-\left(k_{ads} + k_{des}\right)t\right]\right] \tag{4.12}$$

The concentration of monomethylgallium(C_{MM}) can be estimated from an earlier kinetic study in which removal of the first methyl from TMGa was observed to be the rate limiting step.

$$C_{MM}=N_g\{1-\exp[-k_{TMGa}\,\tau]\} \qquad (4.13)$$

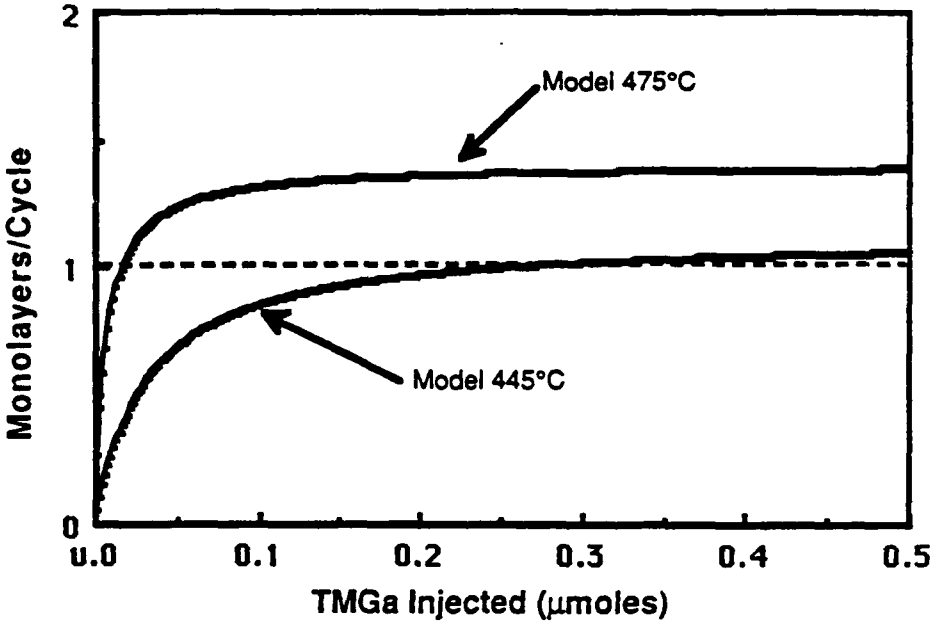

Figure 4.19
ALE growth rate as predicted by first order adsorption model with added deposition term accounting for decomposition of monomethylgallium to involatile gallium.

Utilizing the rate constants shown in Table 4.2 which have been determined from previous results published in the literature[13,14] we can then model the ALE deposition process. As shown in the calculated curves of Figure 4.19, we have been able to qualitatively explain the observed ALE growth behavior. We have also used the pyrolysis rate constant for the decomposition of arsine on the catalytic GaAs(100) surfaces with a first order adsorption model. As shown in Figure 4.20 below, there will be sufficient arsine adsorption for monolayer coverage until the temperature drops below 350°C.

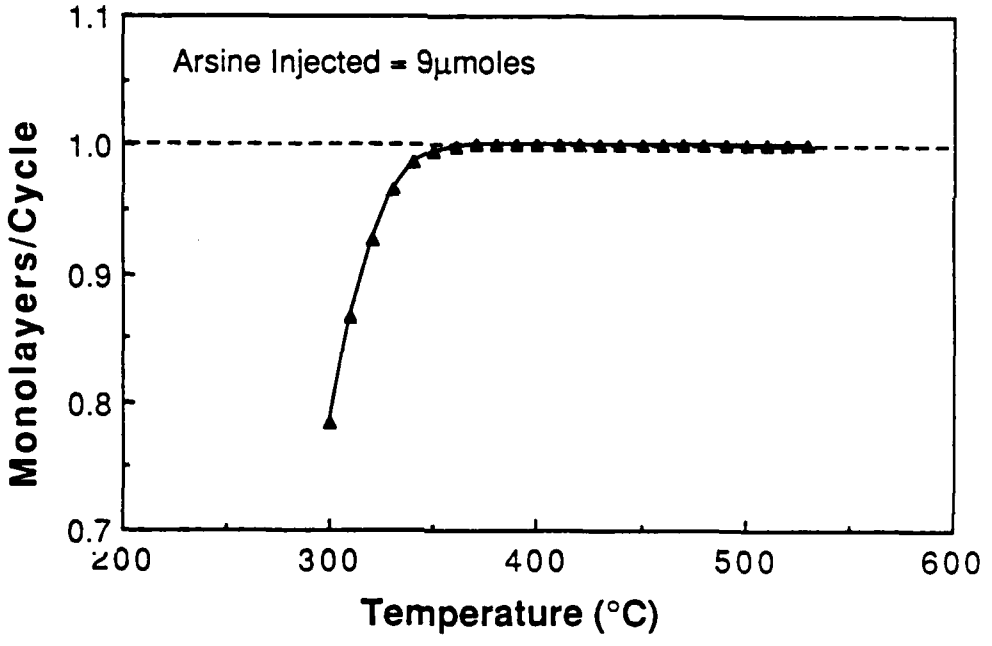

Figure 4.20
Monolayer coverage from arsine adsorption model.

Table 4.3 Rate Constants
$k_{TMGa} = 1 \times 10^{18} \exp\left(-\frac{60kcal}{RT}\right)$
$k_{MMGa} = 5 \times 10^{22} \exp\left(-\frac{77.5kcal}{RT}\right)$
$k_{des} = 333 \exp\left(-\frac{4.6kcal}{RT}\right)$
Arsine on GaAs(100) Surfaces
$k_{AsH_3} = 5.2 \times 10^{3} \exp\left(-\frac{18kcal}{RT}\right)$

4.5.3.3 Boundary Layer

The width of the boundary layer will determine the amount of gas heated to the reaction temperature. For laminar flow across a flat plate and assuming a typical velocity profile of the form:

$$v_x = az + bz^3 \tag{4.14}$$

the thermal boundary layer can be expressed as:[15]

$$\delta(x) = 4.64\sqrt{\frac{x(\nu')}{V_\infty}} \tag{4.15}$$

where x is the distance along the plate from the leading edge, V_∞ is the average gas velocity, and v' is the kinematic viscosity. For a hydrogen carrier gas stream at a temperature of 455°C the kinematic viscosity is 1.51cm^2/sec. For our model we use the average boundary layer thickness across the substrate which we calculate to be 0.68cm (See Appendix B for calculations).

4.5.4 Kinetics of ALE in Nitrogen

To test our kinetic model we have performed ALE growth of GaAs in an N_2 ambient. The data of figure 4.21 show the dependence of the growth rate in N_2 at 500°C as a function of the TMGa exposure. Also shown for comparison is the growth rate data for ALE growth in H_2 at 455°C. Note that the growth rate in N_2 saturates at a thickness considerably less than the lower temperature growth in H_2. This can be explained by the fact that the decomposition rate for TMGa in N_2 is known to be suppressed relative to a H_2 carrier gas because N_2 is nonreactive with the TMGa and has a lower thermal conductivity.[16] As shown in figure 4.22, there is approximately an 80°C temperature difference necessary in nitrogen to obtain the same pyrolysis rate constant. We expect that gas phase reaction rates are depressed in N_2, but not surface. The data of figure 4.21 are consistent with a picture of the gallium methyl complex being chemisorbed in our process.

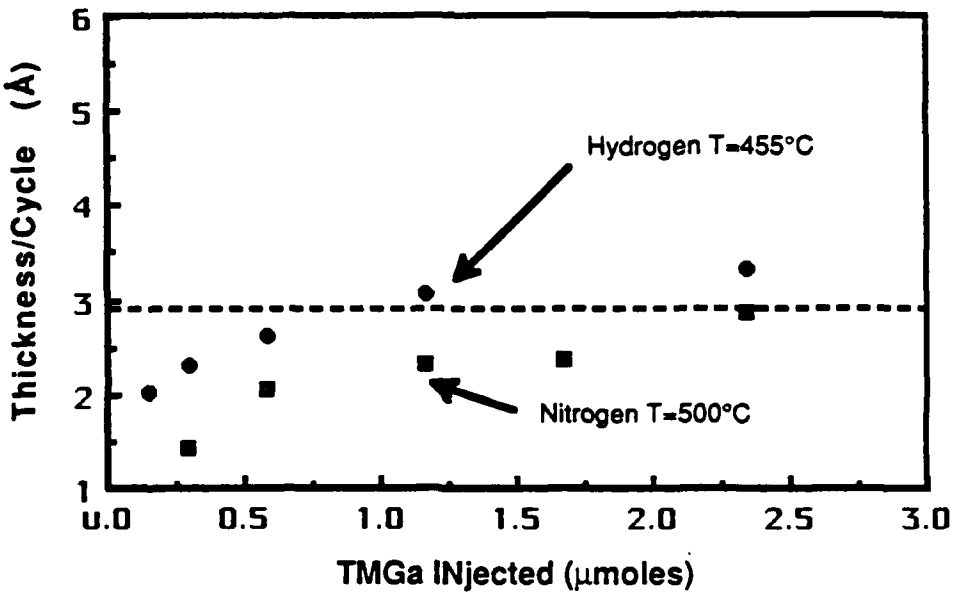

Figure 4.21
Growth rate of ALE GaAs layers in both hydrogen and nitrogen carrier gas ambient as a function of TMGa injected.

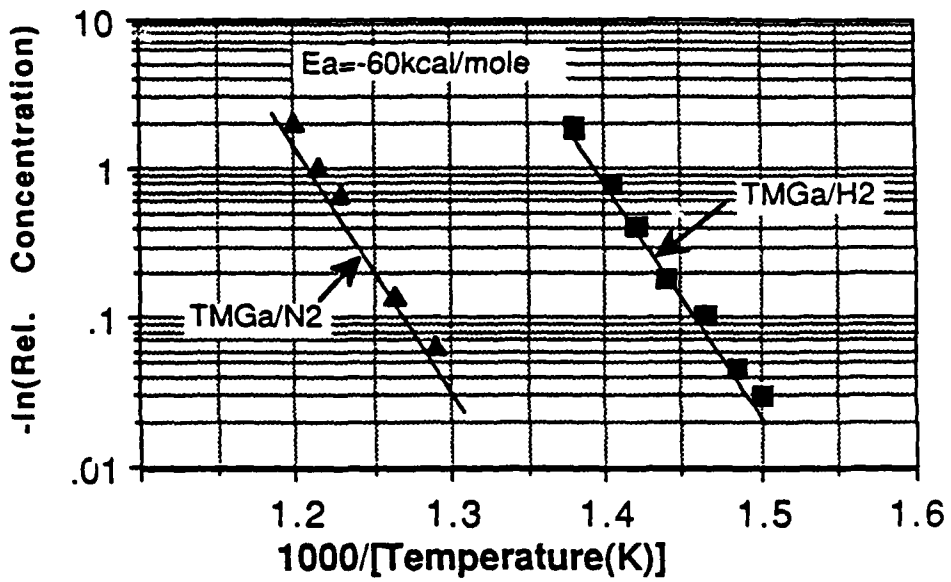

Figure 4.22
Logarithmic plot of the cracking rate of TMGa in nitrogen and hydrogen(data from Yoshida et al.).[17] Note the temperature difference necessary to obtain the same rate constant which corresponds to shift in ALE kinetic temperature range observed in Figure 4.21.

4.6. Conclusions

Saturated monolayer growth of GaAs and AlAs has been observed by using metalorganic precursors at growth temperatures where kinetics of surface reactions dominate the deposition process. We have confirmed some of the inherent advantages of the ALE technique by demonstrating the "digital" nature of the deposition process and growing extremely uniform high quality quantum wells. The data presented distinctly show that ALE proceeds by: the chemisorption of a $Ga(CH_3)_x$ adsorbate (where x is most likely equal to 1), followed by the heterogeneous reaction of arsine with this adsorbate to complete the molecular monolayer. The kinetics for the ALE process have been determined and are shown to behave in accordance with a first order adsorption model. The resultant process, carried out at atmospheric pressure, is compatible with conventional MOCVD and can be used to grow high quality materials and heterostructures by a hybridization of ALE and MOCVD.

REFERENCES-CHAPTER 4

1 H. Kakibayashi and F. Nagata, Surface Sci, **74**, 84 (1986).

2 L. J. Van der Pauw, Philips Res. Rept. **13**, 13 (1958).

3 M. A. Tischler, N. G. Anderson, and S. M. Bedair, Appl. Phys. Lett. **49**, 1199, (1986).

4 J. Nishizawa, T. Kurabayashi, H. Abe, and N. Sakuri, J. Electrochem. Soc. **134**, 945 (1986).

5 T. F. Keuch and E. Veuhoff, J. Crystal Growth, **68**,148 (1984).

6 E. Colas, R. Bhat, and B. J. Skromme,**D-8**, International Symposium on GaAs and Related Compounds, Atlanta, GA (1988).

7 S.Ito, T. Shinohara, and Y. Seki, J. Electrochem. Soc., **120**, 1419 (1972).

8 J. Nishizawa, T. Kurabayashi, H. Abe, and A. Nozoe, Surface Sci., 185, **249** (1987).

9 J. Nishizawa, T. Kurabayashi,H. Abe, and N. Sakurai, J. Electrochem. Soc. **134**, 945 (1986).

10 J. Nishizawa, H. Abe and T. Kurabayashi, J. Electrochem. Soc. **132**, 1197 (1985).

11 G.H. Geiger, D. R. Poirier, Transport Phenomena in Metallurgy, (Addison-Wesley Publishing Co., Menlo Park, CA 1980) p. 8.

12 M. G. Jacko and S. J. W. Price, Can. J. Chem. **41**, 1560 (1963).

13 S. P. DenBaars, B. Y. Maa, P. D. Dapkus, A. D. Danner and H. C. Lee, J. Crystal Growth, **77**, 188 (1986).

14 Y. Aoyagi, A. Doi, S. Iwai, S. Namba, J. Vac. Sci. Technol. **B5**, 1460 (1987).

15 G.H. Geiger, D. R. Poirier, Transport Phenomena in Metallurgy, (Addison-Wesley Publishing Co., Menlo Park, CA 1980) p. 63.

16 M. Yoshida, H. Watanabe and F. Uesugi, J. Electrochem. Soc. **137**, 677 (1985).

17 M. Yoshida, H. Watanabe and F. Uesugi, J. Electrochem. Soc. **137**, 677 (1985).

CHAPTER 5
ATOMIC LAYER EPITAXY OF AlGaAs/GaAs HETEROSTRUCTURES AND QUANTUM WELL LASERS

5.1 Introduction

Recent research efforts have made it clear that heterostructure devices will play an important role in high speed electronics and communications systems. A heterostructure is a material in which a semiconductor with a narrow energy gap is sandwiched between two layers of a wider energy gap semiconductor. Heterostructures offer several physical benefits to electronic and opto-electronic devices such as optical waveguiding, selective absorption, and selective minority carrier injection and confinement. Heterojunction technology has made possible the realization of the continuous room-temperature operation of semiconductor injection lasers at low threshold currents.[1] This elevated the technology from a laboratory curiosity to what has become the key component of the fiber-optic communications systems. Also, the observation of the quantum size effect (QSE) in ultrathin heterostructures has given rise to a whole new generation of electronic and opto-electronic devices.

Advanced heterojunction device concepts that rely on ultra-thin layers and abrupt interfaces require unprecedented control and uniformity of layer properties for high yield implementation. Transistor structures such as high electron mobility transistors (HEMTs) and

modulation doped field effect transistors (MODFETs) have also been shown to be dependent on monolayer level thickness variations.[2] Threshold current density and lasing wavelength of quantum well injection lasers have been found to be extremely dependent upon the active layer thickness.[3] Therefore, active layer thickness uniformity in the range of one to two monolayers is necessary for these devices. Such control is difficult to achieve by conventional epitaxial techniques. Because atomic layer epitaxy operates with a self-limiting monoatomic growth mechanism, it appears to be especially well suited for the growth of these devices with the desired thickness control.

In this chapter we establish that ALE is capable of producing high quality GaAs/AlGaAs quantum well structures. Hybridization of the ALE and MOCVD growth technologies is demonstrated by utilizing ALE to grow the critical ultra-thin layers and MOCVD to grow the thicker AlGaAs regions. We show that under the proper growth conditions, extremely uniform layers of high-quality GaAs can be grown by ALE and that these layers can be incorporated into quantum wells that exhibit intrinsic photoluminescence (PL) at 8K and 300K. We also present results on the first successful demonstration of a device fabricated by ALE in III-V semiconductors. Injection lasers with ALE quantum well active regions operate at room temperature with threshold current densities as low as 380A/cm^2.

5.2 Quantum Well Properties

5.2.1 Calculation of Eigenvalue in finite potential well

A quantum well is the term used to describe a double heterostructure in which the width of the smaller bandgap region is less than the DeBroglie wavelength of the charge carriers (λ_o=280Å in GaAs)[4] in that material. Due to the quantum size effect in these structures , new discrete energy levels arise as shown in figure 5.1. These new discrete eigenvalues for the charged particles, electrons and holes, can be approximated by solving the Schrodinger equation with a finite square potential well:

$$-\left(\frac{h^2}{2m}\frac{\partial^2}{\partial z^2} + V\right)\psi = E\psi \tag{5.1}$$

We derive the energy levels of an electron in a GaAs/AlGaAs quantum well with the barrier height given by the conduction band discontinuity "ΔE_c." An analogous expression can be derived for the holes in the valence band of the well material with the use of the appropriate effective masses and barrier ΔEv. For the electron, the Schrodinger equation becomes:

$$\left(-\frac{h^2\partial^2}{2m_e^*\partial z^2} - \Delta E_c\right)\psi_n(z) = E_{en}\,\psi_n(z) \tag{5.2}$$

where m^*_e is the effective mass of the electron, h is Planck's constant divided by 2π , and E_{en} the energy level of the electron bound state or confined state.

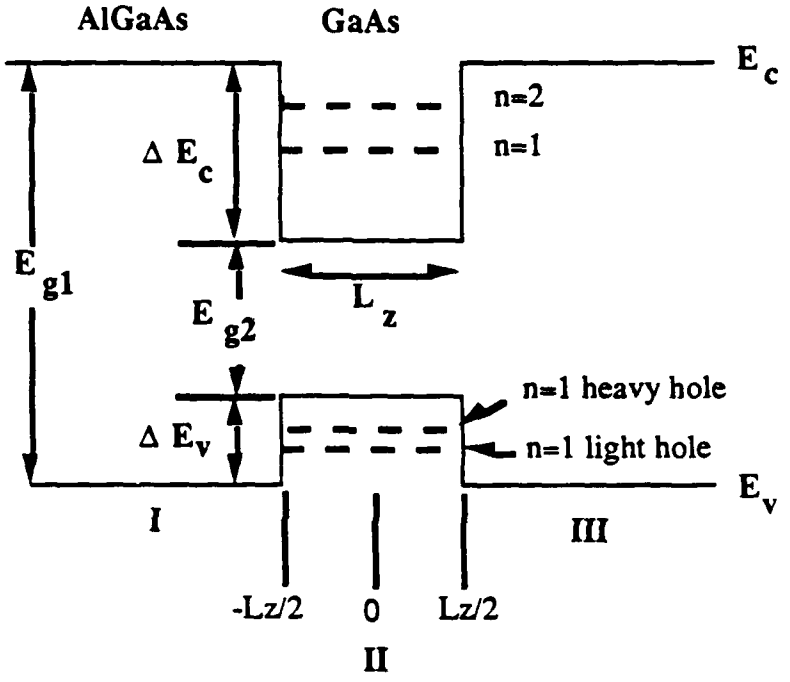

Figure 5.1
Energy band diagram for a GaAs/AlGaAs quantum well structure

The solutions of the eigenvalue equation in the three regions of the heterostructure are:

$$\psi_I = B\exp\left(k_b\left(z + \frac{L_z}{2}\right)\right) \qquad z \le -\frac{L_z}{2} \tag{5.3}$$

$$\psi_{III} = B\exp\left(-k_b\left(z - \frac{L_z}{2}\right)\right) \qquad z \geq \frac{L_z}{2} \tag{5.4}$$

In the well region, the solutions are:

For even parity $$\psi_{II} = A\cos(k_w z) \qquad |z| \leq \frac{L_z}{2} \tag{5.5}$$

For odd pairity $$\psi_{II} = A\sin(k_w z) \qquad |z| \leq \frac{L_z}{2} \tag{5.6}$$

where :

$$k_w = \frac{\sqrt{(2m^*_e(\Delta E_c + E_{en}))}}{\hbar} \tag{5.7}$$

$$k_b = \frac{\sqrt{(2m^b_e(E_{en}))}}{\hbar} \tag{5.8}$$

Where m^*_e and m^b_e are the effective mass of the electron in the well and barrier region,respectively.

There are two types of boundary conditions that can be employed for solution of the eigenvalues in quantum wells. R. Dingle[5] has obtained good agreement of experimental data with a model in which the wavefunction and its first derivative are matched at the interfaces. G. Bastard[6] has proposed that the most appropriate condition at the boundary is that the probability flux is continuous at the interfaces. The continuous flux model accounts for the effective-mass discontinuity at the

interface. For our model we find that continuity of the solutions at the interfaces yield the best fit to both conventional MOCVD[7] and ALE experimental data. Matching solutions and first derivatives of equations 5.3 and 5.4 at the boundary ($z=L_z/2$) yields the transcendental equation for even parity :

$$\tan^2\left[\frac{\sqrt{(2m_e^*(\Delta E_c + E_{en}))}}{\hbar}\left(\frac{L_z}{2}\right)\right] = \left(\frac{m_e^b}{m_e^*}\right)\left(-\frac{E_{en}}{\Delta E_c + E_{en}}\right) \quad (5.9)$$

Similarly we can obtain the equation for odd parity:

$$\cot an^2\left[\frac{\sqrt{(2m_e^*(\Delta E_c + E_{en}))}}{\hbar}\left(\frac{L_z}{2}\right)\right] = \left(\frac{m_e^b}{m_e^*}\right)\left(-\frac{E_{en}}{\Delta E_c + E_{en}}\right) \quad (5.10)$$

These equations are then solved numerically to obtain the eigenvalue E_{en} of the electron bound states. For the eigenvalues of the hole bound states we solve similar eigenvalue equations which utilize the valence band discontinuity "ΔEv". The PL emission energy is given by the transition from the n=1 electron level $E_{1en}(Lz)$ to the n=1 heavy-hole level ($E_{1hh}(Lz)$ minus the exciton binding energy E_{ex}:

$$h\nu_{PL} = E_g + E_{1e}(L_z) + E_{1hh}(L_z) - E_{ex}(L_z) \quad (5.11)$$

The materials parameters, energy dependence of the band gaps, and effective mass values for our model have been reported elsewhere.[8] We use an energy band discontinuity in our calculations in which 65% of the

energy gap difference between the heterojunction materials is attributed to the conduction band discontinuity.

As shown in figure 5.2, there is good fit of the predicted emission energy in comparison to the expected well thicknesses in the range from 50-120Å. Below 50Å, there is some discrepancy between the model and results. At this thickness tunneling of the wavefunction into the AlGaAs barriers becomes significant and further refinement of the wavefunction continuity model is necessary. Many quantum well thicknesses were measured by cleaved corner TEM measurements. Others were estimated by extrapolation of growth rates determined by SEM and angle lapping evaluation of thicker structures. Because there is good agreement of the model with measured well thicknesses at 70Å, all the ALE quantum wells of varying parameters were grown with 25 cycles (2.83Å x 25= 70.75Å). Therefore, all of the 5 QW thicknesses in the ALE study, shown in figure 4.3 of the previous chapter, can be measured relative to each other without the large discrepancies observed in smaller well structures.

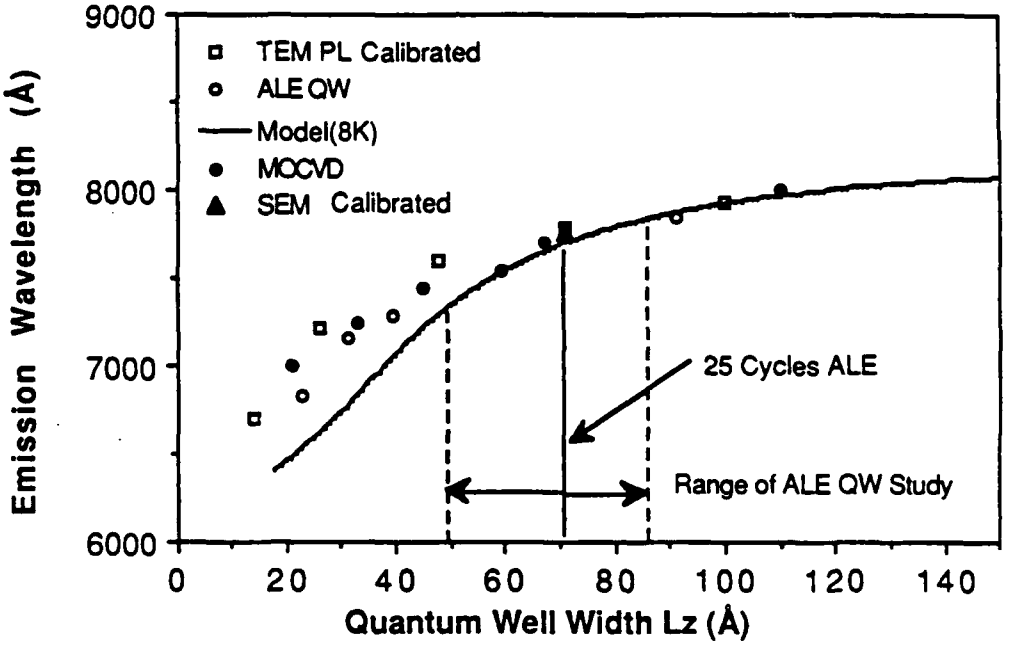

Figure 5.2
Shows the fit of experimental QW data to predicted emission wavelength

5.3 ALE Quantum Wells

Single quantum wells are generally evaluated using low temperature photoluminescence (PL). The linewidth at these temperatures is a measure of the abruptness of the interface. Both the well width and the interface abruptness can be determined by modeling the SQW and comparing the predicted peak energy and linewidth with those measured experimentally. In order to evaluate the quality of ALE grown GaAs for quantum wells a five SQW test sample was studied, as shown schematically in figure 5.3. The five QW's of varying width are arranged such that the thinnest layer is grown last because it does not absorb luminescence from the wider QWs below which produce lower emission energy. The highest quality AlGaAs is produce by conventional MOCVD at high growth temperatures. Therefore, we grew the thick AlGaAs barriers at high temperatures (750°C), the temperature was then lowered to the ALE temperature regime (445-500°C), where the QWs were grown by the pulsed gas injection method.

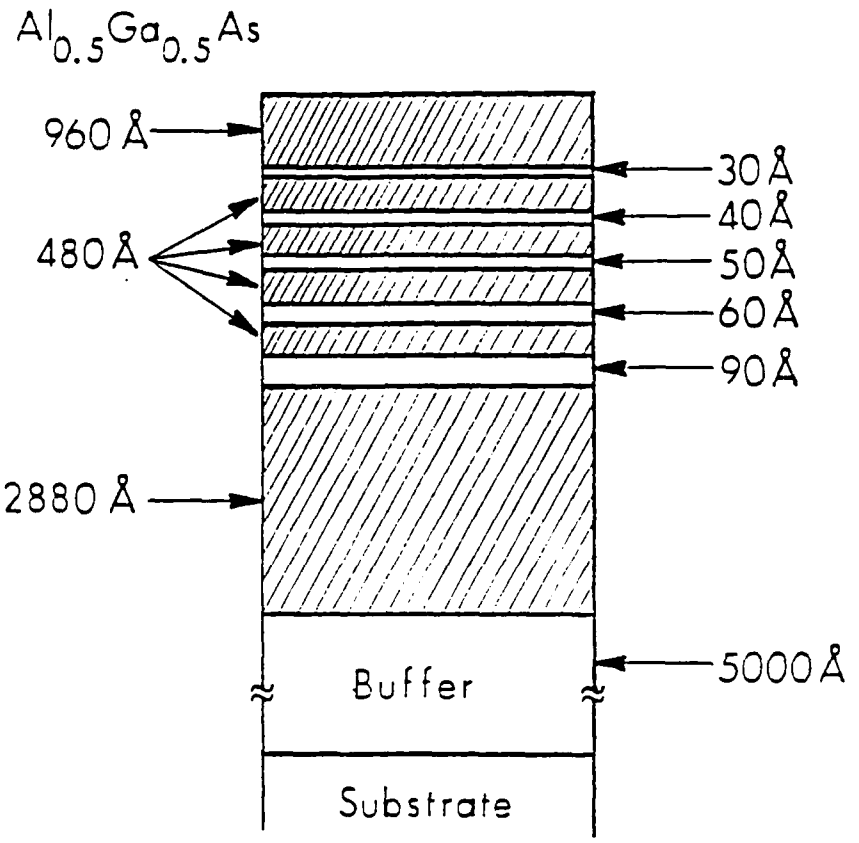

Figure 5.3
5 SQW sample grown for low temperature PL study.

5.3.1 PL Linewidths

The quality of quantum wells formed by the ALE growth of the GaAs and MOCVD growth of $Al_{0.5}Ga_{0.5}As$ at higher temperatures is demonstrated in the 8K photoluminescence spectra as shown in figure 5.4. Note that all five quantum wells exhibit intrinsic radiative emission with narrow linewidths. The PL linewidths for each corresponding well thickness compare quite favorably with quantum wells grown in our laboratory or reported in the literature[9] by conventional MOCVD. The 1-3meV increase in the linewidth of the ALE grown quantum well in comparison to conventional grown MOCVD QWs is presumably caused by a small amount of impurity incorporation that may occur during the three-minute cool-down. The linewidth of the PL spectra is determined by a number of factors. At low measurement temperatures, the linewidth broadening is dominated by interface abruptness[10] and alloy clustering. The latter causes fluctuations in the composition that, in turn, can cause local potential differences. Other factors that may lead to linewidth broadening are electric fields from ionized impurities[11] and band filling due to high carrier concentrations.[12]

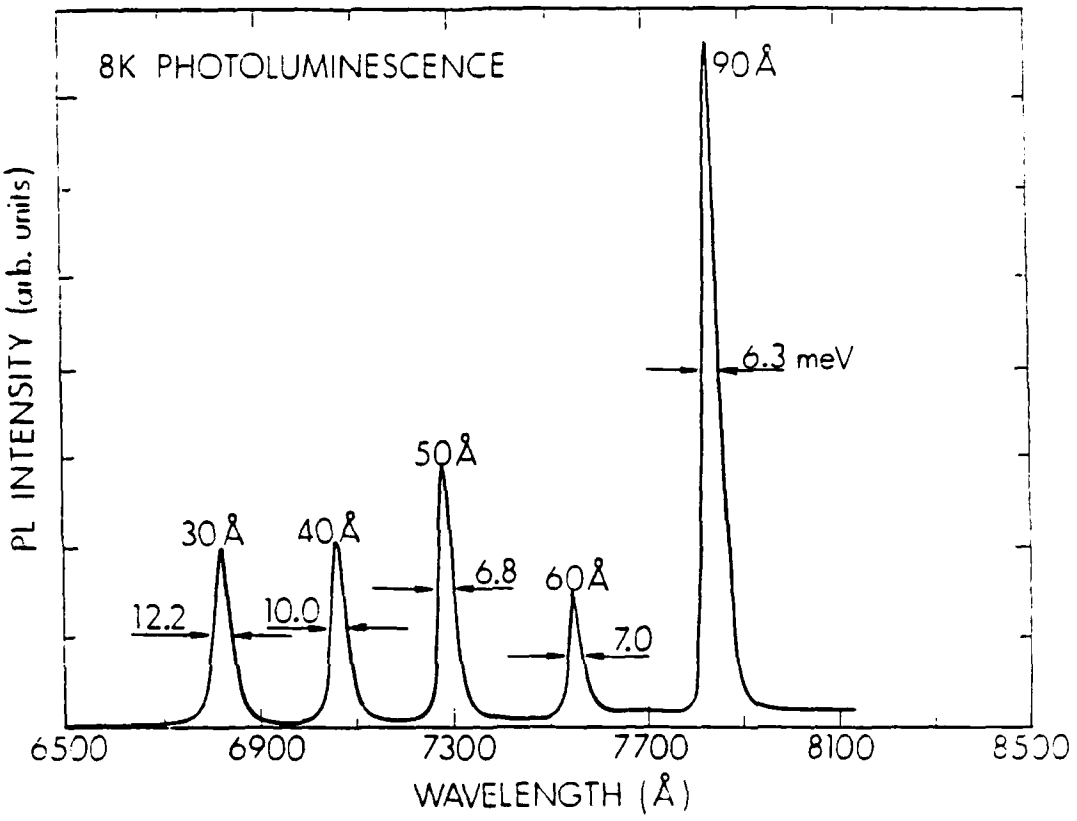

Figure 5.4
Low Temperature PL spectra of 5SQW exhibits narrow line intrinsic luminescence.

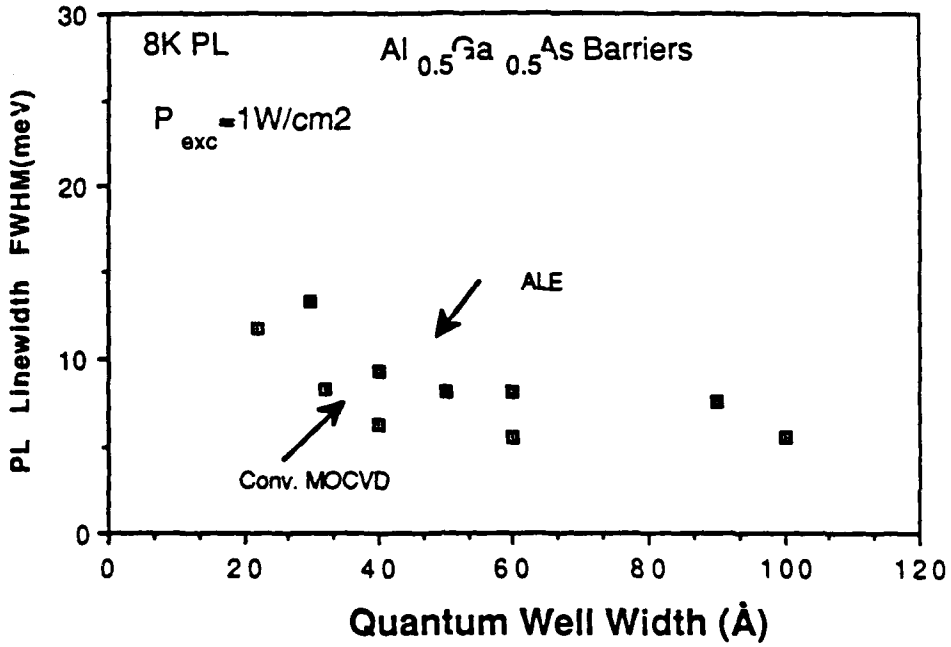

Figure 5.5
PL linewidth (FWHM) comparison of ALE and conventional grown MOCVD quantum wells

5.3.1.1 Interface Broadening

In thin quantum well structures monolayer variations at the heterointerface will result in spectral broadening. This phenomena is illustrated in figure 5.5. Typically, the QW is not uniform in L_z within the layer, but is a assembly of lateral islands in the plane of the layer (See Figure 5.6). If the adjacent lateral island has a different thickness L_z*, it therefore yields a different PL emission energy. When the lateral extent, W, of the island is larger the than Bohr diameter of the exciton, the PL spectrum exhibits multiple peaks. This has been observed in the PL spectrum of MBE-grown QW where long pauses at the heterointerface cause smoothness by surface migration and allows larger islands to grow.[13] In the case where the lateral island size is smaller than the exciton diameter, an exciton experiences different values of L_z which causes spectral broadening. In this case, we can see the approximate effect of broadening ΔE caused by fluctuations in the well width by taking the derivative of the energy dependence of E for an infinite quantum well:

$$\frac{\partial}{\partial L_z}(E) = \frac{\partial}{\partial L_z}\left(\frac{\bar{h}^2}{2(L_z)^2 m_e^*}\right) \tag{5.12}$$

Thus we can see the energy broadening will increase inversely with the cube of the QW width:

$$\Delta E_{PL} = \left(\frac{\bar{h}^2}{2m_e^*}\right)\left[\frac{\Delta L_z}{L_z^3}\right] \tag{5.13}$$

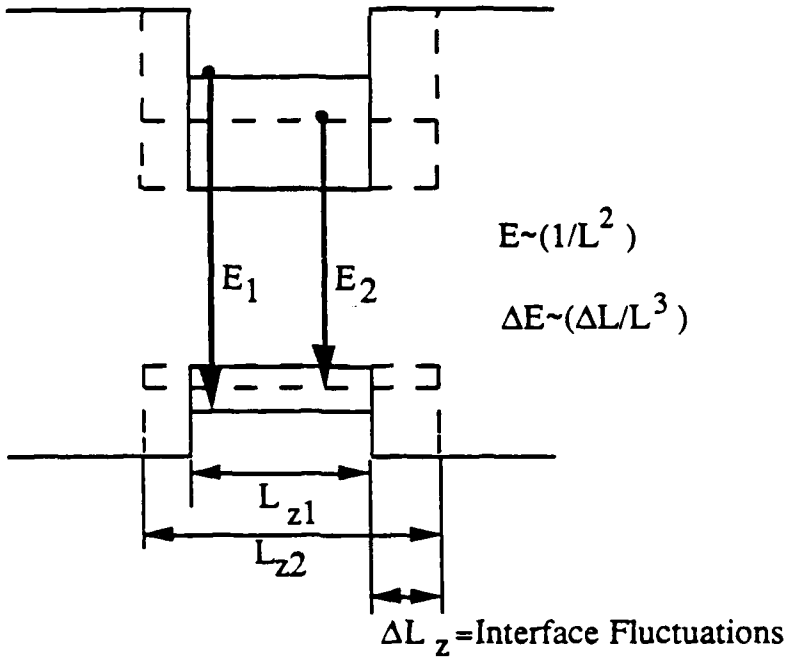

Figure 5.6
Monolayer variations in the width of small quantum wells result in shifts in emission energy.

Singh et al.[14] provide a more detailed model taking into account the finite potential barrier of AlGaAs and GaAs active region. Figure 5.8 shows the dependence of the spectral broadening as a function of the interface fluctuations and lateral island size. By utilizing this PL broadening model with a lateral island size of 100Å, a well width fluctuation of one monolayer can account for the 12.2meV linewidth of the 30Å quantum well grown by ALE.

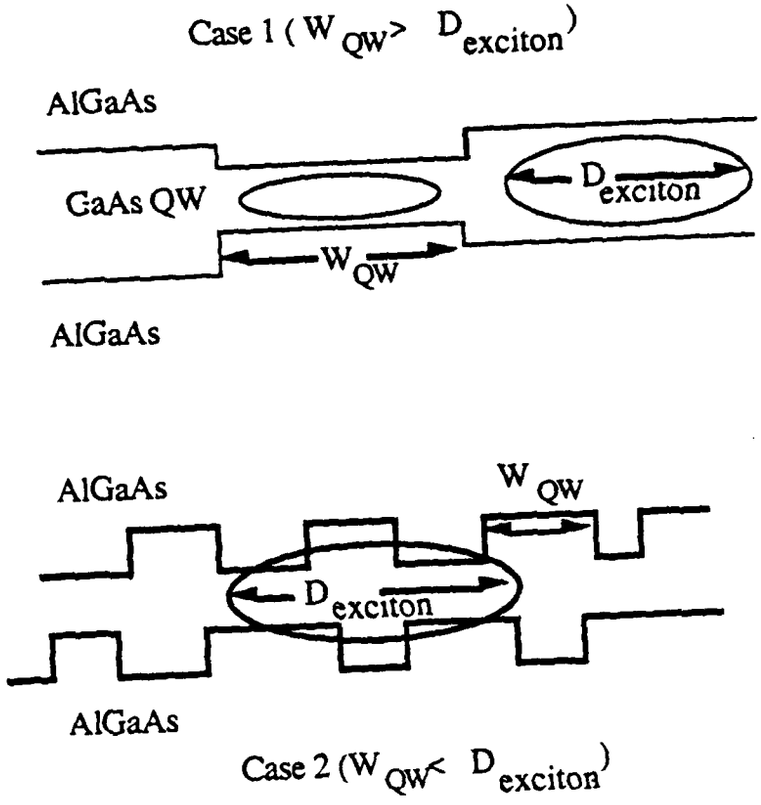

Figure 5.7
Model of interface structure for interface island steps larger than the excitonic diameter (Case 1), and for interface islands steps smaller than excitonic diameter (Case 2).

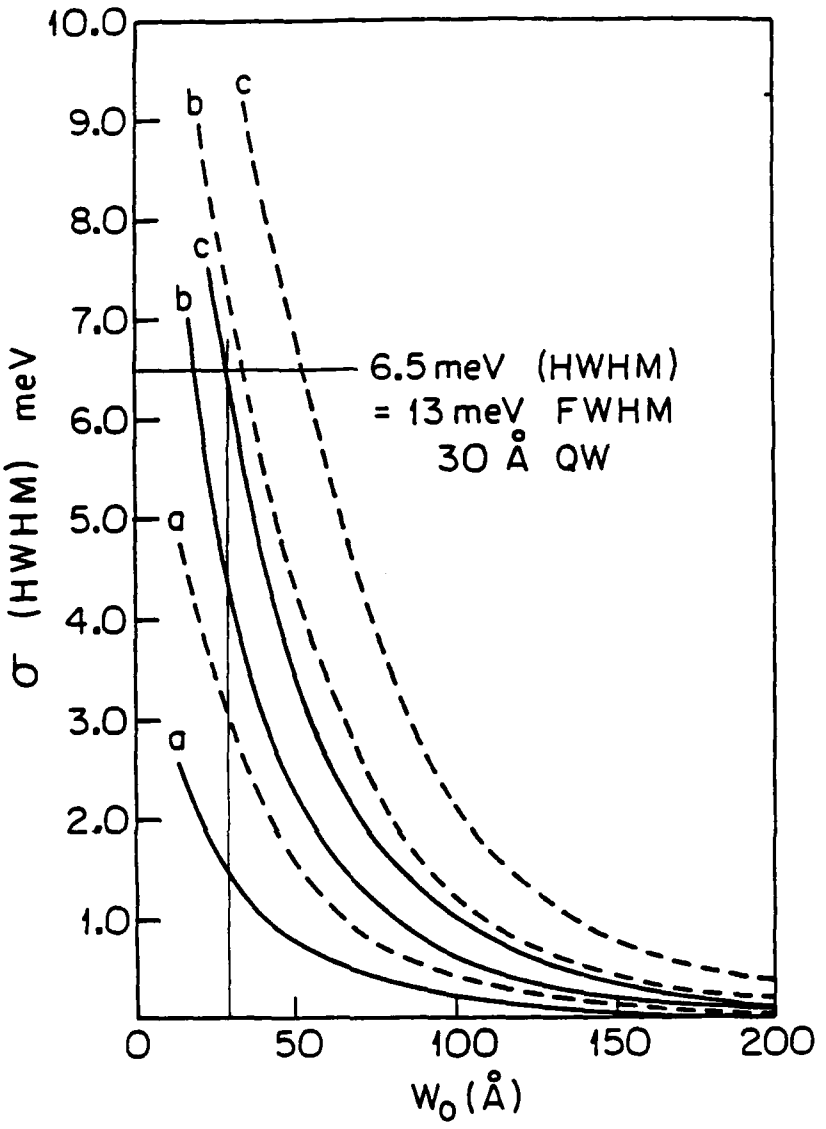

Figure 5.8
Half-width of PL emission as a function of well width L_z for one and two monolayer fluctuations. Lateral island size equals (a) 20Å, (b) 80Å, (c) 100Å (from Singh et al.).[14] Solid line indicates one monolayer interface fluctuations,whereas dashed line indicates two monolayer fluctuation.

5.3.1.2 Alloy Broadening

Another factor contributing to PL line broadening is local fluctuations in the Al composition which will cause barrier height fluctuations. This effect is shown schematically in figure 5.9. S. B. Ogale et al.[15] have developed a rigorous quantum mechanical model which predicts that the PL linewidth will exhibit a $(L_z)^{-1}$ dependence if compositional fluctuations are the dominant broadening mechanism. Figure 5.10 shows the comparison between theory and experimental data for several growth techniques. From this figure we can determine that if compositional fluctuations are the dominant broadening mechanism the observed PL linewidths in the ALE grown QWs can be accounted for by only a 1.0% compositionally fluctuation in the AlGaAs barrier layers. Therefore, the PL spectra of ALE grown SQWs shown in figure 5.4 suggest that the interface abruptness and quality of the quantum wells has not been significantly altered by interrupting the growth to lower the temperature to ALE conditions.

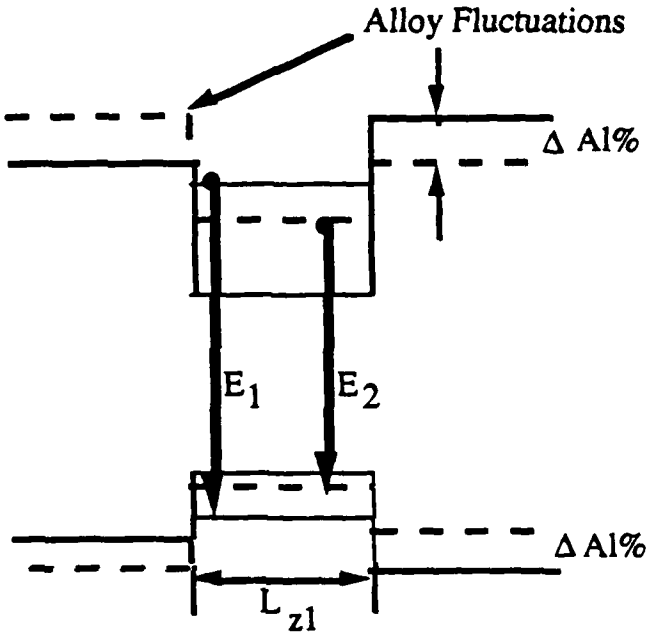

Figure 5.9
Local fluctuations in Aluminum concentration cause broadening of the PL emission.

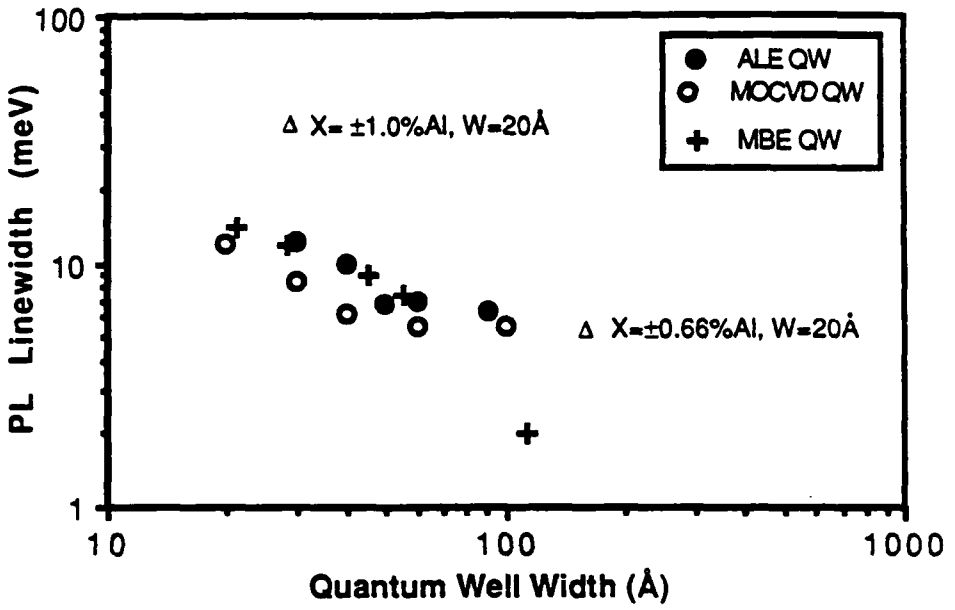

Figure 5.10
The measured dependence of PL linewidth as a function of QW width for various growth methods. Solid lines indicate predicted PL broadening caused by fluctuations in Al composition with 33% Al barriers and 20Å lateral islands widths from S. B. Ogale et al.[16]

5.3.2 Optimization of ALE Quantum Well Luminescence

Several factors influence the quality of luminescence from quantum wells. Poor AlGaAs quality and heavy impurity incorporation in the wells will lower luminescence efficiency. Oxygen incorporation will act as a non-radiative recombination site in both AlGaAs and GaAs. For the ALE growth of quantum wells the most important parameter we have identified that effects the photoluminescence quality is the lack of surface coverage caused by an inefficient arsine exposure. Figure 5.10 shows the detrimental effects produced by reducing the arsine exposure below the amount required to obtain perfect surface coverage "Θ=1." Not only does the luminescence efficiency decrease but also there is significant increase in the linewidth of the emission. The increased linewidth is due to the homogeneous line broadening caused by increased impurity incorporation in these layers. The most likely impurity being incorporated is carbon caused by incompletion of the proposed surface reaction between arsine and the gallium adsorbate.

$$GaCH_{3(ads)} + AsH_3 \rightarrow GaAs_{(s)} + CH_{4(v)} + H_{2(v)} \qquad (5.14)$$

Therefore, sufficient arsine amounts and time of exposures are necessary for high quality GaAs by ALE.

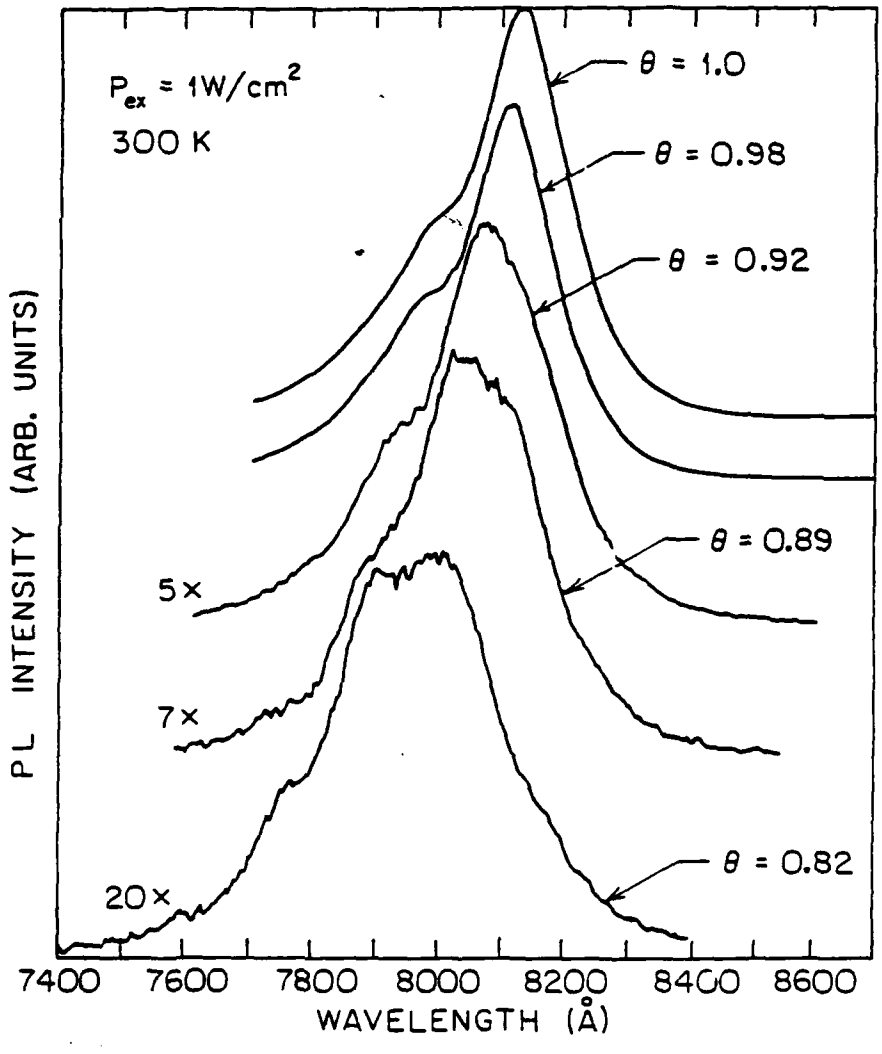

Figure 5.11
Room-temperature PL spectra of 5 SQWs grown with varying surfaces coverages of arsine at 455°C. Note that the insufficient arsine coverages reduce the PL efficiency and increase the PL FWHM linewidths.

The effect of growing quantum wells with various surface coverages of TMGa on the PL spectra is shown in figure 5.11. Interestingly enough the linewidths of the PL spectra at lower TMGa surface coverages appear to be narrower than for the thicker QWs. Therefore for coverages greater than one there appears to an increase in the impurity incorporation. It is likely that putting to much TMGa on the surface blocks the surface exchange reaction between the arsine and the methyl groups. The observation that the thinnest well has the narrowest linewidth might indicate that the exchange reaction is more efficient when the surface is not completely covered by the gallium adsorbate. This is of great interest in comparison to the recent results of E. Colas et al.[17] who obtained the best electrical results of ALE GaAs , μ_{77}=35,000V/cm^{2}sec and 3x10^{15}cm^3 n-type, by growing at 1/2 monolayer per cycle.

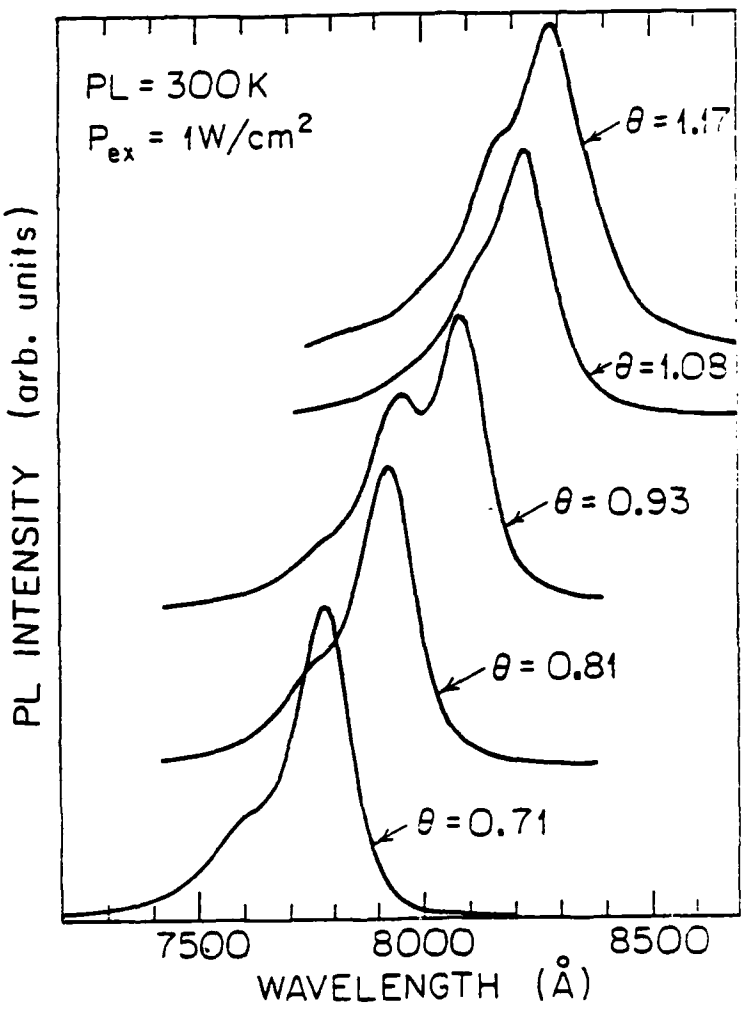

Figure 5.12
Room-temperature PL spectra of 5 SQWs grown with varying surfaces coverages of TMGa at 455°C.

5.3.3 AlGaAs/GaAs heterostructures grown entirely by ALE

ALE of AlGaAs has been achieved by injecting the TMAl both concurrently, and separately from the TMGa pulse. As was shown in the ALE of AlAs in figure 4.6 the deposited thicknesses show the expected saturated growth results. However, as shown in figure 5.13, extrinsic luminescence is observed from the structures in which ALE was also used to grow the barriers. This indicates that further optimization of the process is needed. Luminescence is only observed from structures in which the TMAl is injected simultaneously with the TMGa pulse. We have also grown a 70Å $Al_{0.2}Ga_{0.8}As$ QW by ALE . The barriers for this well were $Al_{0.5}Ga_{0.5}As$ grown by conventional MOCVD at 750°C. The expected emission energy for this well is approximately 6200Å. As we can see PL spectrum in figure 5.14, a small peak exist at the expected energy but lower energy extrinsic luminescence dominates the spectrum.

There are several reasons accounting for the low quality of ALE grown AlGaAs compared to ALE grown GaAs. First, aluminum is thermodynamically a more reactive element than gallium. The reaction of oxygen with an aluminum arsenide surface is 100 times that of a GaAs surface.[18] We have also observed this in the growth on conventional MOCVD QW structures in which we studied the effect of long pauses at the GaAs and AlGaAs interfaces.[19] As shown in figure 5.15 low temperature PL from these studies indicate that pauses at the AlGaAs

interface at high temperatures lead to significant linewidth broadening. This linewidth broadening is attributed to the increased impurity incorporation on the AlGaAs interface.

Another factor that might cause the poor luminescence is the fact that the Al-C bond is much stronger in TMAl than TMGa and thus more carbon might be incorporating in ALE AlGaAs. Using TEAl compounds appears to be a solution to this problem. The aluminum to ethyl bond is weaker than the aluminum to methyl bond[20] and thus less carbon incorporation will occur. By using TEAl in the flow modulated epitaxy scheme Makimoto et al.[21] have grown high quality MQW structures at temperatures as low as 500°C. Low-temperature PL spectra of their QWs with $Al_{0.2}Ga_{0.8}As$ barriers are as narrow as 10.9 and 4.2meV for 18Å and 68Å wells, respectively.

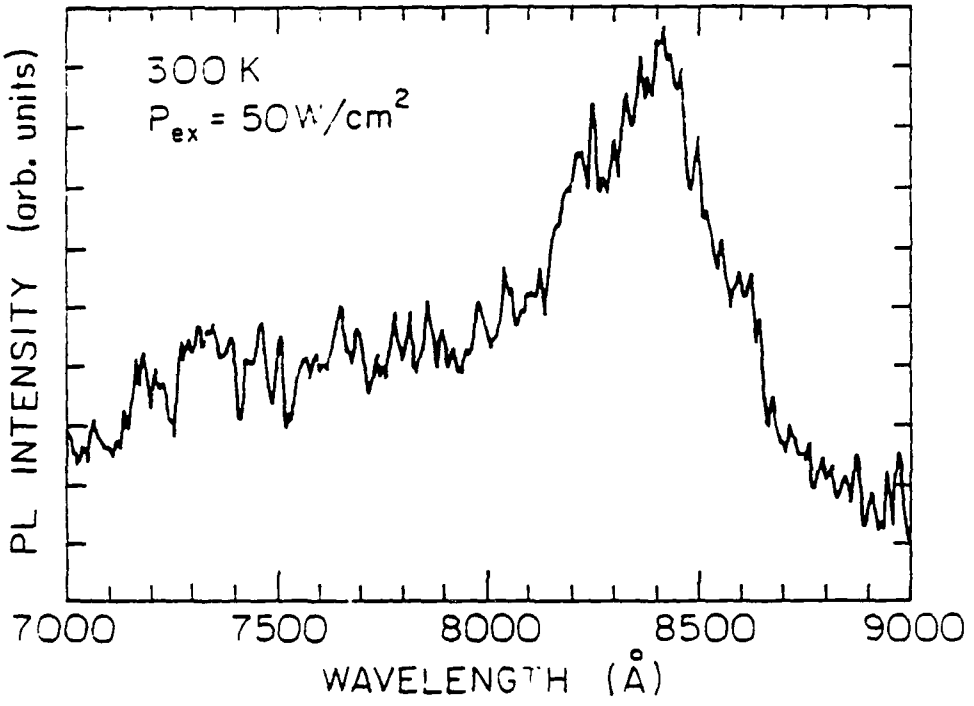

Figure 5.13
PL spectrum of a GaAs/AlGaAs QW structure in which ALE was also used to grow the AlGaAs barrier layers.

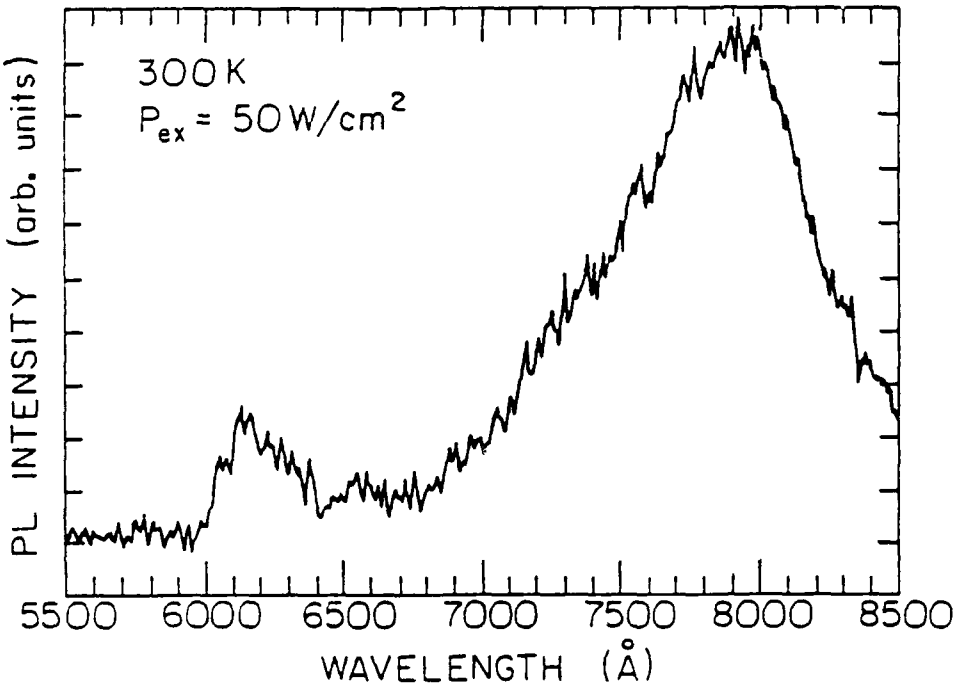

Figure 5.14
PL spectrum of a 70Å QW with $Al_{0.2}Ga_{0.8}As$ ALE active region and $Al_{0.5}Ga_{0.5}As$ barriers.

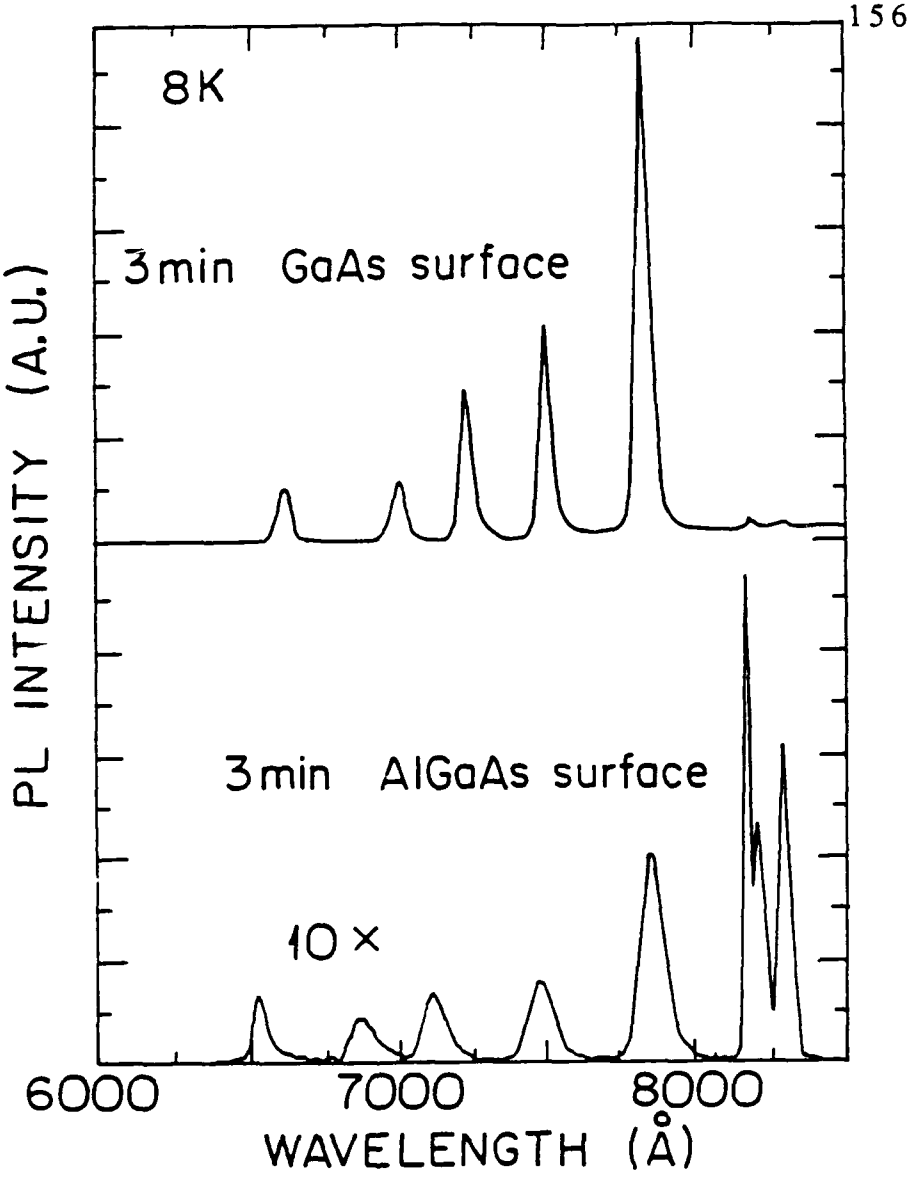

Figure 5.15
Low temperature PL spectra for five MQW structure in which 3 minute pauses at the AlGaAs interface lead to increased impurity incorporation. The uppermost spectrum shows narrow PL from QWs in which the pause was at the GaAs interface only. The lower spectrum shows the extrinsic broadened PL from QWs in which the pause was at the AlGaAs interface only.

5.4 Quantum Well Injection Lasers

Quantum wells, as well as devices incorporating these structures require the ability to produce thin layers with abrupt interfaces. An example of one device is the quantum well injection laser. In this device the threshold current density and lasing wavelength are strongly dependent upon the active layer thickness in the 10-60Å range.[22] We have demonstrated that monolayer uniformity is achievable by the ALE growth technique as shown in figure 4.8. Therefore, as a test vehicle for utilizing ALE in device structures, we have applied ALE to the growth of GaAs/AlGaAs quantum well injection lasers in which the critical thickness GaAs active region is grown by ALE.

Quantum well heterostructures offer several benefits to operation of semiconductor lasers. Extremely low currents threshold current operation are possible because of the step-like 2-dimensional density of states of the quantum well structure. Discrete energy levels exist in the 2-dimensional density of states, thus more efficient utilization of injected carriers at a given energy level is achieved as shown in figure 5.16. This also reduces the temperature dependence of the threshold current density,[23] which typically plague conventional double heterostructure lasers. Carrier confinement in the QW enhances the gain coefficient and reduces the threshold current.[24] For parabolic bands with infinite barriers it can be shown that within each subband there exist a constant density of states, per unit area.

$$\rho(E)\,dE = \left(\frac{m_n^*}{\pi\hbar^2}\right)dE \tag{5.15}$$

For a GaAs/AlGaAs heterostructure the density of states in the conduction band can be shown to be:[25]

$$\rho_c(E) = \left(\frac{m_c^*}{\pi\hbar^2 L_z}\right)\left(INT\left(\frac{E - E_c}{\Delta E}\right)^{1/2}\right) \tag{5.16}$$

Thus, the density of states in a heterostructure is a quasi-two-dimensional density of states which appears as step like function that is asymptotic to the 3-D density of states as Lz becomes large (*See figure* 5.16).

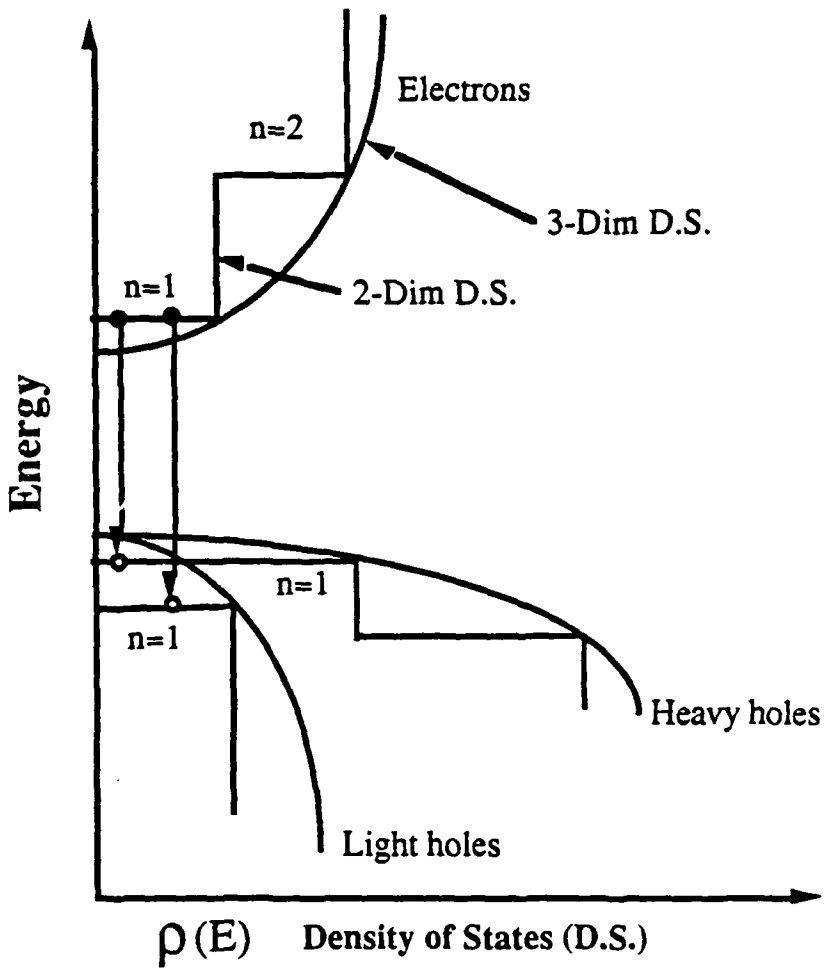

Figure 5.16
Quantum well laser offer discrete transitions energy levels because of the step-like 2-Dimensional density of states.

5.4.2 Growth and Fabrication of ALE Quantum Well Injection Laser

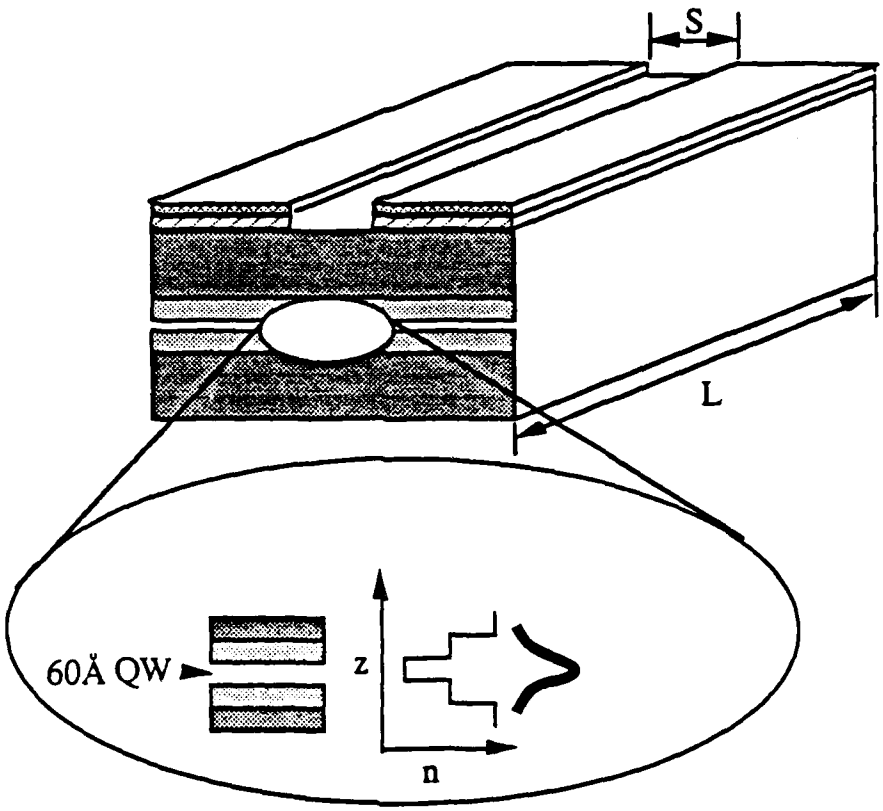

Figure 5.17
Schematic diagram of separate confinement (SCH) heterostructure laser employing 60Å quantum well active region grown by ALE.

Injection laser device structures were formed in three stages in a single growth run. The first stage of growth consists of growing a 0.2μm n+ GaAs buffer layer, a 2μm n-type $Al_{0.5}Ga_{0.5}As$ cladding layer and an 600Å undoped $Al_{0.25}Ga_{0.75}As$ confinement layer. These layers were

grown at a temperature of 750°C. The temperature was lowered to either 455°C or 485°C and the 60Å quantum well active region was grown by ALE. The final stage consisted of the growth of an undoped confinement layer, a p-type cladding layer and a p+ cap layer. These three layers had the same compositions as the layers grown in the first stage and were also grown by conventional MOCVD at 750°C. Laser devices were processed by depositing 100 μm wide Cr-Au stripes and AuGe-Ni contacts on the p- and n-sides of the device, respectively. Injection laser device chips were fabricated by cleaving 400 - 800μm long bars with the cleaved faces perpendicular to the stripe direction. Figure 5.22 shows a micrograph of a typical laser chip. The other sides of the device were scribed and broken to prevent laser operation on internal bounce modes. A schematic illustration of a separate confinement heterostructure (SCH) quantum well laser is shown in figure 5.17.

5.4.3 Device Results

The ALE QW injection laser device chips were tested in a pressure mount fixture under pulsed conditions. The current was applied in 0.3μsec long pulses at a repetition rate of 10kHz. A typical spectrum from a broad area device under spontaneous emission and laser operation is shown in figure 5.18. An expanded view of the laser spectra shows a several longitudinal modes appear above threshold (See figure 5.19). The mode spacing is determined by wavelengths satisfying the phase condition:

$$m\left(\frac{\lambda_o}{\bar{n}}\right) = 2L \qquad (5.17)$$

where m=1,2,3.., and L is the cavity length, and $\bar{n}$ the refractive index. It can then be shown the mode spacing will be given by:[26]

$$\Delta\lambda_o = \left(\frac{\lambda_o^2}{2\bar{n}L\left[1 - \left(\frac{\lambda_o}{\bar{n}}\right)\left(\frac{d\bar{n}}{d\lambda_o}\right)\right]} \right) \tag{5.18}$$

A summary of the threshold current densities obtained for QW injection lasers grown by ALE in comparison to the best conventional MOCVD grown lasers in our lab is shown in Table 5.1. Graded index separate confinement heterostructures (GRIN-SCH) yield the lowest threshold current densities for lasers grown by both techniques. Figure 5.20 illustrates the difference in grading between the SCH and GRIN-SCH laser structures. Increased optical confinement (Γ) along with the pseudo-electric field created by the parabolic graded region have been used to explain the lower threshold currents necessary in the GRIN-SCH structures.[27] This can be shown by examination of the threshold current density J_{th} equation for a double heterostructure (DH) laser which is given as:[28]

$$J_{th} = \frac{J_o d}{\eta_i} + \frac{d}{\eta_i \beta \Gamma}\alpha_i + \frac{d}{\eta_i \beta \Gamma}\left(\frac{1}{L}\ln\left(\frac{1}{R}\right)\right) \tag{5.19}$$

where η is the internal quantum efficiency, Γ the optical confinement factor, L the cavity length, β is the gain constant, and d the active region thickness. The internal loss term is given by:[29]

$$\alpha_i = \Gamma\alpha_{fc} + (1-\Gamma)\alpha_{fcB} + \alpha_s + \alpha_c \qquad (5.20)$$

where α_{fc} is the background free carrier concentration in the active region α_{fcB} is the concentration in the barriers as scattering loss, and α_c the coupling losses.

Threshold current densities as low as 380A/cm^2 were observed for the ALE GRIN-SCH structures.[30] Differential quantum efficiencies as high as 26% per facet were observed in the output power versus drive current curves (See figure 5.21). Equivalent structures with optimized grading and doping of the confinement regions grown in our laboratory by conventional vertical MOCVD have threshold currents as low as 160 A/cm^2. These low thresholds were only achieved after careful calibration of the AlGaAs doping level and the width of the parabolic grading. From the internal loss equations we can see that reduction of the free carrier concentrations in the active regions and the AlGaAs barriers will reduce the losses. We thus anticipate threshold current densities in the range 200-400 A/cm^2 for lasers with ALE-grown active regions with further optimization of the cladding region doping.

Table 5.1 Threshold Current Densities

Structure	Vertical MOCVD	ALE
SCH	400A/cm2	640A/cm2
GRIN-SCH	160A/cm2	370A/cm2

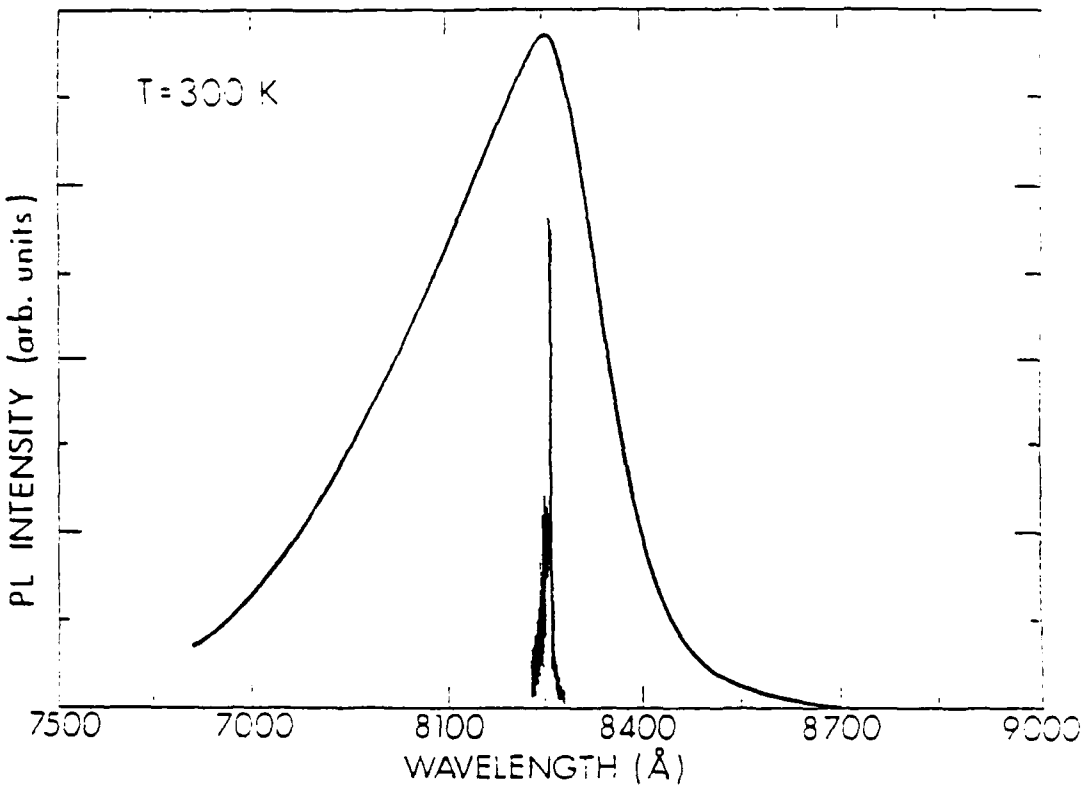

Figure 5.18
Spontaneous and laser emission spectrum from a separate confinement quantum well laser with GaAs QW active region by ALE.

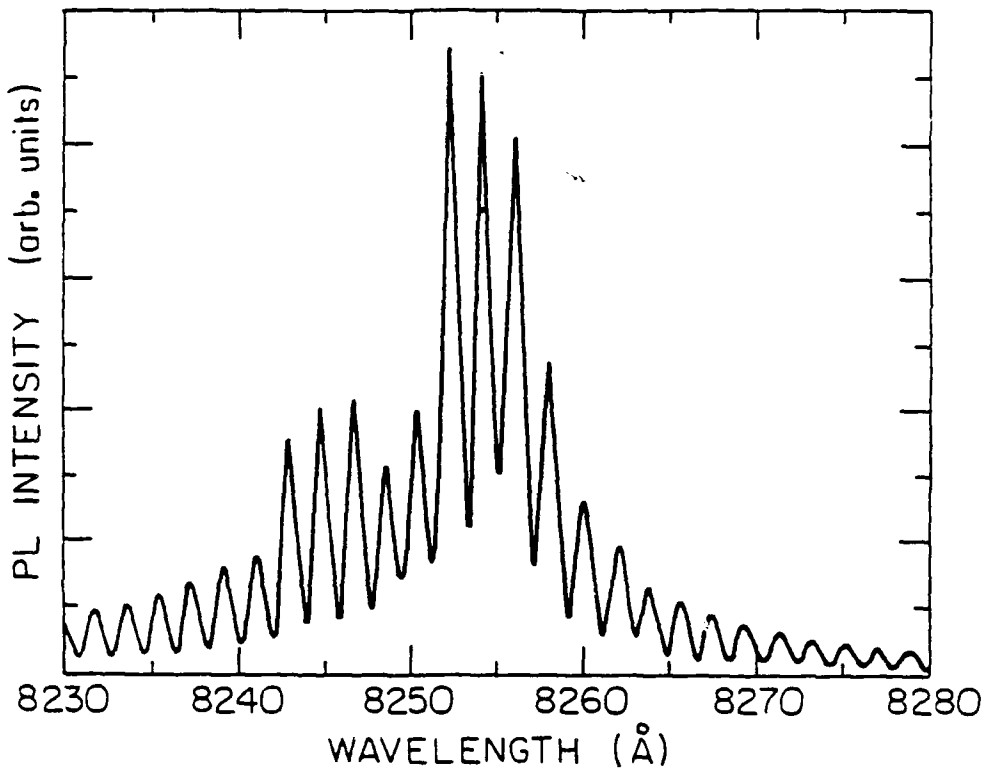

Figure 5.19
Mode spectrum of ALE SCH-QW injection laser showing longitudinal optical modes.

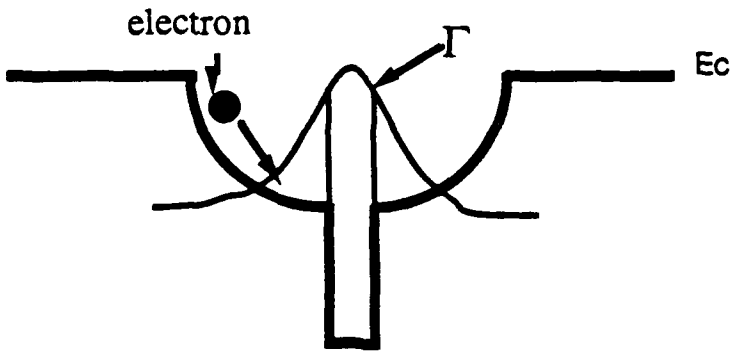

GRIN-SCH Structure

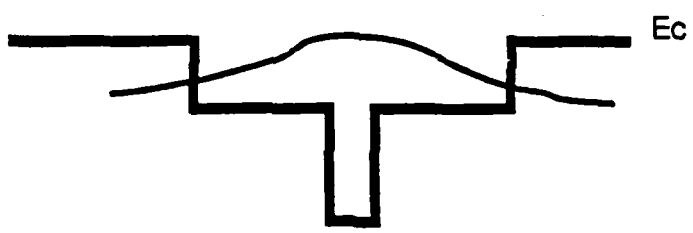

SCH Structure

Figure 5.20
Energy Band diagrams of GRIN-SCH and SCH laser structures
Parabolic grading in GRIN-SCH creates pseudo-electric field and better optical confinement.

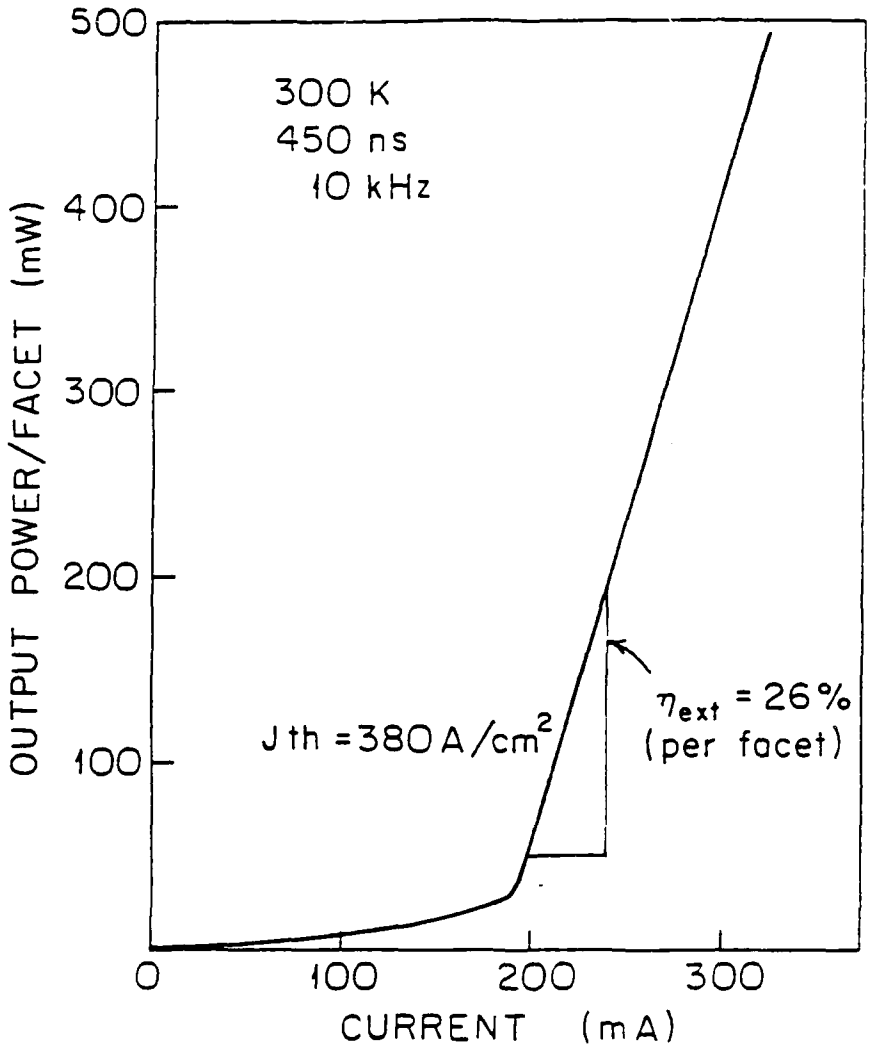

Figure 5.21
Luminescence intensity versus drive current for ALE QW injection laser

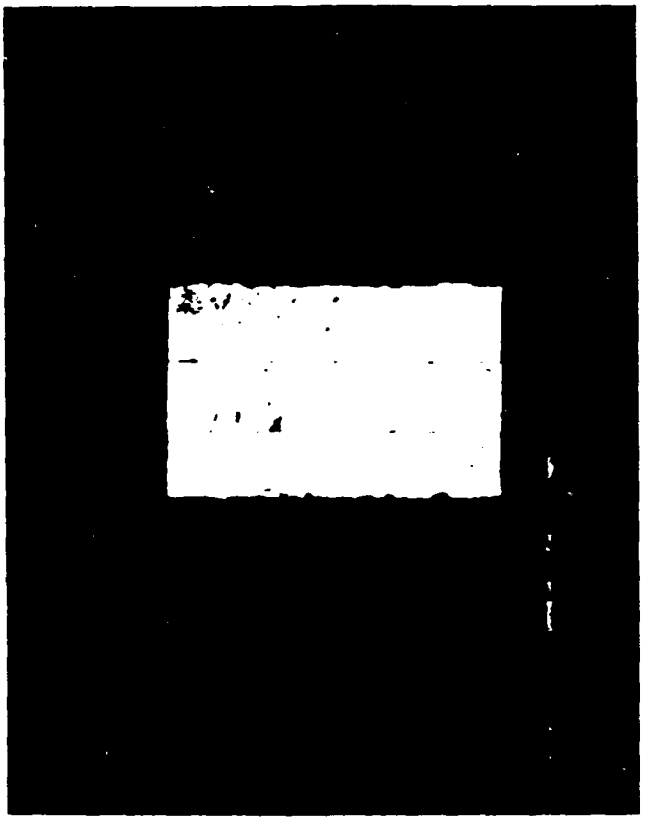

Figure 5.22
Top view of deposited 100μm wide Cr-Au contact stripe on QW injection laser.(MAG=1000X)

5.5 Conclusions

In conclusion, we have demonstrated for the first time operation of an injection laser grown by ALE. Low temperature PL of single quantum well (SQWs) grown by a hybridization of ALE and conventional MOCVD exhibit narrow linewidth intrinsic luminescence. Uniform layer thickness, high quality GaAs quantum well materials have also been demonstrated by utilizing the saturated monolayer growth process inherent to ALE. These results suggest that ALE will play an important role in the fabrication of heterojunction devices with critical layer thickness requirements.

REFERENCES-CHAPTER 5

1 Z. I. Alferov, V. M. Andreev, D. Z. Garbuzov, Y. V. Zhilyaev, E. P. Morozov, E. L. Portinoi, and V. G. Trofim, Sov. Phys. Semicond. **4**, 1573 (1971) [Translated from Fiz. Tekh. Poluprovodn. **4**, 1826 (1970)].

2 P. D. Dapkus, J. Crystal Growth **68**, 345 (1984).

3 L. J. Mawst, M. E. Givens, C. A. Zmudzinski, M. A. Emanuel, and J. J. Coleman, IEEE J. Quantum Electron., **QE-23**, 696, (1987).

4 H. Okamato, Jap. J. Apll. Phys., **26**, 315, (1987).

5 R. Dingle, Festkorperprobleme **XV**, 21 (1975).

6 G. Bastard, Phys. Rev. B, **24**, 5693 (1981).

7 H. C. Lee, PhD. Dissertation, University of Southern California (1987), p.130.

8 H. C. Lee, PhD. Dissertation, University of Southern California (1987), pp.124-127.

9 D. C. Bertolet, J. K. Hsu and K. M. Lau, J. Appl. Phys., **62**,120 (1987).

10 J. Singh K. K. Bajaj and S. Caudhuri, Appl. Phys. Lett. **44**, 805(1984).

11 D. M. Larsen, Phys. Rev. **B8**, 535 (1973).

12 C. F. Schaus, J. R. Shealy, L. F. Eastman, B. C. Cooman and C. B. Carter, J. Appl. Phys. **59**, 678 (1986).

13 T. Fukunaga, K. L. I. Kobayashi, and H. Nakashima, Surface Sci., **174**, 71 (1986).

14 J. Singh K. K. Bajaj and S. Caudhuri, Appl. Phys. Lett. **44**, 805 (1984).

15 S. B. Ogale, A. Madhukar, F. Voillot, M. Thomsen, W. C. Tang, T. C. Lee, Y. Kim and P. Chen, Phys. Rev. B, **36**,1662 (1987).

16 S. B. Ogale, A. Madhukar, F. Voillot, M. Thomsen, W. C. Tang, T. C. Lee, Y. Kim and P. Chen, Phys. Rev. B, **36**, 1662 (1987).

17 E. Colas, R. Bhat, B. Skromme, Paper **D-8**, International Symposium on GaAs and Related Compounds, Atlanta, GA (1988).

18 R. Z. Bachrach, Crystal Growth, 2nd ed., B.R. Pamplin, Pergamon Press, New York, (1980) p.260.

19 S. P. Denbaars, H. C. Lee, A. Hariz, P. D. Dapkus, **N-3**, Electronic Materials Conference, Santa Barbara, (1987).

20 M. Yoshida, H. Watanabe, and F. Uesugi, J. Electrochem. Soc. **137**, 677 (1985).

21 T. Makimoto, Y. Yamauchi, and Y. Horikoshi, Paper **D-7**, International Symposium on GaAs and Related Compounds, Atlanta, GA (1988).

22 L. J. Mawst, M. E. Givens, C. A. Zmudzinski, M. A. Emanuel, and J. J. Coleman, IEEE J. Quantum Electron., **QE-23**, 696, (1987).

23 N. Y. Holonyak, R. M. Kolbas, R. D. Dupuis, P. D. Dapkus, IEEE J. Quantum Electronics, **QE-16**, 170 (1980).

24 W. T. Tsang, Appl. Phys. Lett. **40**, 217 (1982).

25 D. Kasemet, C. Hong, N. B. Patel, and P. D. Dapkus, IEEE J. of Quantum Elec., **QE-19**, 1025 (1983).

26 H. C. Casey, Jr and M. G. Panish, Heterostructure Lasers, (New York, Academic Press, 1978) p.167.

27 P. D. Dapkus, Class Notes, **EE-599**, Heterostructure Materials and Devices, University of Southern California, (1986).

28 W. H. Tsang, Appl. Phys. Lett., **40**, 217 (1982).

29 H. C. Casey, Jr and M. G. Panish, Heterostructure Lasers, (New York, Academic Press, 1978) p.176.

30 S. P. DenBaars, C. A. Beyler, A. Hariz, and P. D. Dapkus, Appl. Phys. Lett., **51**, 1530 (1987).

CHAPTER 6
LASER ASSISTED ATOMIC LAYER EPITAXY

6.1 Introduction

Laser induced chemical vapor deposition (LCVD) has been identified as an attractive alternative for the fabrication of microelectronic devices. Low temperature processing, selective area deposition, and wavelength selective photochemistry are some of the unique aspects offered by LCVD. Because of the spatial and temporal selectivity of depositions available through the use of lasers, new methods of semiconductor processing are anticipated. LCVD of conducting metallic films has recently resulted in excellent metallic films.[1] However, LCVD of semiconductors have been plagued by polycrystalline deposits with high carbon content.

Laser assisted ALE (LALE) has recently been discovered to allow the selective growth of single crystal GaAs.[2] The deposited films were found to be p-type with background doping of the $5x10^{17}/cm^3$. In this method, modulation of both a CW Argon ion laser and the gas stream is performed. The laser irradiates the surface for **1 second during the gallium exposure** to achieve selective decomposition of the TMGa adsorbate on the As atoms. Perfect monolayer saturation of the growth rate is observed over a wide range of trimethylgallium (TMGa) fluxes and temperatures. The selective deposited structure was typically a 0.5mm by 1mm elliptical deposit. Only deposition on GaAs surfaces has been studied to date.

We have elected to study the fast writing potential of LALE on AlGaAs surfaces with the goal of incorporating the GaAs in heterostructure devices. Selective area epitaxy by laser assisted ALE has great potential for the integration of opto-electronic and electronic devices. Optimization of LALE on AlGaAs surfaces would allow the *in situ* deposition of heterostructure devices with different epitaxial structures. The manufacturing benefits of a "laser writing" process which affords the fabrication of various device structures in a single run are enormous. In this study we demonstrate the "fast writing" potential of LALE for depositing small dimension structures .

The approach we have taken is to employ conventional MOCVD reactants to allow for the hybridization of ALE and conventional MOCVD in a novel four chamber reactor. The four chamber reactor allows spatial separation of the column III and column V precursors, thus allowing one monolayer per rotation in as little as 2 seconds. In contrast to the work of Doi et al.,[2] we have employed a scanned laser beam with spot sizes as small as 30μm to selective deposit GaAs stripes on $Al_{0.3}Ga_{0.7}As$.[3] We observe monolayer saturation in the growth rate under a wide range of growth conditions. The LALE deposits exhibit smooth mirror like morphology with a flat-topped profiles of thickness, indicative of a monoatomic growth mechanism.

6.2 Laser CVD Theory

6.2.1 Photocatalytic Deposition

Laser CVD is based on the interaction of laser light with molecules in the gas phase and/or on the substrate surface. The laser CVD approach can be divided into three categories of reactions mechanisms: photocatalytic, photolytic, and pyrolytic. Photocatalytic reactions are defined as an increase in a chemical reaction rate produced by photogenerated carriers in a solid where the solid remains unchanged.[4] A general expression of a photocatalyzed surface reaction in a semiconductor is:

$$S.C._{(Eg)} + h\nu_{(h\nu>Eg)} \Rightarrow e^- + h^+$$

$$e^- + X \Rightarrow X^-$$

$$h^+ + M \Rightarrow M^+$$

$$X^- + M^+ \Rightarrow XM$$

A few of the photocatalytic reactions which are known to occur upon the illumination of a semiconductor are the dehydrogenation of isopropyl alcohol, and the splitting of water molecules.[5] Because the wavelength of the Argon ion laser utilized in the LALE experiments is larger than the bandgap of GaAs, a surface photocatalytic process is a likely growth mechanism.

The deposition rate for a surface photo-reaction will be directly proportional to the power density. Assume the substrate is illuminated with a gaussian laser beam of spot size w_o. For a laser of power P_L the laser power density at a point r_o from beam center is given by:

$$P(r_o, w_o) = \left(\frac{2P_L}{\pi w_o^2}\right)\exp\left(-\frac{2r_o^2}{w_o^2}\right) \tag{6.1}$$

The number of adsorbed molecules per cm^2, will be equal to the surface coverage "Θ," multiplied by the surface sites per unit area N_s:

$$N_a = \theta N_s \tag{6.2}$$

The photon flux per unit surface area will be the power density divided by the photon energy:

$$J_\Phi = \frac{1}{h\nu}\left(\frac{2P_L}{\pi w_o^2}\right)\exp\left(-\frac{2r_o^2}{w_o^2}\right) \tag{6.3}$$

The rate of deposition at a specific point will include the quantum efficiency η, absorption cross-section σ_a of the film, the number of adsorbed molecules, and the photon flux:

$$R_{sur} = J_\Phi(\eta\theta N_s\sigma_a) \tag{6.4}$$

Substituting in above equations the rate of deposition in molecules/cm^2·sec is:

$$R_{sur} = \frac{\eta\theta N_s \sigma_a}{h\nu}\left(\frac{2P_L}{\pi w_o^2}\right)\exp\left(-\frac{2r_o^2}{w_o^2}\right) \qquad (6.5)$$

This expression can be further simplified by noting the fastest rate of deposition will be at the center of the beam (r_o=0). Dividing by the surface site density will yield the number of monolayers deposited per second:

$$R_{sur}^{max} = \frac{\eta\theta(2\sigma_a P_L)}{(h\nu\pi w_o^2)} \qquad (6.6)$$

6.2.2 Pyrolytic Deposition

Pyrolytic deposition is caused by laser radiation absorbed in the substrate which leads to a local increase in temperature at the surface. Molecules either on the surface or in the nearby gas phase dissociate by pyrolysis. The reaction rate is determined principally by the maximum temperature rise ΔT. For a stationary Gaussian beam of power P_L the maximum temperature rise is given by:[6]

$$\Delta\dot{T}_{max} = \frac{P_L(1-R)}{(2\sqrt{\pi}\, w_o \kappa)} \qquad (6.7)$$

where R is the surface reflectivity, κ the thermal conductivity, and w_o the beam radius at $1/e^2$ intensity. For the LALE work of Doi et al.[2] this

equation yields an estimated temperature rise of only 40°C for the stationary irradiation case. If we operate at a low temperatures, where kinetics of surface reactions dominant (T<550°C for MOCVD), then growth is not controlled by the flux of reactant to the surface and we can expresses the growth rate as a temperature activated process:

$$G_r = A\exp\left(-\frac{E_a}{kT}\right) \tag{6.8}$$

where E_a is the activation energy of the process, k is Boltzmann's constant, and A is a proportionality constant. Therefore we should see an exponential increase in the growth rate with laser power if pyrolytic mechanisms dominate.

6.2.3 Photolytic Deposition

Photolytic deposition consists of direct dissociation of one of the molecular bonds of a molecule by absorption of one or more photons. The photodissociation of molecules is typically defined by its dissociation spectrum:[7]

$$\sigma_D(\lambda) = \eta\sigma_A(\lambda) \tag{6.9}$$

where σ_D is the photodissociation cross-section, σ_A is the total absorption cross, and η is the quantum efficiency of the photodissociation process. For a single photon dissociation process, as shown in figure 6.1, η is essentially unity, whereas for a multi-photon dissociation process η can be

quite low. For a gas phase photolytic decomposition process molecules above the substrate will be photodissociated and will contribute to film growth. In this case we can approximate the photolytically decomposed species as a cylindrical column with the same waist as the laser beam w_o. For gas phase photodecomposition the flux impinging on the surface the beam center will be:[6]

$$J_{gas} = \frac{\eta(N_g \sigma_g P_L w_o)}{(2h\nu\pi w_o^2)} \tag{6.10}$$

where ,N_g is the molecular gas phase density, P_L the laser power, w_o the beam radius, and σ_g the absorption coefficient. The rate of deposition on the surface in monolayers per second will be the flux times the photodissociated molecule sticking coefficient β, divided by the surface site density:

$$R_{gas} = \frac{\beta\eta(N_g \sigma_g P_L w_o)}{N_s(2h\nu\pi w_o^2)} \tag{6.11}$$

From the above equation 6.11 we can deduce the growth will be proportional to the inverse of the spot size times the laser power:

$$R_{gas} \sim \frac{P_L}{(w_o)} \tag{6.12}$$

whereas if surface phase deposition dominates, it can be seen from equation 6.6 that growth will be directly proportional to the laser power density:

$$R_{sur} \sim \frac{P_L}{(w_o)^2} \qquad (6.13)$$

Therefore, we will be able to determine if the gas or surface phase photodecomposition process is the dominant mechanism by simply varying the spot size of the laser beam.

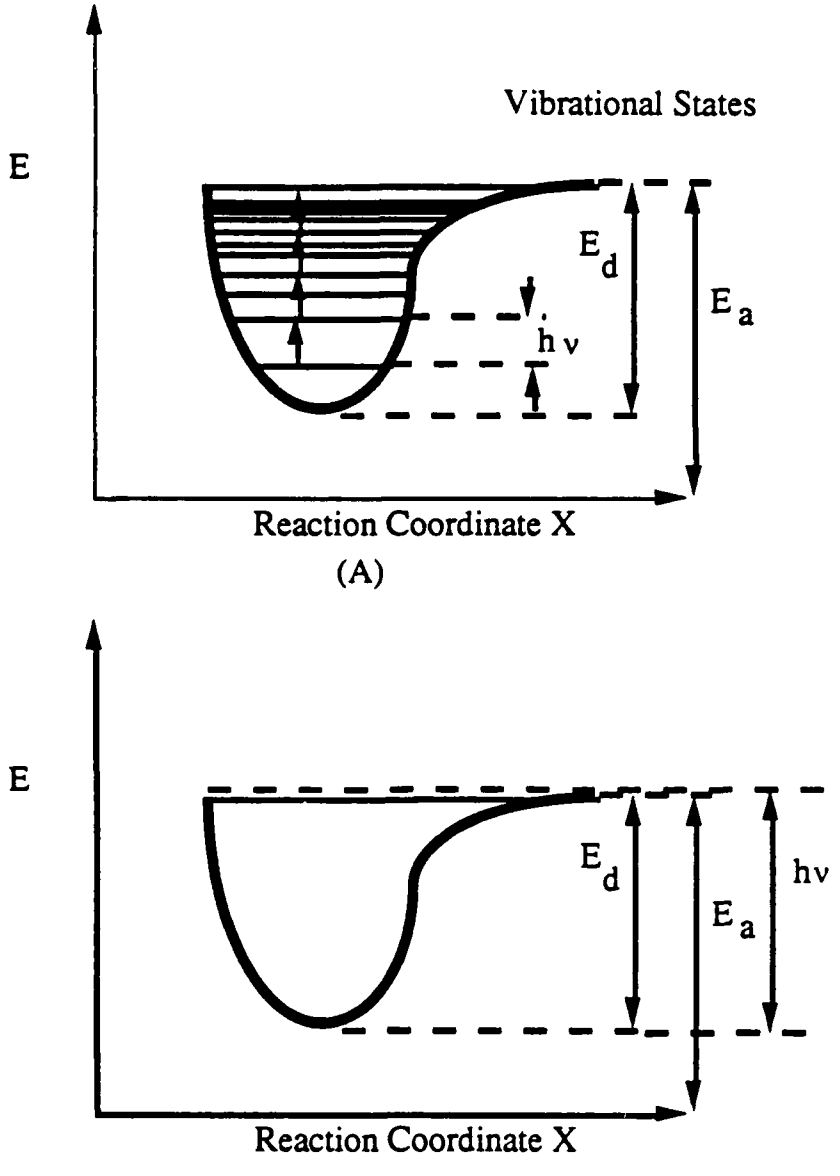

Figure 6.1
Photolytic deposition is achieved by excitation of molecular bonds by either (A) Multi-photon absorption, or (B) a single high energy photon (E_d is the dissociation energy, hν the photon energy)

6.3. EXPERIMENTAL

LALE has been accomplished in this work using conventional MOCVD precursors (TMGa and AsH_3) and conventional vent/run MOCVD reactors altered to allow alternate exposure of the substrate to these precursors. In the new reactor design reactant exposures are separated spatially by utilizing a four chamber vertical reactor in which the substrate is rotated in continuous reactant flows. Figure 6.2 shows a schematic of the experimental setup and new reactor design. RF induction was utilized in this reactor design to heat the susceptor. LALE experiments were performed by directing a focused laser onto the substrate during the TMGa exposure. In this way the laser was effectively scanned across the surface forming an epitaxial stripe. The reactor was equipped with a variable speed rotation control so that exposures to TMGa and AsH_3 could be separately optimized at a given temperature. The sample was then rotated through a high gas velocity hydrogen purge chamber which effectively "flushed" excess TMGa off the surface. The third chamber exposed the substrate to AsH_3 which reacted with the gallium adsorbate to form one monolayer before proceeding through another hydrogen chamber. A complete rotation corresponding to one monolayer could be accomplished in as fast as 2 seconds. Typical rotation speeds were 0.11revolutions/sec.

Under appropriate conditions one monolayer of a Ga adsorbate was formed uniformly only in the region of laser excitation for LALE during

the TMGa exposure. This adsorbate which we believe to be $GaCH_3$ subsequently reacts with AsH_3 to form GaAs. It has been found beneficial to utilized UV illumination during the AsH_3 exposure to improve crystalline morphology. The high energy UV photons *photolytically* decompose the AsH_3 which increase the surface reaction rate with the Ga adsorbate.[8] In this reactor design conventional MOCVD could be performed by raising the substrate temperature and injecting the reactants simultaneously into the same chamber. This gives the ability to overgrow the structures with high quality AlGaAs confining regions

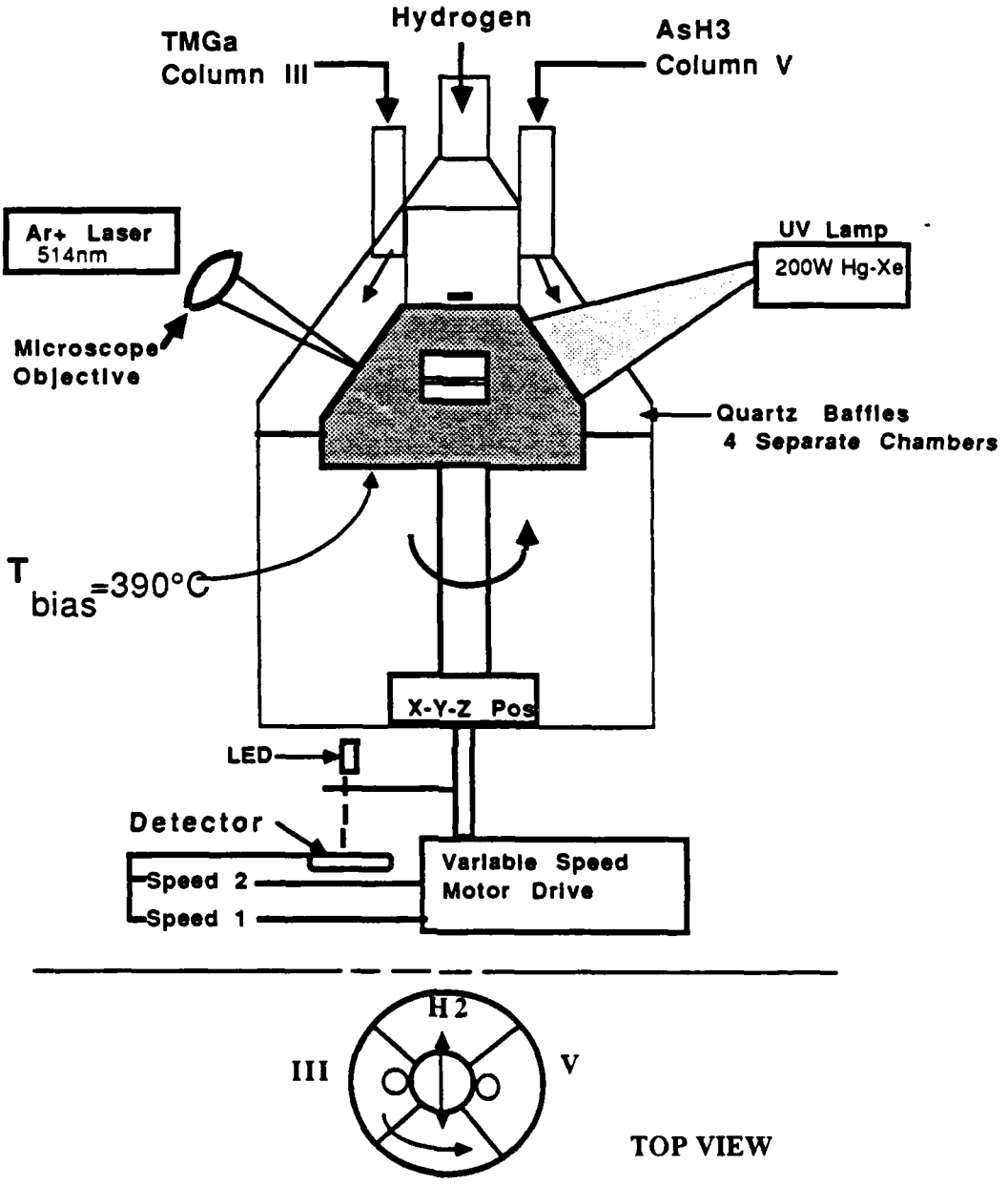

Figure 6.2
Schematic of four chamber reactor used in laser assisted ALE experiments. Note that the column III and column V reactants are separated spatially by two hydrogen purge channels and quartz baffles.

6.4 RESULTS & DISCUSSION

Using the four chamber reactor described previously we have conducted a series of experiments to characterize LALE growth using Argon ion laser irradiation during the TMGa exposure cycle. By scanning the laser spot, 40μm in diameter, at speeds up to 4000μm/sec we have selectively deposited single crystal GaAs stripes on both $Al_{0.3}Ga_{0.7}As$ and GaAs surfaces. As shown in figure 6.3, perfect monolayer saturated growth over an order of magnitude in TMGa pressures is demonstrated. Thickness measurements were made with a surface profilometer accurate to within ±50 Å and correlated to the number of rotations. The typical flat-top deposit profile is illustrated in figure 6.4. The fact that the deposit exhibits a plateau shape, instead of the Gaussian profile of the laser beam intensity, demonstrates the mono-atomic nature of the surface photocatalytic mechanism operative in this process. The flat-top nature of the deposit has also been observed for larger geometry deposits.

6.4. RESULTS & DISCUSSION

Using the four chamber reactor described previously we have conducted a series of experiments to charaterize LALE growth using an Argon ion laser irradiation during the TMGa exposure cycle. By scanning the laser spot, 40μm in diameter, at speeds up to 4000μm/sec we have selectively deposited single crystal GaAs stripes on both $Al_{0.3}Ga_{0.7}As$ and GaAs surfaces. As shown in figure 6.3, perfect monolayer saturated growth over an order of magnitude in TMGa pressures is demonstrated. Thickness measurements were made with a surface profilometer accurate to within ±50 Å and correlated to the number of rotations. The typical flat-top deposit profile is illustrated in figure 6.4. The fact that the deposit exhibits a plateau shape, instead of the Gaussian profile of the laser beam intensity, demonstrates the mono-atomic nature of the surface photocatalytic mechanism operative in this process. The flat-top nature of the deposit has also been observed for larger geometry deposits.

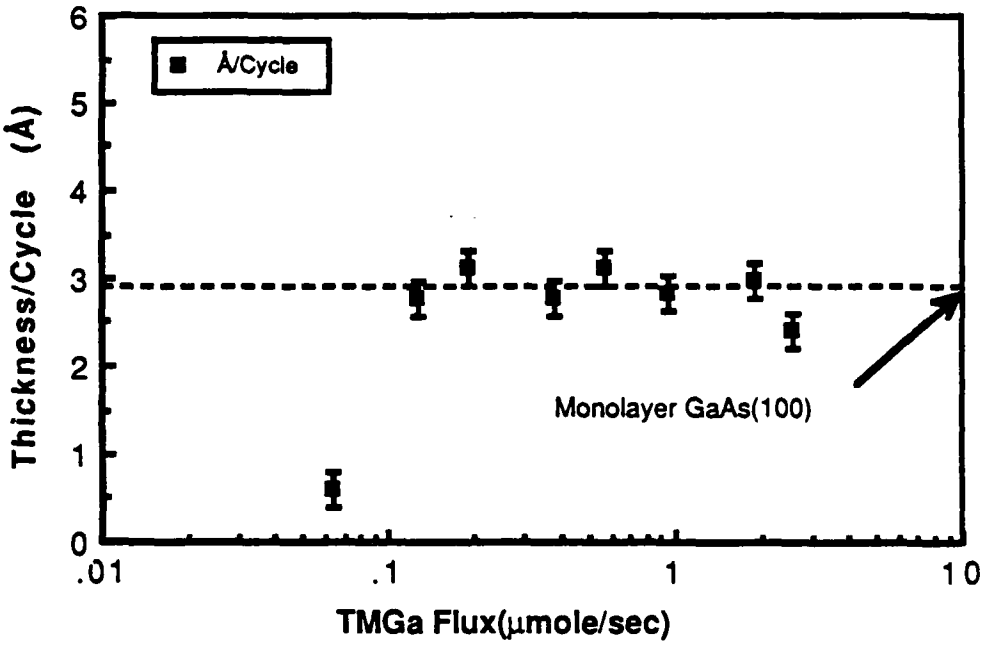

Figure 6.3.
Laser assisted ALE exhibits self-limiting monolayer growth over a wide range of TMGa fluxes.

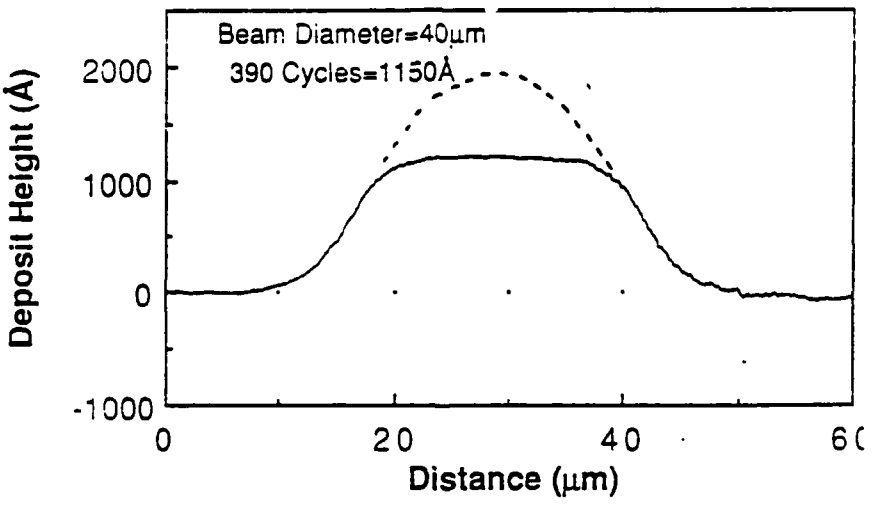

Figure 6.4.
LALE deposits exhibit flat-top profile indicative of mono-atomic growth mechanism.

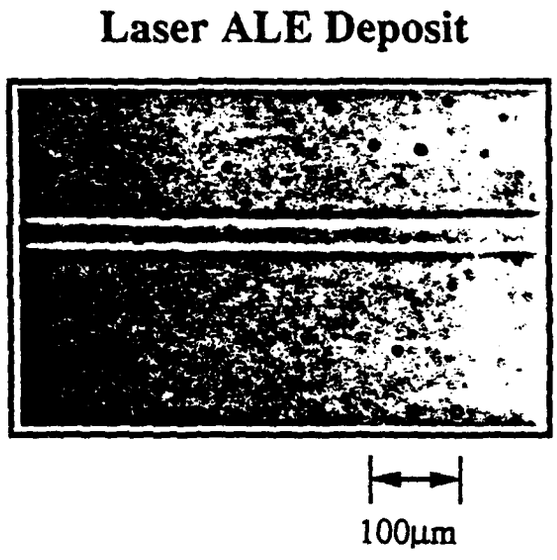

Figure 6.5
Photomicrograph of LALE GaAs stripe deposits exhibits smooth morphology of flat top stripes.(MAG=100X)

Figure 6.5 shows a photomicrograph which illustrates the smooth surface morphology of the deposited stripes. Note the flat-top nature of the deposit is also visible. In order to evaluate the potential of LALE for heterostructure devices, we have overgrown the deposited stripes with AlGaAs. This was performed by conventional MOCVD in the same reactor by heating the sample up to 750°C, and then injecting all reactants simultaneously into the hydrogen purge chamber. Figure 6.6 shows the low temperature PL obtained from a series of closely spaced LALE GaAs stripes which have been overgrown with $Al_{0.3}Ga_{0.7}As$. Donor to acceptor luminescence dominates the spectra. The measured energy difference of the peak from the band edge identify carbon as the dominant impurity in the sample. We believe this to be due to the low bias temperature used in these experiments (T=390°C). The lower temperature would decrease the surface exchange reaction rate between the gallium adsorbate and the arsine

As a means of reducing the carbon content of the films, UV irradiation of the wafer during the arsine exposure step was added High energy UV photons produce photolytic cracking of the arsine and increase the rate of surface reactions. Surface morphology of the deposits was dramatically improved upon the addition of the Hg-Xe UV lamp. The 200W Hg-Xe lamp is housed in an metallic elliptical mirror assembly which produces a highly concentrated optical beam. The power denisity of deep UV irradiation is estimated to be $10W/cm^2$ at the GaAs surface. In addition, we have observed that UV irradiation has improved the PL linewidth of QWs grown by thermal ALE. This is as shown in figure 6.7. Further analysis of UV exposure on the deposits is necessary. Another means of reducing the carbon content in the LALE process would be the addition of thermal pre-cracking of the arsine. Use of an infrared spot heater to locally heat the susceptor upstream of the wafer to above 550°C would generate As_2, As_4, and arsenic hydride radical species which might play a role in reducing carbon incorporation.

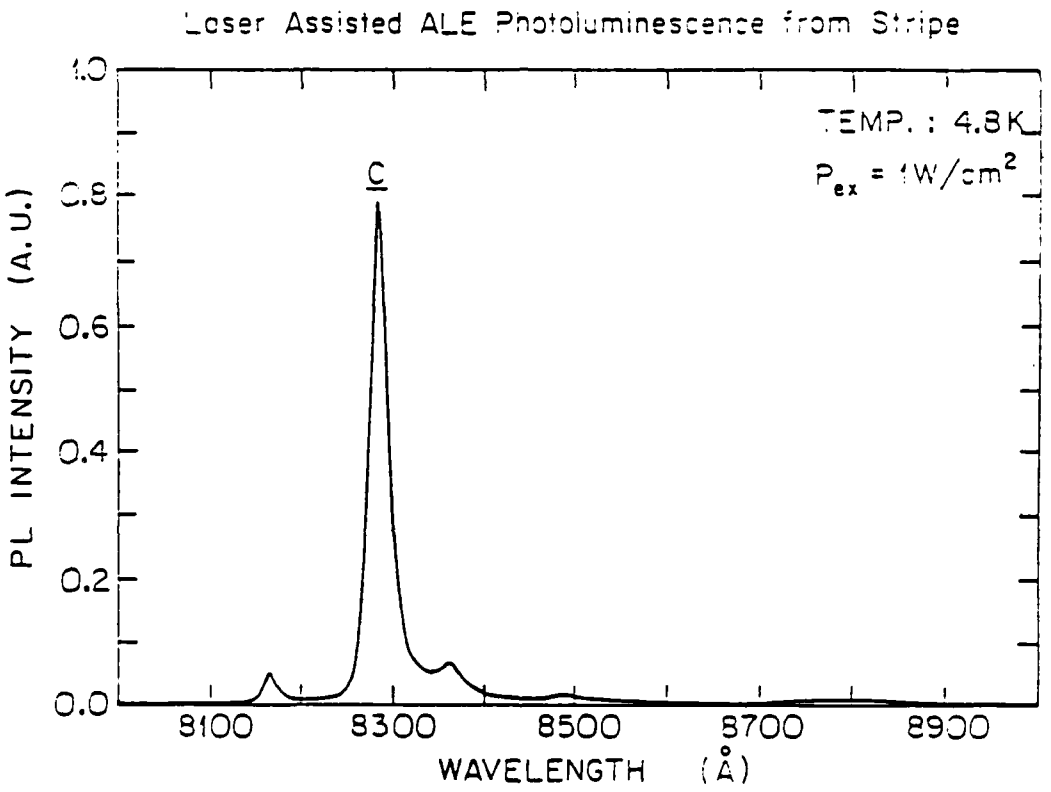

Figure 6.6
Low temperature PL from buried LALE GaAs stripes displays impurity related luminescence

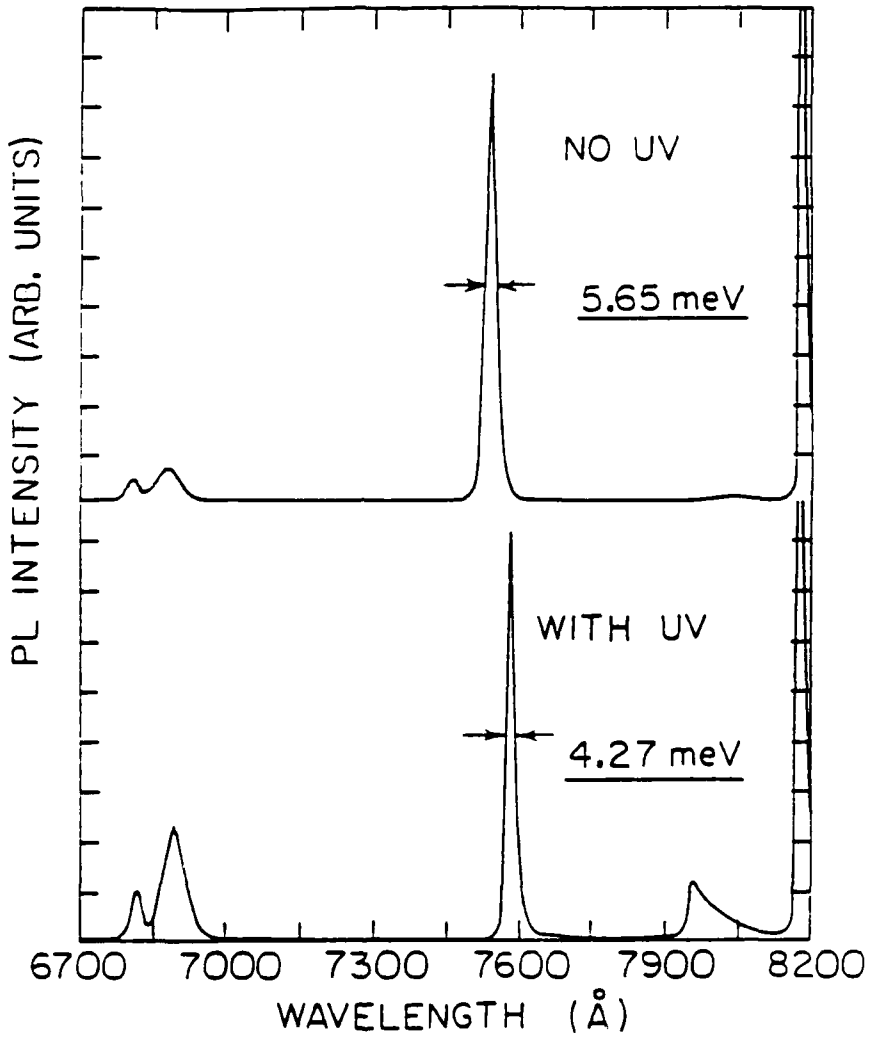

Figure 6.7
UV illumination is observed to decrease the PL linewidth of thermally deposited ALE QWs.

6.4 Proposed LALE Mechanism

The Argon ion laser irradiation locally stimulates the growth by a surface photo-reaction mechanisms. We propose a two mechanism LALE model that takes into account a self-limiting surface photocatalytic mechanism and surface heating. Growth saturation over a range of laser powers, as shown in Figure 6.8, argues against a purely thermally effect. This is also supported by the observation that at these writing speeds the growth saturates over a 50°C range of temperatures. But this data also shows that above critical powers the growth rate increases due to the pyrolytic nature of the laser irradiation. Figure 6.9 provides a comparison of LALE growth data to thermal ALE which suggests different growth kinetics are involved in the two techniques. Thermal ALE requires partial gas or surface phase cracking to yield a Ga adsorbate, while LALE appears to generate selective decomposition by a surface photochemical reaction alone. However, some local heating is necessary to effect single crystal growth since the growth rate starts to drop off with decreasing bias temperature. The deposition rate for LALE is described by modifying the first order adsorption model described in thermally driven ALE to account for the photocatalytic and pyrolytic nature of the laser irradiation:

$$\frac{d\theta}{dt} = k_{laser}^{P_L}(1-\theta) + k_{ads}^{\Delta T}(1-\theta) + k_{des}^{\Delta T}(\theta) + k_{Ga}^{\Delta T} \qquad (6.14)$$

Where k_{laser} is the rate constant for the photocatalytic effect of the laser beam which is directly proportional to the laser power:

$$k_{laser}^{P_L} = \frac{\eta(2\sigma_a P_L)}{(h\nu\pi w_o^2)} \tag{6.15}$$

The thermal effect of the laser beam is taking into account by calculating the temperature rise ΔT_{laser} caused by the scanned beam and substituting this into the rate constant for thermal ALE. Equation 4.7 then becomes:

$$k_{ads}^{\Delta T} = \frac{\delta\,(C_{TMGa})\left(1x10^{18}\exp\left(-\frac{60kcal}{R(T_{bias}+\Delta T_{laser})}\right)\right)}{N_s} \tag{6.16}$$

Where T_{bias} is the temperature at which the substrate held without laser irradiation in the LALE experiments (390°C), R is the gas constant, and C_{TMGa} the concentration of the TMGa in the gas. By similarly altering the thermal rate constant listed in Table 4.2 we can generate a deposition model. The rate of growth caused by the photocatalytic effect can be expressed by an enhancement factor in comparison to the thermal rate constant. This model uses a photocatalytic growth enhancement value of 200, which was observed in cw LALE results.[9]

$$\left(\frac{P_L}{\frac{k_{laser}}{T_b}} \right) = 200 \qquad (6.17)$$

To account for the scanning of the laser beam, the model using the effective reaction time "$\Delta\tau$" which is the time of the laser on the deposited spot area. For our scanned LALE technique this is estimated to be the spot size divided by the linear velocity ($40\mu m/4000\mu m/sec = 1x10^{-2}$ sec $= \Delta\tau$). Figure 6.10 shows the predicted growth rate for laser ALE. Note that the experimentally observed independence of growth rate over a range of temperatures is predicted by the computer generated model.

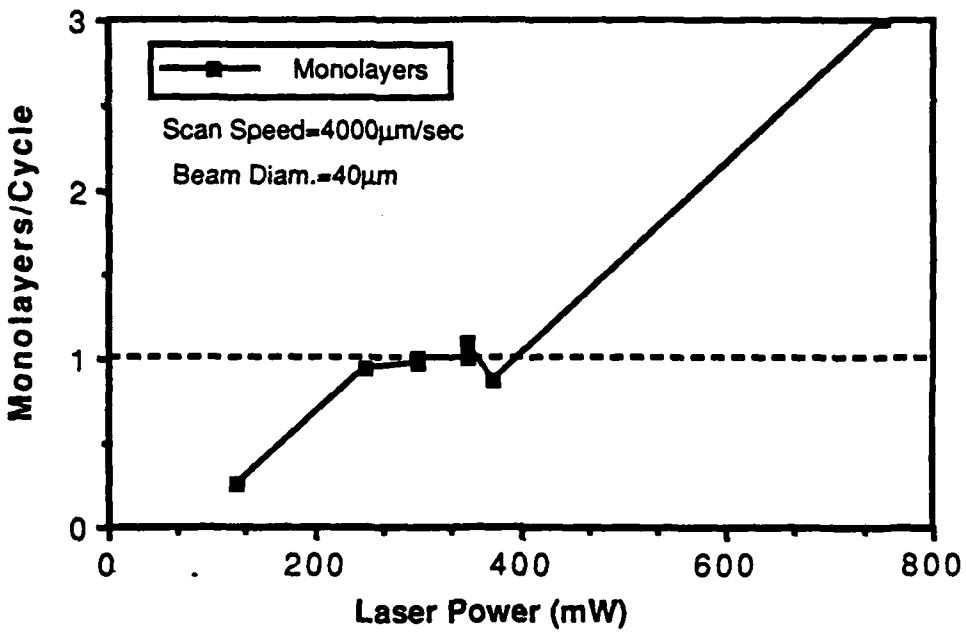

Figure 6.8
Growth rate as a function of laser power for LALE of GaAs on $Al_{0.3}Ga_{0.7}As$.

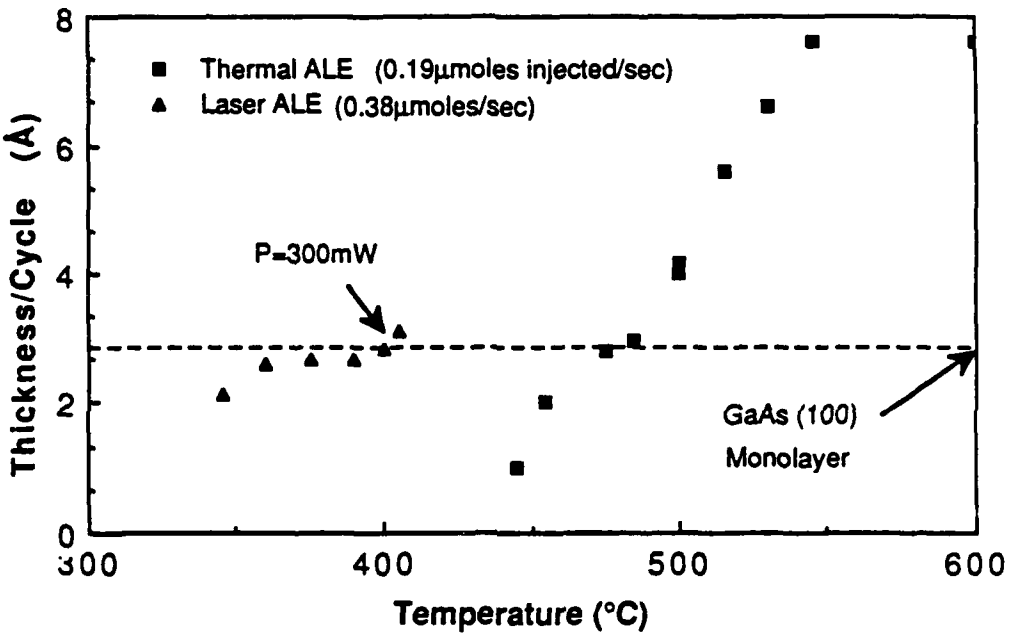

Figure 6.9.
Temperature dependence of Thermal and Laser ALE. Note independence of LALE growth rate over 50°C range which is indicative of photocatalytic mechanism.

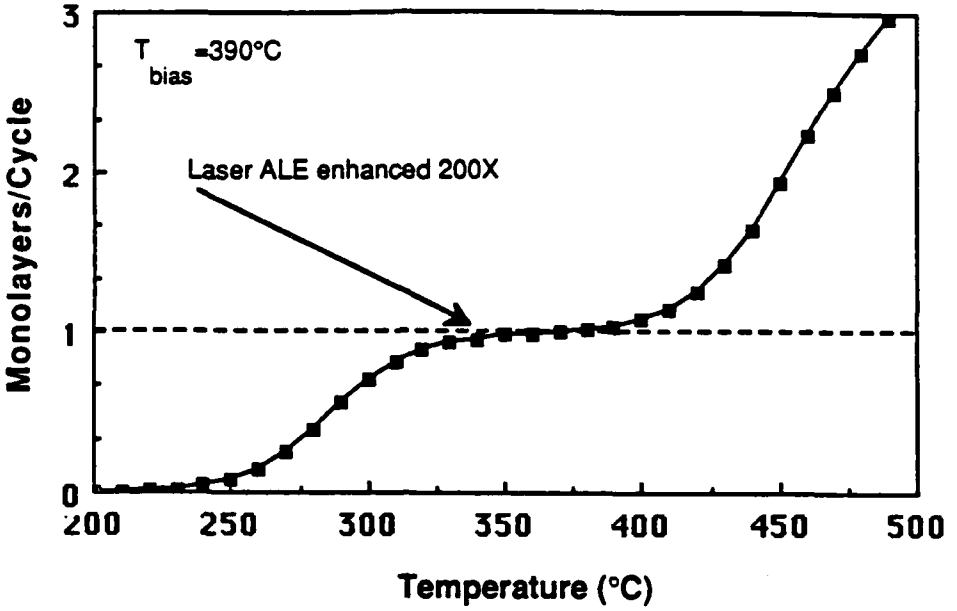

Figure 6.10
Laser ALE model predicts saturated growth over an range of temperatures as was observed in experimental results. The model uses a 300mW laser beam with a 40μm diameter scanned at 4000μm/sec.

Further support for surface photoassisted process can be seen in a comparison of the scanned LALE process demonstrated in this work to the continuous LALE of Aoyagi et al.[8] The growth rate for the small spot sizes scales proportionally with power density in comparison to the larger spot sizes used by Aoyagi. Table 6.1 provides a comparison of the two techniques. In order to compare the techniques we use the "effective" growth rate which uses the effective exposure time "$\Delta\tau$"of the laser on the spot area. Also evident is the observation that approximately the same total number of photons per surface area is necessary in the two cases.

Rearranging equation 6.6 and integrating predicts equivalent deposited thicknesses for the different spot sizes and power densities:

$$R_{sur} = \frac{dz}{dt} = \frac{\eta\theta(2\sigma_a P_L)}{(h\nu\pi w_o^2)} \tag{6.18}$$

Integrating:

$$\int_0^{z(t=\tau)} dz = \int_0^{\Delta\tau} \frac{\eta\theta(2\sigma_a P_L)}{(h\nu\pi w_o^2)} dt \tag{6.19}$$

The deposited thickness is then equal to :

$$z = \left(\frac{\eta\theta(2\sigma_a P_L)}{(h\nu\pi w_o^2)} \right) \Delta\tau \tag{6.20}$$

Since the "effective growth rate" of LALE scales proportionally with laser power density, as shown in Table 6.1, we can conclude that a surface photoassisted process is the dominant mechanism operative in LALE. This is evident when we compare the surface photoassisted rate equation 6.20, to the photolytic gas phase equation 6.11. The observation that growth is only occurring on the surface and no deposition is visible on the quartz windows is further support for a surface photoassisted process. We have also attempted to LALE deposit structures with the use of a Nd:YAG (1.06μm) laser. Below-bandgap irradiation yielded polycrystalline deposits with no sign of a saturated growth mechanism. Therefore, laser wavelengths larger than the band-gap of GaAs are

deemed necessary presumably because they generate electron hole pairs necessary for a surface photocatalytic reaction.

Table 6.1 Comparison of LALE Techniques

Deposited Thickness (T)	"Effective Growth rate" ($T/\Delta\tau$)	Power Density	#Photons cm^2 Cycle	Spot Size
cw LALE				
2.83Å	2.83Å/sec	225W/cm^2	5.85x10^{20}	1.0mm
scanned LALE				
2.83Å	283Å/sec	20,000W/cm^2	5.2x10^{20}	40μm

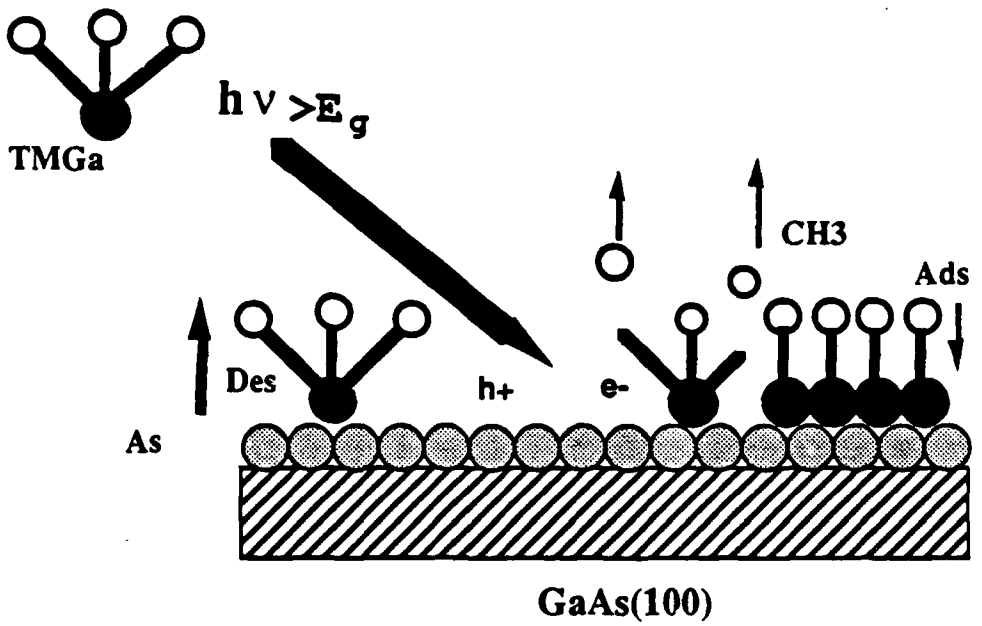

Figure 6.11
Photocatalytic Model for catalytic chemisorption of gallium methyl molecules on a GaAs surface.

6.5.2 Laser Heating Model

A temperature rise of 40°-100°C has been calculated for our conditions by using a model developed by Cline and Anthony.[10] We use aGaussian beam profile to calculate the spatial temperature distribution near the incident spot as a function of substrate thermal properties, beam size and power, and scan speed. As shown in figure 6.11. a temperature rise of 70°C is predicted for a 50μm spot with 200mW of incident power. This yields a power density of 10,000W/cm^2. This temperature rise is greater then the 40°C calculated for the continuously irradiated LALE experiments. However, as we have shown in our model the fact that we scan our laser beam changes the kinetics of the surface reactions.

The equation for heat flow in a solid heated by a laser of power density Q is given as:

$$\frac{\partial T}{\partial t} - \frac{\partial}{\partial x}\left(\kappa\frac{\partial T}{\partial x}\right) - \frac{\partial}{\partial y}\left(\kappa\frac{\partial T}{\partial y}\right) - \frac{\partial}{\partial z}\left(\kappa\frac{\partial T}{\partial z}\right) = \frac{Q}{C_p} \qquad (6.22)$$

where κ is the thermal diffusivity, and C_p the specific heat capacity per volume.

This model uses a moving gaussian intensity distribution normalized to give a total power of P_l for a spot radius R of the form:

$$Q = P_L\left(\frac{\exp\left(-\frac{((x - vt^2) + y^2)}{2R^2}\right)}{2\pi R^2}\right)\left(\frac{h(z)}{\lambda}\right) \tag{6.23}$$

where h is the absorption depth and h(z)=1 for $0<z<\lambda$, and h(z)=0 for $z>\lambda$.

Heat flow from the laser at x'y't' on the surface influences the temperature at x,y,z in the material at a later time t is given as:

$$T = \int_{-\infty}^{t}\int_{-\infty}^{\infty}\int_{-\infty}^{\infty}\int_{-\infty}^{\infty}\left(\frac{Q}{C_p}\right)(x'y'z't')G(x'y'z't'|xyzt)\,dx'dy'dz'dt' \tag{6.24}$$

Which G is Green's function for the diffusion equation at the surface

$$G = \frac{\exp\left(-\gamma^2\{4D(t - t')\}^{-1}\right)}{4[\pi D(t - t')]^{3/2}} \tag{6.25}$$

where D is the thermal diffusivity and:

$$\gamma^2 = (x - x')^2 + (y - y')^2 + (z - z')^2 + (t - t')^2 \tag{6.26}$$

which yields at the surface where z=0, and t=o the following integral.

$$T = \frac{P_1}{C_P}\int_0^{\infty}\frac{\exp\left(-\left(\frac{((x + vt')^2)}{(2R^2 + 4Dt')} + \frac{z^2}{(4Dt')}\right)\right)}{(2R^2 + 4Dt')\sqrt{\pi^3 Dt'}}dt' \tag{6.27}$$

By transforming to dimensionless variables this integral can be further simplified to yield:

$$T(x,y,z) = \frac{P_1}{C_p DR}\int_0^{\infty} \frac{\exp(-H)}{\sqrt{2\pi^3(1+\mu^2)}}d\mu \qquad (6.28)$$

where the following substitution makes the expression readily evaluated by numerical analysis:

$$H = \frac{\left(X + \frac{\rho}{2\mu^2}\right)^2 + Y^2}{2(1+\mu^2)} + \frac{Z^2}{2\mu^2} \qquad (6.29)$$

The dimensionless variables are:

$$\mu^2 = (2Dt')/R, \rho = R/(DV), X = x/R, Y = y/R, Z = z/R \qquad (6.30)$$

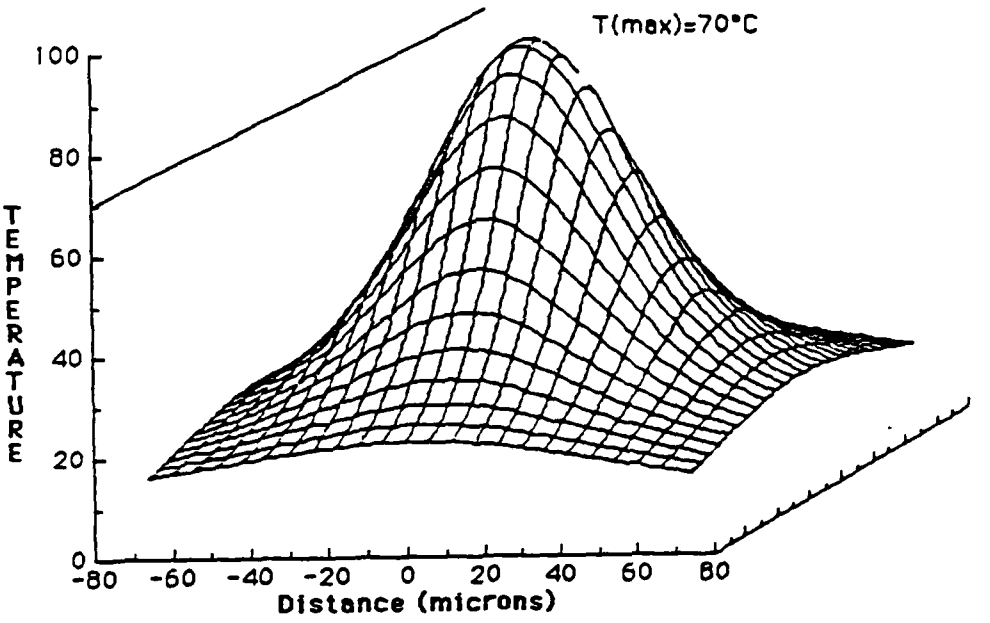

Figure 6.12
Calculated temperature rise for 50μm diameter laser beam at 200mW scanned at 4000μm/sec.

6.5.2 Theoretical Limits on LALE Spatial Resolution

Theoretically the spatial resolution of LALE deposits will be given by either the diffraction limited optical resolution or the thermal diffusion length. The diffraction limited optical spot size (FWHM) is given by:

$$\delta_o = \frac{1.03\lambda}{N.A} \tag{6.30}$$

which yields a FWHM of 0.7μm for an immersion objective (N.A.=1.33). If the thermal diffusion length, $L_t=[2Dt_p]^{0.5}$, limits the spatial resolution we can minimize the deposits size by decreasing the laser exposure time. For GaAs the thermal diffusivity is $0.072cm^2/sec$ at 390°C which yields diffusion lengths of less than 1.2μm when scan speeds are increased to yield an effective 100 nanosecond exposure. It is highly unlikely that photogenerated carrier diffusion lengths will limit the resolution, since the surface recombination velocities at the GaAs surface are very large ($10^6cm/sec$).[11]

Surface migration of the adsorbed species is another factor which might limit the deposit resolution. However, surface migration of the photogenerated adsorbate should be minimal because of the strong bonds formed in chemisorption and low temperatures involved. Recently, coworkers have observed that surface migration lengths in conventional

MOCVD appear to be less than 5μm at 750°C.[12] They also observe a decrease in the mobility of the surface species upon lower the temperature to 650°C. Surface diffusion should decrease exponentionally with temperature. Therefore, it is highly probably that surface migration at 400°C will be minimal and 1μm deposits readily achievable.

6.6 CONCLUSIONS

The "fast writing" potential of LALE to selective deposit GaAs on $Al_{0.3}Ga_{0.7}As$ is demonstrated. The resultant process is carried out in a four chamber atmospheric MOCVD reactor which can also grow conventional MOCVD layers. High quality materials and heterostructures have been accomplished by a hybridization of thermal ALE and MOCVD. The demonstration in the previous chapter on fabrication of high quality quantum wells and quantum well lasers with low threshold current densities, indicates that this process should eventually result in the selective deposition of opto-electronic and electronic components on the chip in a single run.

REFERENCES-CHAPTER 6

1 T. Cacouris, G. Scelsi, R. Scarmozzino, R. M. Osgood, Jr., R. R. Krchnavek, Laser and Particle Beam Chemical Processing for Microelectronics, edited by D. Ehrlich, G. S. Higashi, and M. M. Oprysko (MRS Research Symposium Proceedings, Pittsburgh 1987) Vol 101, p.43.

2 A.Doi , Y. Aoyagi, S. Namba, Appl. Phys. Lett. **49,** 785 (1986).

3 S. P. DenBaars, P. D. Dapkus, J. S. Osinski, M. Zandian, C. A. Beyler, and K. M. Dzurko, **D6,** 15th International Symposium on Gallium Arsenide and Related Compounds, Atlanta, GA (1988).

4 S. R. Morrison, The Chemical Physics of Surfaces, (Plenum Press, New York 1977), p.301.

5 V. F. Kiselev, O. V. Krylov, Adsoprtion Proccesses on Semiconductors and Dielectric Surfaces (Springer-Verlag, Berlin 1985) p.785.

6 M. Lax, J. Appl. Phys. **48,** 3919 (1977).

7 C. J. Chen, J. Vac. Sci. Technol., **A5**(6), 3386 (1987).

8 J. Nishizawa , T. Kurabayashi, H. Abe and A. Nozoe, Surface Science, **185,** 249 (1987).

9 Y. Aoyagi, A. Doi, S. Namba, J. Vac. Sci. Technol., **B5**, 1460 (1987).

10 H. E. Cline, and T. R. Anthony, J. Appl. Phys., **48**, 3897 (1977).

11 H. J. Hovel, Semiconductors and Semimetals, Vol 11 Solar Cells,(Academic Press, New York 1975) p.15.

12 K.M. Dzurko, E. P. Menu, P. D. Dapkus, **D-11**, 15th International Symposium on Gallium Arsenide and Related Compounds, Atlanta, GA (1988).

CHAPTER 7
CONCLUSIONS AND RECOMMENDATIONS FOR FUTURE RESEARCH

7.1 Conclusions from this Work

In this work, atomic layer epitaxy of GaAs, AlAs and AlGaAs has been demonstrated. Saturated monolayer growth of GaAs and AlAs has been observed by using metalorganic precursors at growth temperatures where kinetics of surface reactions dominate the deposition process. These surface reactions can be driven by thermal processes alone or by photo-assisted ALE. We have established some of the inherent advantages of the ALE technique by demonstrating the "*digital*" nature of the deposition process and growing extremely uniform ultrathin layers. We have measured ALE QW thickness variations of less than one monolayer across an entire sample grown in our small residence time reactor.

We have established for the first time that ALE can be hybridized with conventional MOCVD to grow device quality structures. This has been demonstrated by the operation for the first time of an injection laser with an active grown by ALE.[1] Quantum well lasers with threshold current densities as low as 380A/cm^2 have been achieved. Low temperature PL of single quantum wells (SQWs) grown by a hybridization of ALE and conventional MOCVD exhibit narrow linewidth intrinsic luminescence. These results suggest that ALE will play

an important role in the fabrication of heterojunction devices with critical layer thickness requirements.

In laser assisted ALE, selective area growth can occur by photolytically controlled surface reactions at substrate temperatures well below that at which purely thermal ALE will occur. The "*fast writing*" potential of LALE to selective deposit GaAs at scan speeds of 4000μm/sec is demonstrated.[2] We have employed a scanned laser beam with spot sizes as small as 30μm to selective deposit GaAs stripes on $Al_{0.3}Ga_{0.7}As$. We observe perfect monolayer saturation in the growth rate over an order of magnitude range of TMGa fluxes. Saturated monolayer LALE growth also occurs over a variety of power densities and a 50°C range of growth temperatures. The LALE deposits exhibit smooth mirror like morphology with flat-tops thickness profiles indicative of a mono-atomic growth mechanism.

The ALE and LALE of this work was accomplished using conventional MOCVD precursors and vent/run MOCVD reactors modified to allow alternate exposures of the substrate to the column III and column V precursors. In one case the reactant exposures are separated temporally by alternately injecting the reactants for one second each into a short residence time horizontal reactor. In the second design reactant exposures are separated spatially by utilizing a four chamber vertical reactor in which the substrate is rotated between continuous reactant flows. Under appropriate conditions one monolayer of the III-V

compound is formed uniformly in thermally driven ALE and only in the region of laser excitation for LALE. Both reactors are designed with the ability to grow conventional MOCVD layers thus allowing a hybridization of ALE and MOCVD, in the same reactor.

The kinetics for the ALE process have been investigated and are shown to behave in accordance with a first order adsorption model. The kinetics of the process are controlled by the chemisorption of the appropriate precursor on the GaAs surface. Chemisorption of a gallium methyl adsorbate appears to be the controlling step in the growth process. The formation of the adsorbed species, most likely $GaCH_3$, can be achieved by purely thermal processes or photo-assisted process. In thermal ALE removal of the first methyl radical in the gas or surface phase is theorized to be the rate limiting step. In laser assisted ALE selective area growth occurs by photochemical surface reactions of either photocatalytic or pyrolytic nature. The addition of the As monolayer appears to occur by the heterogeneous reaction of arsine with the Ga adsorbate.

By using reaction rates measured by sampled gas infrared spectroscopy we obtain good qualitative agreement between experimental results and predicted behavior from the first order ALE model. The pyrolysis of TMGa was found to occur in stages, with the first two methyl groups releasing in the 350-450°C range. It is not definite that all stages of alkyl elimination are homogeneous. The only gas phase by-product of the decomposition observed is CH_4. Arsine decomposition on the other hand is strongly catalyzed by wall deposits, GaAs surfaces, and gaseous mixtures with TMGa. The activation energy for AsH_3 decomposition is reduced for the reactor at the GaAs surface. We emphasize that these catalytic reactions play an important role in the MOCVD and ALE growth of GaAs and must be taken into account when modeling a large scale reactor.

Alternative gaseous arsenic sources that decompose at low temperatures were also studied. Thermal decomposition of TEAs in H_2 occurs via a ß-hydride elimination mechanism, producing DEAsH and C_2H_4 as the organic by-products. Thermal decomposition of DEAsH was observed to produce predominantly C_2H_6 , C_2H_4 and a small quantity of arsine. Both DEAsH and TEAs decomposition was discovered to be catalyzed by the addition of single crystal GaAs(100) surfaces to the reactor. Since DEAsH does not form an adduct with TMGa, whereas TEAs does, DEAsH is concluded to be the more attractive group V alternative source. Application of these sources to ALE should be studied, since they are significantly less toxic than arsine and decompose at lower temperatures

7.2 Recommendations for Future Research

Selective area epitaxy by laser assisted ALE has great potential for the integration of optoelectronic and electronic devices on the same chip. Optimization of the LALE process for the growth of GaAs/AlGaAs and InP/InGaAs heterostructures would allow the *in situ* deposition of heterostructure devices with differing epitaxial structures requirements. Growth and fabrication of buried heterostructure lasers by selectively depositing the GaAs active region using LALE is an attractive process for the demonstration of low threshold lasers. In addition, integration of multiple wavelength lasers on the same chip will be possible. The minimum spatial resolution achievable by LALE should be studied. Theoretically spatial dimensions of 1-2μm are obtainable if optimum scan rates and optical components are used. Surface migration of the photogenerated adsorbate should be minimal because of the strong bonds formed in chemisorption and low temperatures involved.

The manufacturing benefits of the *in situ* aspects of the LALE process for multiple wafer throughput is particularly attractive. In this study we have established the "fast writing" potential of LALE for depositing small dimension structures. An extension of this work would be the demonstration of multiple stripe lasers fabricated by a parallel optical laser writing setup. Another attractive process would be the the use of holographic projection for the concurrent deposition of multiple devices. Fabrication of heterojunction bipolar transistors (HBTs)

requires deposition of base, emitter, and collector regions. We envision a LALE process using a set of three holographic plates to deposit the different epitaxial layers. Figure 7.1 illustrates the *in situ* deposition of multiple transistor elements on the same wafer.

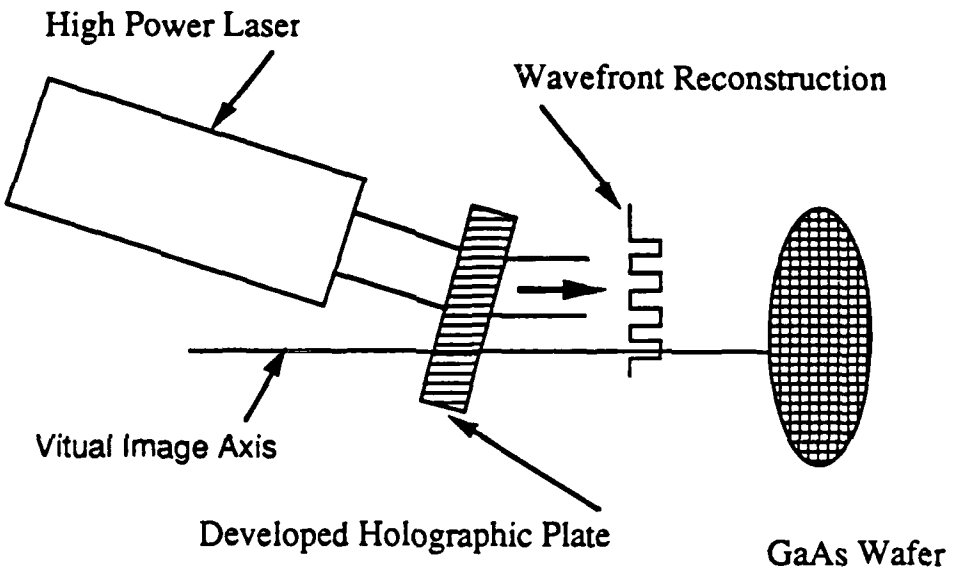

Figure 7.1
LALE process using holographic projection for multiple device fabrication.

The uniformity benefits inherent in the ALE process should be applied to large area epitaxial growth. By utilizing lower pressure short residence time reactors large area deposition of several III-V semiconductors should be possible by pulsed gas injection. Rotation of wafers in a small cross-section four chamber reactor could also yield highly uniform large area deposits. One can envision high reactant utilization if the wafers are rotated in relatively stagnant flows of column III and column V, under conditions of surface catalyzed reactions only. By using cylindrical lenses to induce monolayer photodeposition on the GaAs wafer surfaces 100% utilization of sources is achievable. Such a process could be obtained by simply increasing the power densities and rotation rates in demonstrated in our work by a factor of 10. Figure 7.2 shows a proposed design to achieve such an ambitious process.

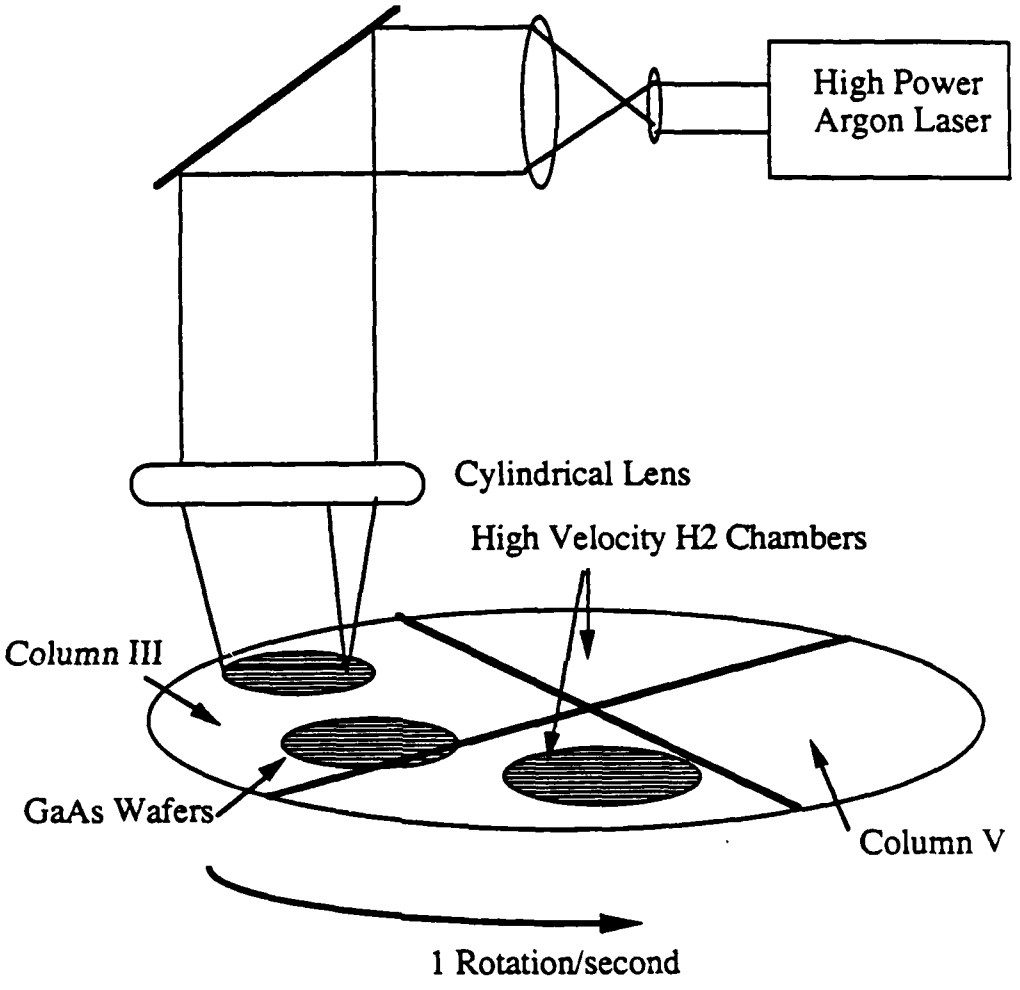

Figure 7.2
Multiple Wafer LALE deposition process

Another aspect of ALE that warrants research is growth on structured substrates. Coworkers have recently demonstrated low threshold lasers with small active regions grown on structured substrates by conventional MOCVD in our laboratory.[3] By using LALE to grow the selective area GaAs/AlGaAs and the etched features to define the small active region, localized low threshold lasers could be deposited. Coupling this technique with LALE of transistors structures would result in integrated electronic and opto-electronic devices on same chip.

Many other devices and materials would greatly benefit from the advantages of ALE. The ability to grow extremely uniform ultrathin layers with the digital ALE method should have impact on several device structures. Successful fabrication of high electron mobility transistors (HEMTs) requires the ability to grow highly uniform monolayer abrupt interfaces.[4] Quantum wells, as well as devices incorporating these structures, require the ability to produce thin layers with abrupt interfaces. In the quantum well injection laser the threshold current density and lasing wavelength are strongly dependent upon the active layer thickness in the 10-60Å range.[5] ALE growth of GaAs on Si and Ge is another area of future research. It is highly probable that ALE will reduce the dislocation density and antiphase domains which appear when a III-V zincblende material is deposited on the diamond lattice of Si or Ge.

n conclusion, this work has demonstrated several advantages of the A E and LALE techniques. Monolayer thickness uniformity in quant m well structures has been accomplished. We have achieved the first I -V device fabricated by ALE. Quantum well injection laser with active regions grown by ALE operate with threshold current densities as low a 380A/cm^2. Low temperature PL of single quantum well (SQWs) with ctive regions grown by ALE exhibit narrow linewidth intrinsic lumir scence. LALE shows great potential as a fabrication technology for in grated optoelectronics.

REF RENCES-CHAPTER 7

1 S. P. DenBaars, C. A. Beyler, A. Hariz, and P. D. Dapkus, Appl. Phys. Lett., **51**, 1530 (1987).

2 S. P. DenBaars, P. D. Dapkus, J. S. Osinski, M. Zandian, C. A. Beyler, and K. M. Dzurko, **D6**, 15th International Symposium on Gallium Arsenide and Related Compounds, Atlanta, GA (1988).

3 K.M. Dzurko, E. P. Menu, P. D. Dapkus, **D-11**, 15th International Symposium on Gallium Arsenide and Related Compounds, Atlanta, GA (1988).

4 P. D. Dapkus, J. Crystal Growth, **68**, 345, (1984).

5 J. J. Mawst, M. E. Givens, C. A. Zmudzinski, M. A. Emanuel, and J. J. Coleman, IEEE J. Quantum Electron., **QE-23**, 696, 1987).

BIBLIOGRAPHY

V. Aebi, C. B. Cooper, R. L. Moon, and R. R. Saxena, J. Crystal Growth **55**, 517 (1981).

Z. I. Alferov, V. M. Andreev, D. Z. Garbuzov, Y. V. Zhilyaev, E. P. Morozov, E. L. Portinoi, and V. G. Trofim, Sov. Phys. Semicond. **4**, 1573 (1971) [Translated from Fiz. Tekh. Poluprovodn. **4**, 1826 (1970)].

Y. Aoyagi, A. Doi, S. Iwai, and S. Namba, J. Vac. Sci. Technol. **B5**(5),1460 (1987).

R. Z. Bachrach, Crystal Growth, 2nd edition(London, Pergamon Press Ltd., 1980) B. R. Pamplin ed., pp. 221-271.

S. J. Bass, J. Crystal Growth **31**, 172 (1975).

S. J. Bass, J. Crystal Growth **44**, 29 (1978).

G. Bastard, Phys. Rev. B, **24**, 5693 (1981).

S. W. Benson, Thermochemical Kinetics , 2nd Ed, (John Wiley & Sons, New York, 1976) pp.17-85.

S. Berkman, V. S. Ban, and N. Goldsmith, Heterojunction Semiconductors for Electronic Devices, eds., G. W. Cullen and C. C. Wang (Springer-Verlag, Berlin 1979) p. 264.

D. C. Bertolet, J. K. Hsu and K. M. Lau, J. Appl. Phys., **62**,120 (1987).

R. Bhat, J. Electron. Mater. **14**, 433 (1985).

R. Bhat, J. R. Hayes, E. Colas, and R. Esagui, IEEE Electron Device Lett., **9**, 442 (1988).

R. Bhat, M.A. Koza, and B.J. Skromme, Appl. Phys. Lett. **50**, 1194 (1987).

T. Cacouris, G. Scelsi, R. Scarmozzino, R. M. Osgood, Jr., R. R. Krchnavek, Laser and Particle Beam Chamical Processing for Microelectronics, edited by D. Ehrlich, G. S. Higashi, and M. M. Oprysko (MRS Research Symposium Proceedings, Pittsburgh 1987) Vol 101, p.43.

H. C. Casey, Jr and M. G. Panish, Heterostructure Lasers, (New York, Academic Press, 1978) pp.167-176.

C. J. Chen, J. Vac. Sci. Technolo., A5(6), 3386 (1987).

H. E. Cline, and T. R. Anthony, J. Appl. Phys., **48**, 3897 (1977).

E. Colas, R. Bhat, B. Skromme, Paper **D-8**, International Symposium on GaAs and Related Compounds, Atlanta, GA 1988.

J. J. Coleman, and P. D. Dapkus, Gallium Arsenide Technology,(Indianapolis, Howard W. Sams & Co., Inc., 1985) D. K. Ferry ed., p.91.

A. D. Danner, PhD. Dissertation, University of Southern California (1987) p.72-74.

P. D. Dapkus, Class Notes, EE-599, Heterostructure Materials and Devices, University of Southern California, (1986).

P. D. Dapkus, J. Crystal Growth **68**, 345 (1984).

S. P. DenBaars, B. Y. Maa, P. D. Dapkus, A. D. Danner and H. C. Lee,J. Crystal Growth, **77**, 188(1986).

S. P. DenBaars, H. C. Lee, A. Hariz, P. D. Dapkus, **N-3**, Electronic Materials Conference, Santa Barbara, (1987).

S. P. DenBaars, C. A. Beyler, A. Hariz, and P. D. Dapkus, Appl. Phys. Lett., **51**, 1530 (1987).

S. P. DenBaars, P. D. Dapkus, C. A. Beyler, A. Hariz, and K. M. Dzurko, J. Crystal Growth, **202T**, Proceedings of the IV International Conference on OMVPE, Hakanoe, Japan (1988).

S. P. DenBaars, P. D. Dapkus, J. S. Osinski, M. Zandian, C. A. Beyler, and K. M. Dzurko, **D6**, 15th International Symposium on Gallium Arsenide and Related Compounds, Atlanta, GA (1988).

R. Dingle, Festkorperprobleme **XV**, 21 (1975).

A. Doi, Y. Aoyagi, S. Namba, Appl Phys. Lett. **48**, 1787, (1986).

A.Doi , Y. Aoyagi, S. Namba, Appl. Phys. Lett. **49**, 785 (1986).

R. D. Dupuis, P. D. Dapkus, R. D. Yingling, and L. A. Moudy, Appl. Phys. Lett., **31**, 201 (1977).

R. D. Dupuis and P. D. Dapkus, Appl. Phys. Lett., **32**, 472 (1978).

T. Fukunaga, K. L. I. Kobayashi, and H. Nakashima, Surface Sci., **174**, 71 (1986).

G.H. Geiger, D. R. Poirier, Transport Phenomena in Metallurgy, (Addison-Wesley Publishing Co., Menlo Park, CA 1980) pp.8-63.

B. K. Gilbert, Gallium Arsenide Technology,(Indianapolis, Howard W. Sams & Co., Inc., 1985) D. K. Ferry ed., p.28.

C. H. L. Goodman and M. V. Pessa, J. Appl. Phys. **R65**, 60 (1986).

S.R. Gunn, Inorg. Chem., **11**, 796 (1972).

M. A. Herman, M. Vulli, and M. Pessa, J. Cryst. Growth **67**,339 (1985).

N. Y. Holonyak, R. M. Kolbas, R. D. Dupuis, P. D. Dapkus, IEEE J. Quantum Electronics, **QE-16**, 170 (1980).

S. Ito, T. Shinohara, and Y. Seki, J. Electrochem. Soc., **120**, 1419 (1972).

M. G. Jacko and S. J. W. Price, Can. J. Chem. **41**, 1560(1963).

S. J. Jeng, C. M. Wayman, G. Costrini, and J. J. Coleman, Materials Lettters **2**, 359 (1984).

H. Kakibayashi and F. Nagata, Surface Sci, **74**, 84 (1986).

D. Kasemet, C. Hong, N. B. Patel, and P. D. Dapkus, IEEE J. of Quantum Elec., **QE-19**,1025 (1983).

H. Kawai, I. Hase, K. Kaneko and N. Watanabe, J. Crystal Growth **68**,508 (1984).

T. F. Keuch, and E. Veuhoff, J. Crystal Growth, **68**, 148 (1984).

V. F. Kiselev, O. V. Krylov, Adsorption Proccesses on Semiconductors and Dielectric Surfaces (Springer-Verlag, Berlin 1985) p.785.

N. Kobayashi, T. Makimoto, and Y. Horikoshi, Jap. J. Appl. Phys. **24**, L962 (1985).

N. Kobayashi, T. Makimoto, and Y. Horikoshi, Appl. Phys. Lett, **50**, 1435 (1987).

M. Kumagawa, H. Sunami, T. Terasaki, and J. Nishizawa, Japan J. Appl. Phys. **7**, 1332 (1968).

D. M. Larsen, Phys. Rev. **B8**, 535 (1973).

M. Lax, J. Appl. Phys. **48**, 3919 (1977).

H. C. Lee, PhD. Dissertation, University of Southern California, (1987) pp.106-130.

P. Lee, D. McKenna, D. Kapur and K.F. Jensen, J. Crystal Growth. **77**,120 (1986).

I. R. Levine, Physical Chemistry, McGraw-Hill Publ. Co., (New York 1978) p.771.

M.R. Leys and H. Veenvliet, J. Crystal Growth, **55**, 145 (1981).

T. Makimoto, Y. Yamauchi, and Y. Horikoshi, Paper **D-7**, International Symposium on GaAs and Related Compounds, Atlanta, GA 1988

H. M. Manasevit, Appl. Phys. Lett. **12**, 156 (1968).

H. M. Manasevit, J. Electrochem. Soc. **118**, 647 (1971).

H. M. Manasevit and W. I. Simpson, J. Electrochem. Soc. **116**, 1725 (1969).

H. M. Manasevit and K. L. Hess, J. Electrochem. Soc. **126**, 2031 (1979).

L. J. Mawst, M. E. Givens, C. A. Zmudzinski, M. A. Emanuel, and J. J. Coleman, IEEE J. Quantum Electron., **QE-23**, 696, (1987).

S. R. Morrison, The Chemical Physics of Surfaces, (Plenum Press, New York 1977) p.301.

J. Nishizawa, H. Abe and T. Kurabayashi, J. Electrochem. Soc. **132**, 1197 (1985).

J. Nishizawa, T. Kurabayashi,H. Abe, and N. Sakurai, J. Electrochem. Soc. **134**, 945 (1986).

J. Nishizawa and T. Kurabayashi, J. Electrochem. Soc. **130**, 413 (1983)

J. Nishizawa , T. Kurabayashi, H. Abe and A. Nozoe, Surface Science, **185**, 249 (1987).

S. B. Ogale, A. Madhukar, F. Voillot, M. Thomsen, W. C. Tang, T. C. Lee, Y. Kim and P. Chen, Phys. Rev. B, **36**,1662 (1987).

H. Okamato, Jap. J. Appl. Phys., **26**, 315 (1987).

M. Pessa, P. Huttunen, M. A. Herman, J. Appl. Phys. **54**, 6047 (1983).

M. Pessa, R. Makela, R. Suntola, Appl. Phys. Lett. **38**, 131 (1980).

W. H. Petzke, V. Gottschalch and E. Butter, Krist. Tech. **9**, 763 (1974).

D. H. Reep and S. K. Ghandi, J. Electrochem. Soc. **130**, 675 (1983).

W. Richter, "Physics of Metal Organic Chemical Vapour Deposition," Festkorperprobleme XXVI (Pergamon Press, New York, 1986).

C. F. Schaus, J. R. Shealy, L. F. Eastman, B. C. Cooman and C. B. Carter, J. Appl. Phys. **59**, 678 (1986).

Y. Seki, K. Tanno, K. Lida, and E. Ichiki, J. Electrochem. Soc. **122**, 1108 (1975).

J. Singh K. K. Bajaj and S. Caudhuri, Appl. Phys. Lett. **44**, 805(1984)

D.M. Speckman and J.P. Wendt, Appl. Phys. Lett. **50**, 676 (1987).

K. Tamura, J. Phys. Chem. **59**, 777 (1955).

V. P. Tanninen, M. Oikkoinen and T. Tuomi, Thin Solid Films **109**, 283 (1983).

M. A. Tischler, N. G. Anderson, and S. M. Bedair, Appl. Phys. Lett. **49**, 1199 (1986).

M. A. Tischler, N. G. Anderson, T. Katsuyama, and S. M. Bedair, Electronic Materials Conference, Boulder, CO, June (1985).

W. T. Tsang, Appl. Phys. Lett. **40**, 217 (1982).

W.T. Tsang, Appl. Phys. Lett. **45**,1234 (1984).

A. Usi and H. Sunakawa, Inst. Phys. Conf. Ser. No. **79**, 753 (1985).

J. S. Yuan, C. C. Hsu,, R. M. Cohen, and G. B. Stringfellow, Appl. Phys Lett., (1985).

M. Yoshida, H. Watanabe, and F. Uesugi, J. Electrochem. Soc. **130**, 413 (1985).

M. Yoshida, H. Watanabe and F. Uesugi, J. Electrochem. Soc. **137**, 677 (1985).

APPENDIX

Appendix A

Integration of first order adsorption model

$$\frac{d\theta}{dt} = k_{ads}(1-\theta) - k_{des}(\theta) + k_{Ga}$$

Integrating:

$$\int_0^{\theta} \frac{d\theta}{\left(k_{ads}(1-\theta) - k_{des}(\theta) + k_{Ga}\right)} = \int_0^{t} dt$$

Rearranging:

$$\int_0^{\theta} \frac{d\theta}{\left(\left[-\left(k_{ads} + k_{des}\right)\right]\theta + k_{ads} + k_{Ga}\right)} = \int_0^{t} dt$$

From Integral Tables:

$$\int \frac{dx}{Ax + B} = \frac{1}{A}\ln[Ax + B] + C$$

Substituting:

$$\text{Let : } A=[-(k_{ads}+k_{des})]$$
$$B=(k_{ads}+k_{Ga})$$

$$\frac{1}{A}\ln[A\theta + B]\Big|_0^{\theta(t)} = |t_0^t$$

$$\ln[B] - \ln[A\theta + B] = -At$$

$$\ln\frac{[B]}{[A\theta + B]} = -At$$

$$\frac{[A\theta + B]}{[B]} = \exp(At)$$

$$A\theta = [B]\exp(At) - B$$

$$\theta = \frac{B}{A}(\exp(At) - 1)$$

Substituting values back in yields:

$$\theta = -\left(\frac{k_{Ga} + k_{ads}}{k_{ads} + k_{des}}\right)\left[\exp\left[-(k_{ads} + k_{des})t\right] - 1\right]$$

Rearranging into final form:

$$\theta = \left(\frac{k_{Ga} + k_{ads}}{k_{ads} + k_{des}}\right)\left[1 - \exp\left[-(k_{ads} + k_{des})t\right]\right]$$

Appendix B

Kinematic Viscosity of Hydrogen

The viscosity of nonpolar gases such as hydrogen gas can be calculated at any temperature by using Newton's law of viscosity corrected for the energy of interaction between molecules in the gas. The Lenard-Jones parameters are used to account for the potential energy of interaction between a pair of molecules in the gas. These parameters are the characteristic diameter of the molecule $\sigma(H_2=2.915\text{Å})$, and the collision integral $\Phi_\eta(H_2=0.7432)$.[1] Using these parameters the viscosity of nonpolar gases can be determined from:

$$\eta = 2.67 \times 10^{-5}\frac{\sqrt{MT}}{\sigma^2\Phi_\eta}$$

where M is the gram molecular weight, η is the viscosity in poises, and T in °K. For hydrogen at 455°C, this yields a viscosity of 1.28×10^4 poise (1 poise =gm/cm-sec). For the boundary layer calculations we need to use the kinematic viscosity which is a measure of the momentum diffusivity:

$$\nu' \equiv \frac{\eta}{\rho}$$

where ρ is the density of the gas ($\rho = 8.49 \times 10^{-5}$gm/cm^3 for hydrogen).The boundary layer thickness is determined from equation 4.15:

$$\delta(x) = 4.64 \sqrt{\frac{x(\nu')}{V_\infty}}$$

For our experimental conditions the average distance of the wafer from the leading edge is 0.5cm and the average gas velocity is 35cm/sec. These values give us an average boundary layer thickness of 0.68cm.

REFERENCES-APPENDIX

1 G.H. Geiger and D. R. Poirier, Transport Phenomena in Metallurgy, (Addison-Wesley Publishing Co., Menlo Park, CA 1980) p.11.